Efficient Robust Structural Topology Optimization Under Material Uncertainties

by

Linxi Gary Li

A thesis submitted in conformity with the requirements
for the degree of Master of Applied Science

Graduate Department of Aerospace Science and Engineering
University of Toronto

Efficient Robust Structural Topology Optimization Under Material Uncertainties

Linxi Gary Li
Master of Applied Science

Graduate Department of Aerospace Science and Engineering
University of Toronto
2024

Abstract

Topology optimization (TO) is a structural design method, and its principle is to distribute material resources throughout a loaded structure to minimize a cost function subject to performance constraints. Additive manufacturing has a symbiotic relationship with TO as it can manufacture components with complex geometries, such as designs from TO. However, additively manufactured components have uncertainties in the material properties, which must be accommodated in structural design. Experimental and theoretical studies show that these uncertainties are represented by high dimensional stochastic surrogates. Robust topology optimization (RTO) is a popular stochastic variant of TO for design under uncertainties. RTO includes a linear combination of the mean and variance of a quantity of interest (QOI) in the optimization statement, which are estimated using an uncertainty quantification (UQ) scheme. In the existing RTO approaches that account for material uncertainties, there is a lack of algorithms that target high dimensional stochastic inputs. The standard approach for this problem is Monte Carlo-based RTO (MCTO), but it requires high computational cost to produce high quality designs. This thesis develops two novel UQ schemes targeting high dimensional material uncertainties, which are incorporated into the RTO framework. Numerical studies show that under moderate to high dimensional stochastic input, both of the proposed RTO algorithms are more computationally efficient than MCTO, can generate accurate estimations of the statistics of QOI, and also produce designs with a similar level of optimality as the designs from MCTO.

Acknowledgements

Just as it takes a village to raise a child, I received a tremendous amount of support from professors, family, and friends which led to the completion of this project.

First and foremost, I would like to thank my supervisor, Professor Craig Steeves, for being a fantastic mentor and sharing his wealth of knowledge regarding research and academic life. His insightful guidance and meticulous suggestions are paramount to the completion of this thesis. Also, I am very appreciative that he provided a supportive and encouraging environment, which is critical for my growth as a student.

I would like to sincerely thank Professor Masayuki Yano for the countless fruitful conversations regarding not only technical details but also career and life advice. His passion and dedication to work greatly inspire me everyday.

Thank you to my family for their encouragement and unconditional support. They are the cornerstones of my life, and I cannot thank them enough for everything they have done for me.

Thank you to the MF gang, Ali, Cathy, Katrina, Mohammad, Satoshi, and Yazdan, for bringing joy during the fun times and providing support through tough moments. Their companionship is what makes this journey so special and memorable. Also, I would like to thank my friends William and Laster for their support and chats, which brightened up my day. To my friends, I would like to borrow a quote from The Office: "I'm still just thinking about my old pals, only now they're the ones I made here. I wish there was a way to know you're in the good ol' days before you've left them."

Thank you to all my lab mates at the AASL for the good times. I would like to especially thank Dr. Daniel Pepler for his help with setting up the code base for this thesis work and for providing insightful technical discussions.

The financial support from The Natural Sciences and Engineering Research Council of Canada is gratefully acknowledged.

Contents

List of Tables

List of Figures

Chapter 1

Introduction

Multifunctional and lightweight structural designs are integral to efficient engineering systems. Typical designs following the conventional frameworks lead to classic structures such as trusses and frames. Predetermining the structural forms severely restricts the design space, and hence the structures may not be the most efficient in the application context. With computer aided design and advanced manufacturing methods such as additive manufacturing, the capability of 3D modeling and component fabrication in engineering has increased rapidly. It is worthwhile to exploit these technologies as means to produce high performance structures.

Topology optimization (TO), is one of the most promising computational methods for designing lightweight structures in aerospace applications [1]. TO aims to distribute material efficiently based on an imposed objective coupled with a set of constraints. Such a systematic optimization-based framework allows for the best compromise between the material usage and performance of structural designs. TO allows for the introduction and removal of structural elements in design iterations, hence enabling more freedom on the structural form. The resulting components tend to have complex geometries and are tailored for specific performance objectives, such as maximizing structural stiffness for a limited amount of material. The complex features means that structures designed with TO are best fabricated using additive methods. However, additive manufacturing leads to significant uncertainties in material properties as demonstrated in Figure 1.1. Unless the material model used for design accounts for the variability in material properties, the component may not perform as predicted. This necessitates the propagation of material uncertainties into TO algorithms.

Robust topology optimization (RTO), a method for design under uncertainty is employed in this thesis as the stochastic counterpart to deterministic TO. The uncertain material properties are typically represented as correlated random fields, which

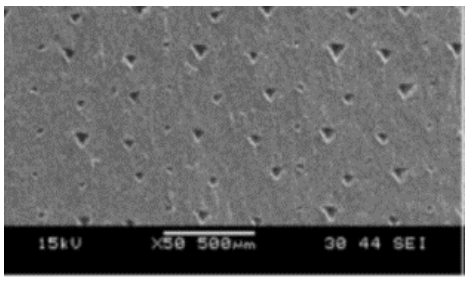

(a) Micro-CT image showing the pores in the cross section of a 3D printed component [6].

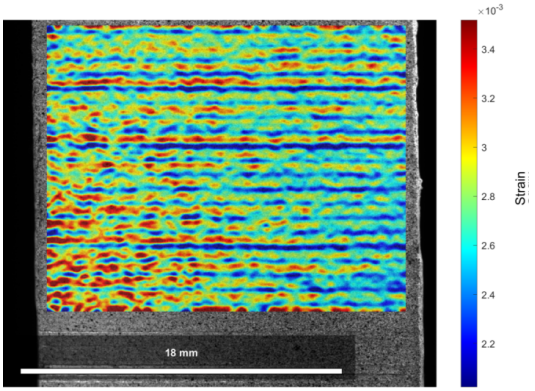

(b) Significant inconsistencies in the strain field of a unidirectionally 3D printed specimen under tensile loading [2].

Figure 1.1 Examples of varabilities in additively manufactured component leading to randomness in material properties.

are approximated with statistical surrogates that depend on a finite set of random variables. For additively manufactured components, the randomness in material properties is effectively modeled using random fields with short correlation lengths [2], which result in high stochastic dimensions. RTO is more costly due to the additional stochastic dimensions and the need to compute statistics of interest every iteration. Typically, the Monte Carlo-based RTO (MCTO) are used to compute the statistics and the gradients for optimization. However, MCTO is very inefficient and hence this thesis aims to develop RTO algorithms that are more efficient than MCTO and also produce structural designs with similar qualities.

Ultimately, the efficient propagation of material uncertainties that are characteristic of additively manufactured components into RTO and the design of uncertainty-aware structures are the main motivations behind this thesis. The layout of the thesis is as follows, Chapter 2 covers the general framework of TO and RTO, in addition to filtering schemes, sensitivity analysis, and models for material uncertainty. A summary of RTO algorithms in literature is also presented. Chapters 3 to 5 are devoted to discussions of novel RTO algorithms and their associated uncertainty quantification schemes for computing the statistics of interest. Numerical studies are conducted to assess the performance of these algorithms. Chapter 6 concludes this dissertation.

As an additional note, a paper [3] was generated during the thesis work, but has not been included in this manuscript for reasons of space.

Chapter 2

Robust Topology Optimization

2.1 Structural Topology Optimization

Since the seminal work on topology optimization (TO) in 1988 by Bendsøe and Kikuchi [4], a plethora of TO variants have emerged in literature [1, 5], including homogenization [4], level set method [6], genetic algorithms [7], the moving morphable components-based method [8], and solid isotropic material with penalization (SIMP) [9]. These ensure that TO is well-studied in deterministic contexts, where the boundary conditions and objectives are constants.

For its simplicity in both conception and numerical implementation, the SIMP method, a density-based approach, is the most popular TO framework [1] and is employed in this thesis. In the SIMP approach, the design domain is discretized using the finite element method (FEM) and each element is assigned a density, which are the optimization variables. In the discrete settings, the densities are either zero, corresponding to void, or one, corresponding to solid material. Binary densities lead to a large-scale integer programming problems that are computationally expensive. In SIMP, the density is relaxed to be continuous between zero and one, enabling the application of very efficient gradient-based optimizers.

For compliance (c) minimization under a set of boundary conditions and physical constraints, the mathematical statement of TO is:

$$\min_{\boldsymbol{\rho}} \quad c(\boldsymbol{\rho}) = \mathbf{F}^T \mathbf{u}(\boldsymbol{\rho}), \tag{2.1}$$

$$\text{s.t.} \quad : \mathbf{K}(\boldsymbol{\rho})\mathbf{u}(\boldsymbol{\rho}) = \mathbf{F}, \tag{2.2}$$

$$: 0 < \rho_{min} \leq \rho_e \leq 1 \quad \forall e, \tag{2.3}$$

$$: \boldsymbol{\rho}^T \boldsymbol{v} - V^* \leq 0, \tag{2.4}$$

where $\mathbf{F}$ the applied load, $\mathbf{u}(\boldsymbol{\rho})$ the nodal displacement, $\boldsymbol{\rho} = \{\rho_e\}$ the element density vector, $\boldsymbol{v} = \{v_e\}$ the element volume vector, and V^* is the total allowed design volume. $\mathbf{K}(\boldsymbol{\rho})$ is the symmetric positive definite (SPD) FEM stiffness matrix, constructed from the summation of element stiffness matrices ($\mathbf{K}_e(\rho_e)$) as: $\mathbf{K}(\boldsymbol{\rho}) = \sum_e \mathbf{K}_e(\rho_e)$. The scalar lower bound for the densities of the elements is ρ_{min}, as this ensures that $\mathbf{K}(\boldsymbol{\rho})$ is non-singular, leading to the existence of a unique displacement solution. In practice, ρ_{min} is set to a small value of 0.001.

However, this optimization formulation leads to designs with patches of intermediate density regions, which do not have a clear physical meaning. Hence, the SIMP approach further penalizes the Young's modulus of each element as a function of the density:

$$\mathbf{K}_e(\rho_e) = {\rho_e}^p E_e \, \mathbf{D}_0, \tag{2.5}$$

where $\mathbf{D}_0$ is the unit modulus element stiffness matrix and p is the penalization parameter, usually 3. The Young's modulus is constant over each element. This power law representation discourages elements from having intermediate densities by reducing their effective moduli. In this thesis, a 4-node plane stress bilinear element with unit thickness is used.

2.2 Filtering Schemes

2.2.1 Density Filter

Solving the problem in Equations (2.1)–(2.3) and (2.4) using low order elements, such as bilinear quadrilateral, results in mesh dependent designs and checkerboarding pathology [5]. Both are undesirable behaviors from modeling and physical perspectives. The linear density regularization filter [10], a type of design restriction method, is often used to alleviate these issues. This filter introduces a filter density set ($\bar{\boldsymbol{\rho}} = \{\bar{\rho}_e\}$), which is obtained from a weighted product of the nearby optimization variables ($\tilde{\boldsymbol{\rho}} = \{\tilde{\rho}_e\}$):

$$\bar{\rho}_i(\tilde{\boldsymbol{\rho}}) = \frac{\sum_e w(x_i, x_e) v_e \tilde{\rho}_e}{\sum_e w(x_i, x_e) v_e}. \tag{2.6}$$

The cone smoothing kernel $w(\cdot, \cdot)$ is defined by $w(x_i, x_e) = \max(0, r_{min} - \|x_i - x_e\|)$, where x_i and x_e are the centroid locations for elements i and e, and r_{min} is the filter radius. This filter also serves as a feature control mechanism, as r_{min} dictates the minimum structural size.

2.2.2 Heaviside Filter

The application of the regularization filter in Equation (2.6) leads to a large number of transitional elements with intermediate density, a phenomenon known as the boundary diffusion effect [11]. A Heaviside projection filter (HPF) is applied to recover a strictly solid-void design, which is desirable.

In this thesis, two different HPFs are employed. The first is a non-volume preserving HPF, proposed by Wang et al. [12]:

$$\rho_e(\bar{\rho}_e) = \frac{\tanh(\beta\eta) + \tanh(\beta(\bar{\rho}_e - \eta))}{\tanh(\beta\eta) + \tanh(\beta(1-\eta))}. \tag{2.7}$$

This function approximates the Heaviside step function and is differentiable. The η controls the position of the transition from 0 to 1 and is typically set to 0.5. The β controls the sharpness of this transition. As β tends to 0, Equation (2.7) becomes a linear function where $\rho_e = \bar{\rho}_e$, and as β approaches infinity the unit step is recovered. The characteristic of a non-volume preserving filter is its application leads to a change in the total volume, meaning $\sum_e \bar{\rho}_e \neq \sum_e \rho_e$. Hence, the volume or weight constraints are applied to the physical densities $\boldsymbol{\rho}$, not the design variables $\tilde{\rho}$.

The other HPF scheme considered is a volume preserving method, proposed by Xu et al. [11]:

$$\rho_e(\bar{\rho}_e) = \begin{cases} \eta\Big[\exp\left(-\beta\left(1 - \bar{\rho}_e/\eta\right)\right) - (1 - \bar{\rho}_e/\eta)\exp(-\beta)\Big], & 0 \leq \bar{\rho}_e \leq \eta; \\ (1-\eta)\Big[1 - \exp(-\beta\frac{\bar{\rho}_e - \eta}{1-\eta}) + (\bar{\rho}_e - \eta)\exp(-\beta)/(1-\eta)\Big] + \eta, & \eta \leq \bar{\rho}_e \leq 1. \end{cases} \tag{2.8}$$

This function also approximates the Heaviside function. The η and β parameters have the same functionalities here as the non-volume preserving case. A bisection algorithm is used every iteration to select the η that maintains $\sum_e \bar{\rho}_e = \sum_e \rho_e$ before and after filtering, hence leading to volume preservation. Volume preserving HPFs typically have better stability and convergence properties [11]. Since the density filter in Equation (2.6) is also a volume preserving scheme, a combination of these two schemes leads to $\sum_e \tilde{\rho}_e = \sum_e \rho_e$.

Having a sufficiently high β in the HPF is necessary to produce a solid-void topology. However, imposing an aggressive filter as a baseline tends to trap the optimization in local minima. Hence, a continuation scheme is applied where β starts at a low value and gradually increases. At the initial optimization stages, the HPF has a weak influence on the intermediate densities and hence the SIMP scheme plays a pre-

dominant role in penalizing the intermediate densities. As the design iterates closer to an optimal solution, the HPF begins to play a more important role in removing the intermediate densities.

With the application of a regularization filter and a HPF, the physical densities ($\boldsymbol{\rho}$) are functions of the optimization variables ($\tilde{\rho}$) through the compositional relation: $\boldsymbol{\rho}(\bar{\boldsymbol{\rho}}(\tilde{\boldsymbol{\rho}}))$.

2.3 Sensitivity Analysis

SIMP-based topology optimization problems are solved by gradient-based methods, which require the derivatives of the objective and the constraints with respect to the optimization variables.

With filtering, the physical densities (ρ_e) are functions of the optimization variables ($\tilde{\rho}_e$) and hence gradients with respect to the physical densities are developed. The sensitivities of the compliance objective in Equation (2.1) with respect to the physical density of element e is formulated using the adjoint method [13], leading to:

$$\frac{\partial c}{\partial \rho_e} = -\mathbf{u}^T(\sum_e p\rho_e^{p-1} E\mathbf{D}_0)\mathbf{u}. \tag{2.9}$$

The computational advantage of the adjoint method is that the cost of performing the sensitivity analysis is similar to the cost of solving the linear equilibrium equation, regardless of the number of design variables. Since the compliance is self-adjoint, the cost of computing the derivatives are even cheaper. The sensitivities of the volume constraint in Equation (2.4) are:

$$\frac{\partial(\boldsymbol{\rho}^T\boldsymbol{v} - V^*)}{\partial \rho_e} = v_e. \tag{2.10}$$

To obtain the sensitivities with respect to the optimization variables, the effects of the filters are accounted through the chain rule:

$$\frac{\partial(\cdot)}{\partial \tilde{\rho}_e} = \frac{\partial(\cdot)}{\partial \rho_i}\frac{\partial \rho_i}{\partial \bar{\rho}_i}\frac{\partial \bar{\rho}_i}{\partial \tilde{\rho}_e}, \tag{2.11}$$

which requires the gradients of the filters. For the regularization filter in Equation (2.6), it is

$$\frac{\partial \bar{\rho}_i}{\partial \tilde{\rho}_e} = \frac{w(x_i, x_e)v_e}{\sum_e w(x_i, x_e)v_e}. \tag{2.12}$$

The gradient of the non-volume preserving HPF in Equation (2.7) is

$$\frac{\partial \rho_i}{\partial \bar{\rho}_i} = \frac{\beta(\text{sech}(\beta(\bar{\rho}_i - \eta)))^2}{\tanh(\beta\eta) + \tanh(\beta(1-\eta))}, \tag{2.13}$$

while the gradient of the volume preserving HPF in Equation (2.8) is

$$\frac{\partial \rho_i}{\partial \bar{\rho}_i} = \begin{cases} \beta \exp(-\beta(1 - \bar{\rho}_e/\nu) + \exp(-\beta), & 0 \leq \bar{\rho}_e \leq \eta; \\ \beta \exp\left(-\beta \frac{\bar{\rho}_e - \nu}{1-\nu}\right) + \exp(-\beta), & \eta \leq \bar{\rho}_e \leq 1. \end{cases} \tag{2.14}$$

The Method of Moving Asymptotes (MMA) [14] is the gradient-based optimizer to update the design variables in TO problems. Unless specified otherwise, convergence is defined as when the largest change in the design variables between iterations is less than 0.01. An even distribution of material is always used to initialize the design variables.

2.4 Design Under Uncertainty

One of the motivations for this thesis is to account for the variability of material properties in TO and ensure consistency of the expected performance of the designs in practical applications where material uncertainties are inevitable.

To address the existence of uncertainties, two stochastic variants of TO have received considerable attention, namely, robust topology optimization (RTO) and reliability-based topology optimization (RBTO). Comprehensive reviews of these two frameworks are available [15, 16]. RTO incorporates uncertainties by changing the quantity of interest (QOI) in TO to a weighted sum of the mean and the standard deviation of the QOI [15, 17, 18]. This approach focuses on the central statistical moments of the QOI and improves the consistency of the performance of the structures under uncertainties. RBTO is concerned with optimization according to a fail-safe criterion, which is achieved by constraining the undesired behavior of the QOI to be less than a specified probability [15, 17, 19]. The RBTO approach focuses on the tail of the distribution of the QOI and hence controlling the likelihood that the designed structure exhibits extreme behaviors in the presence of randomness. Comparatively, the RTO framework is more intuitive to understand and implement for designers as it avoids analyses related to failure region, which is required in RBTO. Also, computing the failure criterion leads to an additional (costly) optimization problem [19, 20] and the result is very sensitive to the probabilistic model of the input uncertainty. In

practical problems where efficiency is paramount and knowledge of the uncertainty is typically limited, these are undesirable traits and hence, this thesis focuses on the RTO framework. Ultimately, both RTO and RBTO require manipulating the deterministic QOI into a function that involves some statistical measures [15, 18]. In this thesis, the QOI is the structural compliance. Stochastic TO necessitates the usage of compatible and efficient uncertainty quantification (UQ) schemes to propagate material uncertainties and estimate the statistics of QOI.

2.5 Representation of material uncertainty

Material properties and their variability are continuous in the design domain. A common practice is to model the spatial distribution of the stochastic material properties using a homogeneous random field [21, 22, 23]. A random field is an extension of a random variable, in the sense that every spatial point is a random variable with a mean and a variance. A correlation function is employed to describe the interdependency of pointwise variables at different spatial positions. For a homogeneous random field, the mean and the variance are further limited to constants across the spatial domain.

For a concrete example, consider a two dimensional Gaussian random field characterized by a uniform mean (μ), a uniform variance (σ^2), and a correlation function $C_H(\cdot,\cdot)$ [23, 24]. A valid $C_H(\cdot,\cdot)$ needs to be positive definite [24, 25] and in this thesis, the two-dimensional exponential correlation function is used:

$$C_H(\boldsymbol{x},\boldsymbol{x}') = \exp\left(-\frac{|x_1 - x_1'|}{l_1} - \frac{|x_2 - x_2'|}{l_2}\right), \tag{2.15}$$

where l_1 and l_2 are the axial correlation lengths, while $\boldsymbol{x} = [x_1, x_2]$ and $\boldsymbol{x}' = [x_1', x_2']$ are two arbitrary spatial positions. In practice, these parameters are influenced by the material choice and the manufacturing process, and are determined experimentally [2, 26, 27]. A physical interpretation of these parameters is that having a higher variance means an increase in the likelihood of having a local defect. When a defect is present, the longer the correlation lengths, the larger the defect area is likely to be. The covariance of the random field is defined as $\text{CoV} = \frac{\sigma}{\mu}$. In the numerical studies, the random fields are set with $\mu = 1$ and hence the square of CoV is the pointwise variance.

2.5.1 Karhunen–Loève Expansion

Due to the continuity of the random field in both the stochastic and spatial domains, it is difficult to employ this model directly in problems. Hence, the truncated Karhunen–Loève expansion (KLE) is typically applied to discretize the random field into a mathematically tractable form with finite stochastic dimensions [23, 24]. The KLE representation of a Gaussian random field, truncated to M terms, is given by a series sum:

$$\mathrm{E}_{\mathrm{gau}}(\boldsymbol{x}, \boldsymbol{\xi}) = \mu + \sigma^2 \sum_{m=1}^{M} \sqrt{\lambda_m} \phi_m(\boldsymbol{x}) \xi_m. \tag{2.16}$$

The ξ_m are independent random variables and follow the standard normal distribution. They are called the stochastic coordinates or randomness dimensions. The λ_m are real and positive scalar eigenvalues and the $\phi_m(\boldsymbol{x})$ are orthonormal functional eigenvectors that depend on the spatial position. These deterministic eigenpairs are obtained from solving a continuous eigenvalue problem (Fredholm integral equation of the second kind) using $C_H(\cdot, \cdot)$ as the kernel. For the exponential correlation function in Equation (2.15), the eigenpairs have closed form equations [23, 24].

The value of M depends on the desired accuracy of the representation of the random field variance, which is associated with the rate of decay of λ_m, which in turn is dictated by the correlation lengths. Weakly correlated random fields have short correlation lengths and need more truncation terms, while strongly correlated random fields are the opposite. As an example, the plot of the eigenvalues of a Gaussian random field over a domain of 100 by 50 units is shown in Figure 2.1(a) for the case of long correlation lengths, and Figure 2.1(b) for the case of short correlation lengths. For long correlation lengths, the first 10 modes have considerably higher values than the rest, while for short correlation lengths, the eigenvalues are significant up to a few hundred modes.

The desired accuracy of the random field representation, which guides the choice of M, is typically measured by the variance of the truncation error of the KLE at spatial points [28, 29]. For a Gaussian random field, let $\widehat{\mathrm{E}_{\mathrm{gau}}}(\boldsymbol{x})$ be the exact random field (in the limit $M \to \infty$). The variance of the difference between the truncated KLE and the exact random field at each spatial point is described by:

$$\mathrm{var}[\widehat{\mathrm{E}_{\mathrm{gau}}}(\boldsymbol{x}) - \mathrm{E}_{\mathrm{gau}}(\boldsymbol{x}, \boldsymbol{\xi})] = \sigma^2 \left(1 - \sum_{m=1}^{M} \lambda_m \phi_m(\boldsymbol{x})^2 \right). \tag{2.17}$$

Various error measures have been developed using this equation. This thesis employs

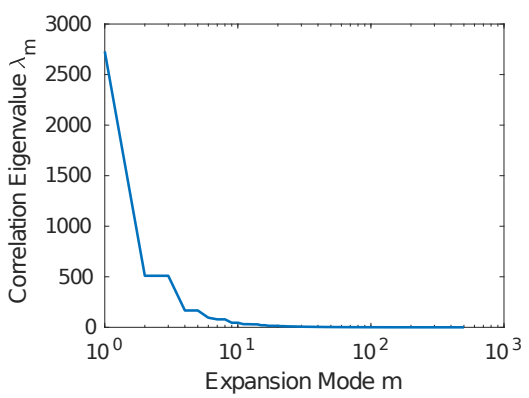

(a) Case of a long correlation length field with $l_x = 100$ and $l_y = 50$ units.

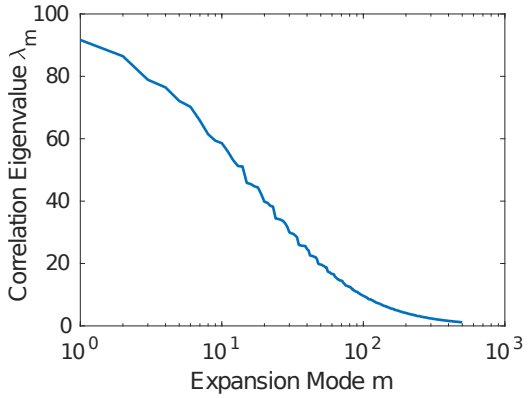

(b) Case of a short correlation length field with $l_x = 5$ and $l_y = 5$ units.

Figure 2.1 KLE eigenvalue decay for 2D Gaussian random fields on a 100 by 50 units spatial domain with various correlation lengths.

a global relative error measure from Sudret and Der Kiureghian [28]:

$$e_{\text{KLE}} = \frac{1}{\int_\Omega d\boldsymbol{x}} \int_\Omega \frac{\text{var}[\widehat{\text{E}_{\text{gau}}}(\boldsymbol{x}) - \text{E}_{\text{gau}}(\boldsymbol{x}, \boldsymbol{\xi})]}{\text{var}[\widehat{\text{E}_{\text{gau}}}(\boldsymbol{x})]} d\boldsymbol{x}, \tag{2.18}$$

where Ω is the spatial domain and $\int_\Omega d\boldsymbol{x}$ is the volume of the domain. To compute e_{KLE} for the case of a homogeneous random field and a domain discretized with finite elements, the integrand is approximated as piecewise continuous over each element, with the value taken at the centroids of the elements ($\boldsymbol{x}_c$), yielding:

$$e_{\text{KLE}} = \frac{1}{\int_\Omega d\boldsymbol{x}} \int_\Omega \left(1 - \sum_{m=1}^{M} \lambda_m \phi_m(\boldsymbol{x})^2\right) d\boldsymbol{x}, \tag{2.19}$$

$$e_{\text{KLE}} \approx \frac{1}{\sum_e \Omega_e} \sum_e \left(\left(1 - \sum_{m=1}^{M} \lambda_m \phi_m(\boldsymbol{x}_c)^2\right) \Omega_e\right), \tag{2.20}$$

where Ω_e is the volume of an element. From the definition of e_{KLE}, it is bounded between $[0, 1]$ and hence a percentage value is often applied to threshold e_{KLE}. A truncated KLE is deemed to be a sufficient approximation of the random field if the M truncation terms lead to e_{KLE} above the imposed threshold.

For physically admissible systems, the Gaussian random field is not always applicable. For instance, in the case of stochastic Young's modulus (E), it must be strictly positive at all spatial positions. This requires distributions with strictly positive support, such as the lognormal, gamma, or beta distributions. To obtain these

distributions from an underlying Gaussian process, additional transformations are employed. The truncated KLE representation of a lognormal random field is formulated using an exponential transformation [23]:

$$\mathrm{E}_{log}(\boldsymbol{x}, \boldsymbol{\xi}) = \exp\left(\mu + \sigma^2 \sum_{m=1}^{M} \sqrt{\lambda_m}\phi_m(\boldsymbol{x})\xi_m\right). \tag{2.21}$$

To incorporate the truncated KLE into FEM and TO framework, the midpoint approximation method is employed [23, 30], where the material random field is approximated as piecewise constant over each element, with the value at the centroid of the element. Hence, the truncated KLE representation of material properties at each element only depends on the stochastic variables, $\boldsymbol{\xi}$. The UQ schemes make use of the truncated KLE to parametrize the material uncertainties, which enables the estimation of the statistical quantities pertaining to the QOI.

2.6 Robust Topology Optimization Framework

With the material properties modeled as random fields, the compliance (c) is a scalar random variable, the nodal displacement vector ($\mathbf{u}$) is a stochastic field, and the stiffness matrix ($\mathbf{K}$) is a random matrix. RTO augments the QOI in TO into a weighted sum of the mean ($\mathbb{E}[\cdot]$) and standard deviation (Std[$\cdot$]) of QOI. For the compliance minimization problem with a volume constraint, the RTO counterpart is

$$\begin{aligned} \min_{\tilde{\boldsymbol{\rho}}} \quad & c_R(\tilde{\boldsymbol{\rho}}) = \mathbb{E}[c\,(\tilde{\boldsymbol{\rho}}, \boldsymbol{\xi})] + \kappa\,\mathrm{Std}\,[c(\tilde{\boldsymbol{\rho}}, \boldsymbol{\xi})]\,, \\ \text{s.t.} \quad & : \mathbf{K}(\tilde{\boldsymbol{\rho}}, \boldsymbol{\xi})\mathbf{u}(\tilde{\boldsymbol{\rho}}, \boldsymbol{\xi}) = \mathbf{F}, \\ & : 0 < \rho_{min} \leq \rho_e(\tilde{\boldsymbol{\rho}}) \leq 1 \quad \forall e, \\ & : \boldsymbol{\rho}(\tilde{\boldsymbol{\rho}})^T \boldsymbol{v} \leq V^*, \end{aligned} \tag{2.22}$$

where the weight κ dictates the trade-off between optimized average performance and expected variations due to uncertainty. The objective function, c_R, is the robust compliance, and the $\boldsymbol{\xi} = \{\xi_m\}_{m \leq M}$ is a vector containing the M stochastic coordinates from KLE. The stochastic equilibrium equation in the second line is satisfied almost-surely, meaning that the equality constraint holds for all realizations of $\boldsymbol{\xi}$.

An alternative RTO formulation is the minimum volume design with a robust

compliance constraint:

$$\begin{aligned} \min_{\tilde{\boldsymbol{\rho}}} \quad & \boldsymbol{\rho}(\tilde{\boldsymbol{\rho}})^T \boldsymbol{v}, \\ \text{s.t.} \quad & : \mathbf{K}(\tilde{\boldsymbol{\rho}}, \boldsymbol{\xi})\mathbf{u}(\tilde{\boldsymbol{\rho}}, \boldsymbol{\xi}) = \mathbf{F}, \\ & : 0 < \rho_{min} \leq \rho_e(\tilde{\boldsymbol{\rho}}) \leq 1 \quad \forall e, \\ & : \mathbb{E}[c\left(\tilde{\boldsymbol{\rho}}, \boldsymbol{\xi}\right)] + \kappa \operatorname{Std}\left[c(\tilde{\boldsymbol{\rho}}, \boldsymbol{\xi})\right] \leq c_{\max}. \end{aligned} \tag{2.23}$$

The total volume, or equivalently, the volume fraction, is used as the objective function, while $c_{\max}$ is the maximum allowable robust compliance.

For SIMP-based RTO frameworks, estimations of the robust complance and its gradient with respect to density are required. Hence, the UQ schemes employed need to be compatible with gradient-based optimizers. The general expression of the sensitivities of c_R with respect to $\tilde{\boldsymbol{\rho}}$:

$$\frac{\partial c_R}{\partial \tilde{\rho}_e} = \frac{\partial \mathbb{E}[c]}{\partial \tilde{\rho}_e} + \kappa \frac{\partial \mathrm{Std}[c]}{\partial \tilde{\rho}_e}. \tag{2.24}$$

The detailed formulae for the statistical measures and their gradients vary depending on the applied UQ schemes.

2.7 Robust Topology Optimization Algorithms

This section discusses existing gradient-based RTO algorithms that target material or geometric uncertainties. The algorithms are classified based on their characteristics. The practical motivation of this thesis is to incorporate uncertainties from additive manufacturing, which can be modeled using random fields with very short correlation lengths according to experimental observations [2, 27]. The truncated KLE representations of these random fields have high stochastic dimensions and hence this section also discusses the applicability of existing RTO algorithms for high input dimensions.

The two key ingredients in a gradient-based RTO algorithm for solving the problems defined in Equations (2.22) and (2.23) are an uncertainty quantification (UQ) scheme for computing the statistics of the QOI (c_R), as well as a design update scheme for computing the gradients of statistics (Equation (2.24)) and updating the design variables. Two popular types of approaches address these ingredients. One type focuses on efficient and high-quality design updates by employing the stochastic gradient descent (SGD) algorithm [31, 32, 33, 34, 35]. A sampling-based UQ scheme, such as Monte Carlo, is used to compute the statistics of QOI and sample-wise gra-

dients. These approaches require the sample sets at each iteration to have a small size for cost reduction and a sufficient level of independence from sample sets of other iterations. This leads to a coarse estimation of the statistics and noisy gradients, but the application of the SGD optimizer (also known as the Robbins-Monro algorithm [36]) or its variants ensures sufficient optimality of the design. The other type focuses on efficient and reliable UQ schemes. For estimating the statistics, these approaches require the UQ scheme to use either the same sample set every iteration or an analytical formula. Hence, the stochastic optimization becomes a deterministic problem at each iteration and any gradient-based optimizers can be employed. The procedure for computing the gradients varies depending on the UQ scheme and having an accurate estimation of statistics leads to good quality of gradients. In this thesis, the second type of approaches are of particular interest, since they are more versatile and stable [37].

Amongst the second type of approaches, the most popular class of approaches employ sampling-based UQ schemes [22, 25, 38]. These RTO approaches require a set of compliance samples per iteration, and the statistics of the compliance as well as their gradients are computed using a weighted aggregation of the sample-wise results. The most well-developed is Monte Carlo-based RTO (MCTO) [25, 38]. The advantage of Monte Carlo (MC) is that the random sampling process employed is independent of the complexity of the uncertainties and therefore tractable in high stochastic dimensions and for uncertainties that are difficult to parameterize. However, the accuracy of Monte Carlo converges slowly with the number of samples. Hence, the downside of MCTO is the significant computational cost incurred due to solving a large number of FE problems associated with a large number of samples. MCTO is generally considered as the benchmarking algorithm, while other approaches try to improve efficiency while maintaining sufficient accuracy. To this end, the stochastic collocation (SC)-based RTO approach [22, 39] is another popular sampling-based scheme. The sampling process in the SC UQ is guided by multivariate quadrature algorithms according to the distribution of the random variables. For a small number of random dimensions, SC is more efficient than MC since fewer samples and FE solves are required to achieve high accuracy. However, for high dimensional problems, the number of samples required by SC increases drastically (factorial scaling with sparse-grid [40]), hence making it less efficient than MC. The main computational bottleneck for sampling-based RTO is the large number of FE solutions required. To alleviate this issue, one strategy is to replace each FE solution with a cheaper approximation. For instance, Amir et al. [41] employ the reanalysis technique to accelerate the MC,

while Keshavarzzadeh et al. [42] use coarse mesh approximation alongside a neural network mapping to accelerate SC. Another strategy is to use additional samples from other models that are cheaper but coarser compared to the FEM. The multi-resolution sampling process, such as multi-level MC [43] and multi-fidelity MC [44], helps to ensure accuracy while reducing cost.

Another class of RTO approaches employs the perturbation-based UQ scheme. The principle is to approximate the QOI with a Taylor series in the stochastic space and hence the statistics of the QOI are only dependent on the joint statistics of the input random variables. Consequently, the statistics and their gradients admit closed-form expressions, which are extremely efficient to compute. RTO algorithms based on perturbation of the compliance [45], the displacement vector [46], and the FE stiffness matrix [47, 48, 49] have all been investigated in the literature. Note that the perturbation of the stiffness matrix is equivalent to the approximate matrix inversion technique for solving a linear system. In general, the cost of perturbation approaches consists of factorizing and storing one stiffness matrix, which is then used to solve a set of linear systems. The number of linear systems scales linearly or quadratically with the stochastic dimension, corresponding to the 1st and 2nd-order Taylor series, respectively. Hence, perturbation-based approaches scale well for high dimensional problems. The fundamental limitations of these approaches are that they are only applicable for low variance in the input variables and they necessitate storage of a factorized stiffness matrix, which may not be possible for ill-conditioned or large-scale problems. The other downside of these approaches is that the joint statistics and gradients for all permutations of input random variables are required. The complexity and cost for this is significant for high stochastic dimensions. To alleviate this, finite difference schemes have been investigated to approximate the joint statistical gradient [50, 51] and random variable decorrelation schemes have been employed to decrease the number of joint statistics [52, 53].

The class of RTO approaches based on functional decomposition UQ schemes is also popular. These approaches approximate the QOI with a basis of functions in the stochastic space. Obtaining the basis coefficients generally requires a projection procedure and once they are known, the statistics of QOI and their gradients are computed analytically. From a many-query perspective, these approaches are as efficient as the perturbation-based approaches and can also handle high variances in input uncertainties. Polynomial chaos (PC)-based RTO [10, 21, 54] belongs to this class, where the functional basis is composed of orthogonal polynomials. However, the cardinality of the basis of PC increases drastically (exponentially or factorial) with the

stochastic dimension. Consequently, the cost of the projection procedure also rapidly increases, making it less efficient than MC for high dimensional problems. Hence, other decomposition UQ schemes have been investigated for RTO applications, such as the univariate and bivariate dimension reduction [55, 56, 57, 58], and anchored ANOVA [59]. These UQ schemes employ a basis that has a lower order compared to the PC basis and hence the cardinality of the basis and the number of FE solves required for the projection procedure scales polynomially with the stochastic dimensions. These schemes in theory are reliable for high dimensions, provided that the QOI does not exhibit strong nonlinear behaviors.

Some recent RTO approaches employ statistical transformations to approximate the distribution or central moments of the compliance using closed form expressions. Examples are, using the matrix variate distribution scheme [3] or employing the linear transformation properties of Gaussian variables [60].

Ultimately, for RTO approaches applicable to material uncertainties, given a high dimensional stochastic space, not many are more efficient than MCTO while being sufficiently reliable in the estimation of statistics. Also, most of the approaches depend on the existence of a parametric model for the uncertainties, which may not be available, such as a random field with correlation lengths of zero (white noise). Numerical cases for RTO with high dimensional inputs are very sparse in the literature. Hence, further investigations in this direction are required.

As the MCTO approach is extensively studied, it is considered as the benchmark algorithm to provide comparison bases for other, novel, RTO algorithms in this thesis. Regarding implementation, sampling-based (MC) UQ schemes are task-parallel in the sample dimension. This is because the sample-wise computations are independent of each other and no communication is required between these processes. Hence, parallel computing techniques should be employed whenever possible to achieve higher computational speed. In MATLAB, a task parallel `for` loop is implemented using the `parfor` command. More advanced optimization of parallel implementation depends on the computing language used, the available computing resource, and architecture. Detailed discussions and algorithm designs regarding these aspects are much more involved and thus are outside the scope of this thesis.

Chapter 3

Neumann Expansion Robust Topology Optimization

This chapter describes a robust topology optimization (RTO) algorithm based on the Neumann expansion (NE) uncertainty quantification (UQ) scheme. The objective of this thesis is to develop RTO algorithms that efficiently handle high dimensional or multi-source material uncertainties. RTO has an inner UQ module for estimating the statistic of interest and an outer module for updating design variables using a gradient-based optimizer. The statistic of interest is the robust compliance, c_R, which is a weighted sum of the mean and standard deviation of the compliance. The UQ module is required to estimate c_R reliably and accurately, which ensures sufficient quality of the gradients.

The standard UQ approach for handling high dimensional uncertainties is the Monte Carlo (MC) scheme, which requires many samples of compliance for each iteration to achieve accurate c_R. Since computing each sample corresponds to solving a finite element (FE) problem, if n_s compliance samples are needed, this requires n_s linear solves for each iteration, which is very costly. For design updates, MC-based RTO (MCTO) requires solving n_s adjoint problems. Since a compliance objective produces a self-adjoint system, computing the gradients for all samples leads to $n_s n_e$ vector-matrix-vector products between element-wise stiffness matrices and element-wise displacements, totalling $O(n_s n_e n_u^2)$ computational cost, where n_e is the number of elements and n_u is the size of an element displacement vector.

The proposed NE UQ provides an efficient alternative for estimating c_R. The principle is to employ an approximate perturbation model of the FE stiffness matrix and compute the perturbation coefficients using a sampling procedure, such as MC. In terms of cost for each iteration, if n_s samples are used for computing the coefficients,

then estimating c_R requires one linear solve and $O(n_s n_f)$ scalar arithmetic, where n_f is the number of free degrees of freedom in the FE. The NE UQ is compatible with gradient optimization, leading to the NE-based RTO (NETO) algorithm. The design update of NETO requires computing the gradient of one compliance sample at a cost of $O(n_e n_u^2)$, and $O(n_s n_e n_u)$ scalar arithmetic operations without the need to access element-wise operators. Hence, cost reduction compared to MC is achieved. In addition, the proposed NE UQ does not necessitate parametric models of the input uncertainties and it can handle multi-source material uncertainty. The computational complexity also does not have explicit dependency on the input stochastic dimension and hence it does not suffer from the curse of dimensionality. The main disadvantage of NE is the decrease in accuracy of the estimation of c_R compared to MC. However, numerical cases show that this inaccuracy is not detrimental to the quality of the designs, as structures generated from NETO and MCTO achieve similar optimality.

The sections in this chapter are organized as follows: Section 3.1 provides a summary of NE in stochastic mechanics and the concept of the approximate matrix inversion, which allow the random compliance to be represented using a series. The algorithm of NETO is presented in Section 3.2. The ingredients required by NETO include a UQ procedure for estimating the c_R, expressions for computing the design gradients, and a parameter storage method to enable efficient statistics and gradient computations for each iteration. The NE UQ scheme is developed in Section 3.3, where the expression for the c_R is provided. A novel dimension reduction approach is employed, which enables the NE UQ to be efficient under high stochastic dimensions. The equations for the gradient of c_R with respect to the design variables are developed in Section 3.4. The equations of c_R and its gradient require statistics of matrix variables, which are computed using a sampling-based approach. However, repeating the sampling procedure every iteration is very inefficient and hence a novel storage method is developed in Section 3.4.1, which decomposes the matrix variables as products between stochastic components and deterministic scaling from the design variables. The sample-wise stochastic components are computed and stored before optimization, and the scaling components are updated with changes in the design variables. The products of these two components only require scalar arithmetic each iteration and hence the samples of matrix variables are updated efficiently, which enables the equations for c_R and its gradient to be computed with low cost. In Section 3.6, 2D numerical cases are presented to demonstrate the efficacy of the NETO in comparison with the MCTO. The chapter is concluded by Section 3.7.

3.1 Background

NE is based on decomposing a stochastic variable into sum of its mean and random perturbations, then approximating the inverse of this sum with a perturbed series, enabling the computation of output quantities of interest. NE is well-established in stochastic finite element analysis [23, 61, 62, 63], where the stiffness matrix $\mathbf{K}$ is random. The stochastic $\mathbf{K}$ is $\mathbf{K} = \bar{\mathbf{K}} + \Delta\mathbf{K}$, where $\bar{\mathbf{K}}$ is the mean stiffness matrix while $\Delta\mathbf{K}$ is the stochastic perturbation matrix. Since the output displacement field and the compliance require the inverse of $\mathbf{K}$, the perturbed representation is inverted using the approximate matrix inversion method [64, 65], which represents the inverse stiffness matrix as a binomial series:

$$\mathbf{K}^{-1} = \left(\bar{\mathbf{K}}\left(\mathbf{I} - \bar{\mathbf{K}}^{-1}\Delta\mathbf{K}\right)\right)^{-1} = \left(\sum_{i=0}^{\infty}(-1)^i\left(\bar{\mathbf{K}}^{-1}\Delta\mathbf{K}\right)^i\right)\bar{\mathbf{K}}^{-1}. \tag{3.1}$$

A sufficient condition for the convergence of the series in Equation (3.1) is $\|\bar{\mathbf{K}}^{-1}\Delta\mathbf{K}\|_{\mathrm{F}} < 1$, where $\|\cdot\|_F$ is the Frobenius matrix norm [30, 61, 66, 67, 68]. A stronger condition is that the spectral radius of $\bar{\mathbf{K}}^{-1}\Delta\mathbf{K}$ is less than one. The series expansion for the stochastic displacement field ($\mathbf{u}$) given a deterministic forcing ($\mathbf{F}$) is:

$$\mathbf{u} = \left(\sum_{i=0}^{\infty}(-1)^i\left(\bar{\mathbf{K}}^{-1}\Delta\mathbf{K}\right)^i\right)\bar{\mathbf{K}}^{-1}\mathbf{F}. \tag{3.2}$$

The expansion of the random compliance is:

$$\begin{aligned} c = \; & \mathbf{F}^T\bar{\mathbf{K}}^{-1}\mathbf{F} - \mathbf{F}^T\bar{\mathbf{K}}^{-1}\Delta\mathbf{K}\bar{\mathbf{K}}^{-1}\mathbf{F} + \mathbf{F}^T\bar{\mathbf{K}}^{-1}\Delta\mathbf{K}\bar{\mathbf{K}}^{-1}\Delta\mathbf{K}\bar{\mathbf{K}}^{-1}\mathbf{F} \\ & - \mathbf{F}^T\bar{\mathbf{K}}^{-1}\Delta\mathbf{K}\bar{\mathbf{K}}^{-1}\Delta\mathbf{K}\bar{\mathbf{K}}^{-1}\Delta\mathbf{K}\bar{\mathbf{K}}^{-1}\mathbf{F} + \dots \end{aligned} \tag{3.3}$$

For small variance in the randomness of $\mathbf{K}$ (for example, the input material random field has a covariance ratio $\mathrm{CoV} = \frac{\sigma}{\mu} < 0.15$ [52, 62]), the higher order terms are negligible. In addition, having many expansion terms leads to computational inefficiency. Hence, the series representation in Equation (3.3) is typically truncated to the first few terms. The order of the series is conventionally used to represent the number of terms retained. Keeping N expansion terms is denoted as the $(N-1)$th order NE.

3.2 Neumann Expansion RTO Algorithm

The Neumann expansion-based RTO, denoted as NETO, is presented in Algorithm 1. The first phase of NETO describes the novel storage scheme developed in Section 3.4.1,

which stores the sample-wise matrix variables used to computed their statistics required in every iteration of RTO. These matrix variables are highlighted in red in Equations (3.4) and (3.20). The second phase of NETO describes the procedure of RTO, where each iteration requires computing the statistics of the matrix variables using the stored samples and the updated design variables. These statistics are employed to estimate the c_R and its gradient with respect to the design variables using the NE UQ scheme, which are developed in Section 3.3 and 3.4. As mentioned in Section 3.1, the series representation of the random compliance is truncated to qth order in practice. Henceforth, "NETO qth order" denotes the application of the qth order NE UQ scheme to RTO.

Algorithm 3: NETO

Phase 1: *Sample-wise Variable Extraction and Vectorized Storage*

Input: Sample set of $\{\boldsymbol{\xi}_m, w_m\}_{1\leq m\leq n_s}$.
for $m = 1 : n_s$ **do**
for (each (i, j) entry of $\mathbf{K}_{ij}$) **do**
$\rightarrow$ $\forall k \in N_{ij}$ and $\boldsymbol{\xi}_m$, compute $E_k(\boldsymbol{\xi}_m)a_k(\boldsymbol{\xi}_m)$
$\rightarrow$ $\forall k', \hat{k} \in N_{ij}$ and $\boldsymbol{\xi}_m$, assemble $E_{k'}(\boldsymbol{\xi}_m)E_{\hat{k}}(\boldsymbol{\xi}_m)a_{k'}(\boldsymbol{\xi}_m)a_{\hat{k}}(\boldsymbol{\xi}_m) \leftarrow (i, j) \leftarrow (ele\, k', ele\, \hat{k})$
end for
end for
$\rightarrow$ Assemble $\mathbb{E}[E_k a_k] \leftarrow (i, j) \leftarrow (ele\, k)$

Phase 2: *Gradient Based Robust Topology Optimization*

Input: Determine the truncation order for NE, and the $\mathbb{E}[\alpha^q]$ and $\mathbb{E}\left[\alpha^q \frac{\partial \alpha}{\partial \rho_e}\right]$
Input: Initialize $\tilde{\boldsymbol{\rho}}$
while $\|\tilde{\boldsymbol{\rho}}_{iter} - \tilde{\boldsymbol{\rho}}_{iter-1}\|_\infty > 0.01$ **do**
$\rightarrow$ Filter $\tilde{\boldsymbol{\rho}}_{iter}$ to $\boldsymbol{\rho}_{iter}$ via Equation (2.6) and (2.7)
$\rightarrow$ Compute $\rho_k^p \mathbb{E}[E_k a_k]$ and $\rho_k^{p-1} \mathbb{E}[E_k a_k]$
for $m = 1 : n_s$ **do**
$\rightarrow$ Compute the product between $E_{k'}(\boldsymbol{\xi}_m)E_{\hat{k}}(\boldsymbol{\xi}_m)a_{k'}(\boldsymbol{\xi}_m)a_{\hat{k}}(\boldsymbol{\xi}_m)$ and $\rho_{k'}^p \rho_k^p$ or $p\rho_{k'}^{p-1}\rho_k^p$ using $(i, j) \leftrightarrow (ele\, k', ele\, \hat{k})$ mapping
$\rightarrow$ Compute for sample m: $\alpha(\boldsymbol{\xi}_m)$ and $\frac{\partial \alpha(\boldsymbol{\xi}_m)}{\partial \rho_e}$
end for
$\rightarrow$ Aggregate sample results, compute all required $\mathbb{E}[\alpha^q]$ and $\mathbb{E}\left[\alpha^q \frac{\partial \alpha}{\partial \rho_e}\right]$
$\rightarrow$ compute c_R and its sensitivities
$\rightarrow$ update to $\tilde{\boldsymbol{\rho}}_{iter+1}$ using MMA
end while

3.3 Uncertainty Quantification Scheme

3.3.1 Parameter Selection

NE is similar to perturbation approaches where the Taylor series is applied to the stiffness matrix [47, 48, 49]. Hence, many formulations of the perturbation matrix ($\Delta\mathbf{K}$) are proposed in literature [61, 68]. The majority construct $\Delta\mathbf{K}$ from a linear combination of deterministic matrices scaled by a stochastic function that depends on one or more random variables from the random field surrogate, such as the variables ($\boldsymbol{\xi}$) in the Karhunen–Loève expansion (KLE). However, such approaches suffer from a significant increase in computational complexity with increasing stochastic dimensions. To circumvent this issue, a new approximation for the perturbation matrix is:

$$\Delta\mathbf{K} \approx \alpha\bar{\mathbf{K}}; \quad \alpha = \frac{\mathrm{Tr}\left(\bar{\mathbf{K}}^2\right) - \mathrm{Tr}\left(\mathbf{K}^2\right)}{2\mathrm{Tr}\left(\bar{\mathbf{K}}^2\right)}. \tag{3.4}$$

Note that α is a positive scalar random variable, with $\mathrm{Tr}(\cdot)$ the trace operator. The perturbation matrix is an approximation of the exact $\Delta\mathbf{K}$. This approximation is a dimension reduction approach, where various material uncertainties in the system are amalgamated. Hence, regardless of the complexity of the underlying uncertainties, the formulation of the random matrix perturbation is the same, leading to consistent computational complexity. This approximation is specifically intended for computing the statistical values of the stochastic compliance.

The main requirement for the applicability of NE is that $\Delta\mathbf{K}$ satisfies the convergence criterion. For the approximation in Equation (3.4), this corresponds to $\alpha < 1$. It is possible to rescale the perturbation component such that for any realizations of $\mathbf{K}$, convergence is guaranteed [61]. However, such an adjustment is not applied in this thesis. In practical applications, the material uncertainties are typically modeled using physically plausible positive-definite distributions (lognormal, beta, and uniform distributions), and the variations of $\mathbf{K}$ are typically not significant enough to violate the $\alpha < 1$ condition. With this approximate perturbation, the NE of the compliance is:

$$c \approx \left(1 - \alpha + \alpha^2 - \alpha^3 + \alpha^4 - \dots\right) \mathbf{F}^T \bar{\mathbf{K}}^{-1} \mathbf{F} \tag{3.5}$$

The sum in the bracket is truncated according to the required accuracy.

3.3.2 Computation of Statistics

As the random compliance is represented with a truncated series, statistical operators such as the statistical moments are applied to the expression. Hence, the mean is:

$$\mathbb{E}[c] \approx \mathbb{E}\big[(1-\alpha+\alpha^2-\alpha^3+\alpha^4-\dots)\big]\mathbf{F}^T\bar{\mathbf{K}}^{-1}\mathbf{F}. \tag{3.6}$$

Truncating to first order leads to:

$$\mathbb{E}[c] \approx (1-\mathbb{E}[\alpha])\,\mathbf{F}^T\bar{\mathbf{K}}^{-1}\mathbf{F}. \tag{3.7}$$

The second order approximation of the mean is:

$$\mathbb{E}[c] \approx \big(1-\mathbb{E}[\alpha]+\mathbb{E}\big[\alpha^2\big]\big)\,\mathbf{F}^T\bar{\mathbf{K}}^{-1}\mathbf{F}. \tag{3.8}$$

RTO also requires the standard deviation, which necessitates the second statistical moment of the compliance, where the general expansion is:

$$\mathbb{E}\big[c^2\big] \approx \mathbb{E}\big[(1-\alpha+\alpha^2-\alpha^3+\alpha^4-\dots)^2\big](\mathbf{F}^T\bar{\mathbf{K}}^{-1}\mathbf{F})^2. \tag{3.9}$$

The first and second order truncated approximation of the second moment are:

$$\mathbb{E}\big[c^2\big] \approx \big(1+\mathbb{E}\big[\alpha^2\big]-2\mathbb{E}[\alpha]\big)\,(\mathbf{F}^T\bar{\mathbf{K}}^{-1}\mathbf{F})^2, \tag{3.10}$$

and

$$\mathbb{E}\big[c^2\big] \approx \big(1+\mathbb{E}\big[\alpha^4\big]-2\mathbb{E}\big[\alpha^3\big]+3\mathbb{E}\big[\alpha^2\big]-2\mathbb{E}[\alpha]\big)\,(\mathbf{F}^T\bar{\mathbf{K}}^{-1}\mathbf{F})^2. \tag{3.11}$$

As a consequence:

$$\mathrm{Std}[c] = \sqrt{\mathbb{E}[c^2]-\mathbb{E}[c]^2}. \tag{3.12}$$

Hence, the values required to calculate the robust compliance are available, although the exact expression depends on the order of truncation applied.

3.4 Statistical Gradients

The optimization algorithm is gradient-based, requiring the sensitivities of the robust compliance (c_R), which are the gradients of the statistical moments with respect to the physical densities. Define ρ_e as the element density for the eth element, $\boldsymbol{\rho}$ as the vector of element densities, and a nominal compliance and its derivatives with respect

to the physical density of an element as:

$$c_0 = \mathbf{F}^T \bar{\mathbf{K}}^{-1} \mathbf{F}, \text{and } \frac{\partial c_0}{\partial \rho_e} = -\mathbf{F}^T \bar{\mathbf{K}}^{-1} \frac{\partial \bar{\mathbf{K}}}{\partial \rho_e} \bar{\mathbf{K}}^{-1} \mathbf{F}. \tag{3.13}$$

Using the linearity of the expected value and the differentiation operators, the sensitivity of the first statistical moment of compliance with respect to the density of an element are:

$$\frac{\partial \mathbb{E}[c]}{\partial \rho_e} \approx \mathbb{E}[(1 - \alpha + \alpha^2 - \alpha^3 + \alpha^4 - \dots)] \frac{\partial c_0}{\partial \rho_e} + \mathbb{E}\left[\left(-\frac{\partial \alpha}{\partial \rho_e} + \frac{\partial \alpha^2}{\partial \rho_e} - \frac{\partial \alpha^3}{\partial \rho_e} + \frac{\partial \alpha^4}{\partial \rho_e} - \dots\right)\right] c_0. \tag{3.14}$$

Truncating to first and second order leads to the approximations:

$$\frac{\partial \mathbb{E}[c]}{\partial \rho_e} \approx (1 - \mathbb{E}[\alpha]) \frac{\partial c_0}{\partial \rho_e} + \left(-\frac{\partial \mathbb{E}[\alpha]}{\partial \rho_e}\right) c_0, \tag{3.15}$$

and

$$\frac{\partial \mathbb{E}[c]}{\partial \rho_e} \approx \left(1 - \mathbb{E}[\alpha] + \mathbb{E}\left[\alpha^2\right]\right) \frac{\partial c_0}{\partial \rho_e} + \left(-\frac{\partial \mathbb{E}[\alpha]}{\partial \rho_e} + \mathbb{E}\left[2\alpha \frac{\partial \alpha}{\partial \rho_e}\right]\right) c_0. \tag{3.16}$$

The sensitivity of the second statistical moment of compliance with respect to the density of an element are:

$$\frac{\partial \mathbb{E}\left[c^2\right]}{\partial \rho_e} \approx \mathbb{E}[(1 - \alpha + \alpha^2 - \alpha^3 + \alpha^4 - \dots)^2] 2c_0 \frac{\partial c_0}{\partial \rho_e} + \frac{\partial \mathbb{E}\left[(1-\alpha+\alpha^2-\alpha^3+\alpha^4-\dots)^2\right]}{\partial \rho_e} c_0^2. \tag{3.17}$$

Approximating by truncation to first order leads to:

$$\frac{\partial \mathbb{E}[c^2]}{\partial \rho_e} \approx \left(1 + \mathbb{E}\left[\alpha^2\right] - 2\mathbb{E}[\alpha]\right) 2c_0 \frac{\partial c_0}{\partial \rho_e} + \left(\mathbb{E}\left[2\alpha \frac{\partial \alpha}{\partial \rho_e}\right] - \mathbb{E}\left[2 \frac{\partial \alpha}{\partial \rho_e}\right]\right) c_0^2, \tag{3.18}$$

while truncation to second order results in:

$$\begin{aligned} \frac{\partial \mathbb{E}[c^2]}{\partial \rho_e} \approx\ & \left(1 + \mathbb{E}\left[\alpha^4\right] - 2\mathbb{E}\left[\alpha^3\right] + 3\mathbb{E}\left[\alpha^2\right] - 2\mathbb{E}[\alpha]\right) 2c_0 \frac{\partial c_0}{\partial \rho_e} \\ & + \left(\mathbb{E}\left[4\alpha^3 \frac{\partial \alpha}{\partial \rho_e}\right] - \mathbb{E}\left[6\alpha^2 \frac{\partial \alpha}{\partial \rho_e}\right] + \mathbb{E}\left[6\alpha \frac{\partial \alpha}{\partial \rho_e}\right] - \mathbb{E}\left[2 \frac{\partial \alpha}{\partial \rho_e}\right]\right) c_0^2. \end{aligned} \tag{3.19}$$

Given α defined in Equation (3.4), its expected value and sensitivity with respect to the density of an element are:

$$\mathbb{E}[\alpha] = \frac{1}{2}\left(1 - \frac{\mathbb{E}[\mathrm{Tr}\,(\mathbf{K}^2)]}{\mathrm{Tr}\,(\bar{\mathbf{K}}^2)}\right), \text{and } \frac{\partial \alpha}{\partial \rho_e} = -\frac{\mathrm{Tr}\left(\mathbf{K} \frac{\partial \mathbf{K}}{\partial \rho_e}\right)}{\mathrm{Tr}\left(\bar{\mathbf{K}}^2\right)} + \frac{\mathrm{Tr}\left(\bar{\mathbf{K}} \frac{\partial \bar{\mathbf{K}}}{\partial \rho_e}\right) \mathrm{Tr}\left(\mathbf{K}^2\right)}{\left(\mathrm{Tr}\left(\bar{\mathbf{K}}^2\right)\right)^2}. \tag{3.20}$$

The sensitivities of the standard deviation of the compliance with respect to the density of an element are:

$$\frac{\partial \mathrm{Std}[c]}{\partial \rho_e} = \frac{1}{2}(\mathbb{E}\left[c^2\right] - \mathbb{E}[c]^2)^{-\frac{1}{2}} \left(\frac{\partial \mathbb{E}[c^2]}{\partial \rho_e} - 2\mathbb{E}[c] \frac{\partial \mathbb{E}[c]}{\partial \rho_e} \right). \tag{3.21}$$

Computing these for all of the elements in $\boldsymbol{\rho}$ leads to the full set of sensitivities.

3.4.1 Parameter Storage and Update Scheme

In general, the statistical moments and sensitivities of the compliance approximated by NE necessitates the computation of the expressions $\mathbb{E}[\alpha^q]$ and $\mathbb{E}\left[\alpha^q \frac{\partial \alpha}{\partial \rho_e}\right]$, with q a positive integer or zero. The definitions of α in Equation (3.4) and $\frac{\partial \alpha}{\partial \rho_e}$ in Equation (3.20) indicate that statistics of matrix variables associated with $\mathbf{K}$ are required. These matrix variables are highlighted in red in Equations (3.4) and (3.20), and their statistics are computed with sampling methods. However, as the element densities $\boldsymbol{\rho}$ change each iteration, the stiffness matrices require reconstruction and hence the inefficient repetition of the sampling process every iteration. A new storage scheme is developed to enable the efficient update of the samples of these matrix variables in each optimization iteration.

The storage scheme must enable efficient updates for the samples of all matrix variables required in the expressions of α and $\frac{\partial \alpha}{\partial \rho_e}$. For α, $\mathrm{Tr}\left(\mathbf{K}^2\right)$ and $\mathrm{Tr}\left(\bar{\mathbf{K}}^2\right)$ are the key variables. For $\frac{\partial \alpha}{\partial \rho_e}$, $\mathrm{Tr}\left(\bar{\mathbf{K}} \frac{\partial \bar{\mathbf{K}}}{\partial \rho_e}\right)$ and $\mathrm{Tr}\left(\mathbf{K} \frac{\partial \mathbf{K}}{\partial \rho_e}\right)$ are the additional key variables. Have sample-wise realizations of these variables enable expected values of their products to be computed, for example, $\mathbb{E}\left[\mathrm{Tr}\left(\mathbf{K}^2\right) \mathrm{Tr}\left(\bar{\mathbf{K}} \frac{\partial \bar{\mathbf{K}}}{\partial \rho_e}\right)\right]$. The number of matrix variables does not depend on the order of the NE.

In RTO based on the Solid Isotropic Material with Penalization (SIMP) scheme, each entry in $\mathbf{K}$ contains contributions from the adjacent elements in the form of a product between the element stiffness matrix with unit modulus scaled by $E_e {\rho_e}^p$. Consider the assembly of the (i,j)th entry of $\mathbf{K}$, where the contributing elements are denoted by the set $[N_{ij}]$. Each element has a contribution of $(\rho_k)^p a_k E_k$ for $k \in [N_{ij}]$, where ρ_k^p is the element density with SIMP scaling, E_k is the element Young's modulus, and a_k is a constant scalar from the unit modulus elastic matrix, $\mathbf{D}_0$. The expression for a_k depends on the entries to which it corresponds in $\mathbf{D}_0$. The assembly of $\mathbf{K}_{ij}$ is given by $\mathbf{K}_{ij} = \sum_{k \in [N_{ij}]} (\rho_k)^p a_k E_k$. With material uncertainties, E_k and possibly a_k (if the Poisson's ratio is stochastic) are random variables. In this thesis, ρ_k is considered deterministic. Hence, the random quantities are independent of the design variables

and remain unchanged throughout the optimization. The element densities are the only variables that change through the optimization iterations. To keep track of the individual element contributions, the stochastic and deterministic components are stored separately, while their coupling is maintained through a mapping procedure.

Assuming that a set of realizations of the material uncertainties is given, and samples of E_k and a_k are made available through sampling or experimental data. The sample-wise value of $\mathrm{Tr}\big(\mathbf{K}^2\big)$ is:

$$\begin{aligned}\mathrm{Tr}\big(\mathbf{K}^2\big) &= \sum_{j=1}^{n}\sum_{i=1}^{n}(\mathbf{K}_{ij})^2 = \sum_{j=1}^{n}\sum_{i=1}^{n}\left(\sum_{k\in[N_{ij}]}(\rho_k)^p a_k E_k\right)^2, \\ &= \sum_{j=1}^{n}\sum_{i=1}^{n}\left(\sum_{k'\in[N_{ij}]}\sum_{\hat{k}\in[N_{ij}]}(\rho_{k'})^p(\rho_{\hat{k}})^p(a_{k'}a_{\hat{k}})(E_{k'}E_{\hat{k}})\right),\end{aligned} \tag{3.22}$$

where k' and $\hat{k}$ are dummy indices. Similarly, the sample-wise $\mathrm{Tr}\left(\mathbf{K}\frac{\partial\mathbf{K}}{\partial\rho_e}\right)$ is:

$$\mathrm{Tr}\left(\mathbf{K}\frac{\partial\mathbf{K}}{\partial\rho_e}\right) = \sum_{j=1}^{n}\sum_{i=1}^{n}\left(\sum_{k'\in[N_{ij}]}\sum_{\hat{k}\in[N_{ij}]\cap e}2p((\rho_{k'})^p(\rho_{\hat{k}})^{p-1})(a_{k'}a_{\hat{k}})(E_{k'}E_{\hat{k}})\right). \tag{3.23}$$

Note that $k'\in[N_{ij}]\cap e$ denotes the intersection between element e and the set $[N_{ij}]$. The sample-wise formulae for all the other variables are similar to Equations (3.22) and (3.23). The only adjustment required is changing a_kE_k to $\mathbb{E}[a_kE_k]$ when $\bar{\mathbf{K}}$ or $\frac{\partial\bar{\mathbf{K}}}{\partial\rho_e}$ appears in the trace operator.

In practical implementation, storage for the $(a_{k'}a_{\hat{k}})(E_{k'}E_{\hat{k}})$ values are needed for each sample realization, as well as the mapping which describes the exhaustive set of $(k',\hat{k})$ tuples for each (i,j) index. This only needs to be obtained once prior to the optimization stage. Having this mapping available, the samples of any of the matrix variables can be constructed efficiently by multiplying the densities with samples of E_k and a_k corresponding to element tuple $(k',\hat{k})$, and then summing according to the matrix entry tuple (i,j). The expected values of the matrix variables and their products are computed by simple aggregation of sample-wise realizations.

With a set of samples of material properties and the aid of the aforementioned procedure, for each RTO iteration the samples of the matrix variables are dynamically updated, which enables the sample-wise values of α and $\frac{\partial\alpha}{\partial\rho_e}$ to be efficiently computed. Aggregating the sample results enables c_R and its sensitivities to be computed with the application of the chain rule in Equation (2.11).

3.5 Computational Aspects

The storage scheme of NETO is based on samples of material properties combined with the vectorized tuple storage scheme. Given n_s samples, each sample requires vector tuple storage of the set of $E_{k'}E_{\hat{k}}a_{k'}a_{\hat{k}}$. All of these are precomputed and stored before optimization. Each of the vector tuples has lengths of number of non-zero entries in $\mathbf{K}$, which scales with $O(n_f)$, where n_f is the number of free degrees of freedom. Hence, the memory requirement is $O(n_s n_f)$, which is comparable to the cost of storing n_s stiffness matrices.

In NETO, the samples of $E_{k'}(\boldsymbol{\xi}_m)E_{\hat{k}}(\boldsymbol{\xi}_m)a_{k'}(\boldsymbol{\xi}_m)a_{\hat{k}}(\boldsymbol{\xi}_m)$ and the variables $\mathbb{E}[E_k a_k]$ are scaled by the corresponding penalized density ρ_k^p or ρ_k^{p-1}, based on the mapping $(i,j) \leftrightarrow (\text{element } k', \text{element } \hat{k})$. These samples of matrix variables lead to samples of α and $\frac{\partial \alpha}{\partial \rho_e}$. This information is sufficient for computing $\mathbb{E}[\alpha^q]$ and $\mathbb{E}\left[\alpha^q \frac{\partial \alpha}{\partial \rho_e}\right]$ of any order, and also the statistics of compliance and its sensitivities.

In terms of computational cost for each iteration, computing c_0 (see Equation (3.13)) requires solving one linear system and computing $\frac{\partial c_0}{\partial \rho_e}$ costs $O(n_e n_u^2)$. To compute the $\mathbb{E}[\alpha^q]$ and $\mathbb{E}\left[\alpha^q \frac{\partial \alpha}{\partial \rho_e}\right]$, with the storage scheme, the updated sample-wise matrix variables are needed. Updating the one sample of the matrix variables requires only scalar operations and hence if n_s samples are used, the complexity is $O(n_s n_e n_u)$. Even though these variables are matrix related quantities, their computation does not involve traversing through elements, which is very beneficial for memory and arithmetic.

For the representation of material uncertainties, $\Delta\mathbf{K}$ and the sampling process required by NETO are insensitive to the dimensionality and complexity of the underlying uncertainties. For instance, in the case of multiple uncertainty sources (for example, stochastic Young's modulus and Poisson's ratio) or short correlation lengths in the material random field leading to many expansion terms in the truncated KLE representation, the associated storage and computational cost of the NETO does not explicitly scale with the number of stochastic dimensions, which is different from the majority of the existing methods. Also, the sampling-related computations in Algorithm 1 are task parallel, hence parallel computing can be employed to reduce the computation cost.

There are potential disadvantages to the NETO algorithm. The accuracy of the NE UQ varies depending on the underlying levels of uncertainties. For example, large random field variance leads to inaccuracies and divergence in estimating the statistics of compliance. In addition, the cost of storage depends on the sampling

scheme. A large number of samples leads to high storage requirements. For higher order truncation choices, the number of terms in the full expansion of Equation (3.9) grows, potentially leading to difficulties in formulating the closed form expressions.

3.6 Numerical Results

In this section, the NETO algorithm is demonstrated for minimum weight designs of a cantilever beam and a simply supported bridge with a robust compliance constraint (Equation (2.23)). Having the robust compliance as a constraint rather than as an objective is a more demanding application for the calculation of statistics. The domains and boundary conditions of these problems are shown in Figure 3.1. The domains are discretized by unit square elements. All cases have a unit point load ($F = 1$). The uncertainty is a consequence of random Young's modulus, modeled as a homogeneous lognormal field. The bridge design additionally considers Poisson's ratio as random. For the random fields, the mean Young's modulus is one, while the mean Poisson's ratio is 0.3. The CoV and the correlation lengths in $C_H(\cdot, \cdot)$ for all random fields are varied to study the robustness and accuracy of NETO.

MCTO provides a benchmark for comparison of the NETO algorithm. For both problems, 1000 samples of the material random fields are utilized in MCTO. Since the computational procedure is identical across sample realizations, parallel computing techniques are used with four cores to improve the computational efficiency. Since NETO also relies on sample-wise simulation of matrix variables to compute the c_R and its gradient, for all design problems the same 1000 Monte Carlo random samples are used for this purpose. This procedure removes the influence of sample variance when comparing NETO and MCTO designs. These cases illuminate two phenomena: the behavior of the NE UQ scheme and the performance of NETO compared to standard MCTO.

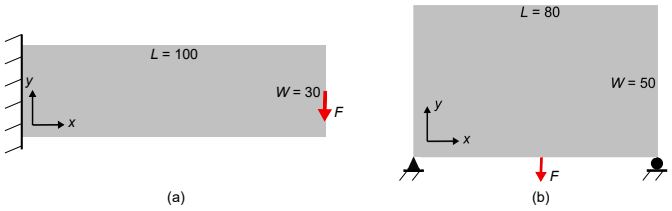

Figure 3.1 Design domain of (a) a cantilever beam with downward loading on the center of right edge, and fixed pin support along the left edge; (b) a simply supported bridge with downward loading at the bottom center, roller condition on the right bottom corner, and pin support on the left bottom corner. The geometries are in non-dimensional units.

The application of the NE approximation in computing the random compliance

leads to error. To assess the behavior of this error, the NE UQ scheme of various orders is used to estimate the statistics of a reference structure, which is the MCTO design. To form a comparison basis, 10,000 samples of the material random fields are generated leading to 10,000 samples of the stiffness matrix and compliances. Using these samples, a MC UQ is employed to compute the robust compliance of the MCTO design. This MC UQ computation is considered as the ground truth, and the resulting robust compliance is the verified compliance, c_V, of the MCTO design. Subsequently, the NE UQ is used to approximate the c_V of the MCTO design. Different truncation orders of NE are applied, where the statistics of the expansion variables, α^q, are computed using the same 10,000 stiffness matrix samples. Provided the ground truth c_V and the approximation of c_V using NE, their relative signed difference is computed and denoted as the relative robust compliance error. This error shows the convergence and the accuracy of NE schemes of different orders. Also, the 10,000 samples of compliance computed through MC is used to compute a ground truth empirical probability density function (PDF) of the compliance through kernel approximation methods [69, 70]. In NE, the random compliance is approximated by Equation (3.5). Using the same pool of samples, the sample-wise compliance is estimated using NE and are aggregated to approximate the PDF of the compliance. The MC generated ground truth PDF of the compliance is compared with the NE approximated PDF of the compliance.

To assess optimization, several values are compared for each problem between MCTO and NETO with various expansion orders. First, the final volume fraction of the designs is presented, denoted as v_f. To verify constraint satisfaction, the ground truth robust compliance, c_V, of each design is computed using the same 10,000 sample MC procedure as above. Each RTO algorithm provides an estimation of the robust compliance, denoted c_E. The absolute difference between c_V and c_E is computed as a relative error with respect to c_V. This error helps to compare the level of accuracy of the NETO and MCTO algorithms. Since the robust designs have different v_f and c_V, in order to provide a more neutral performance comparison of the designs, a robust stiffness per unit volume metric, S_V, is defined. As stiffness is the inverse of the compliance, S_V is computed via $S_V = \frac{1}{v_f * c_V}$. Also, the CPU time per iteration and the total number of optimization iterations are reported to compare the efficiency of different algorithms. For parallel computing, the CPU time includes the total operation time for all parallel cores.

Several topology optimization parameters remain consistent for all algorithms and all problems. In the SIMP scheme, $p = 3$ is imposed as the penalization factor and

$\rho_{min} = 10^{-3}$ is set as the minimum density. For the regularization filter radius, $r_f = 1.5$ is set for all cases, equivalent to 1.5 times the element edge length. The volume preserving HPF in Equation (2.8) is applied with a continuation scheme on β, where it starts with a value of 1 and doubles every 50 iterations until a value of 8, which is maintained until convergence. The maximum β is set to avoid the generation of discontinuous structural members during optimization, which leads to potential instability. The `asyinit` and the `move` parameter in MMA are kept as the default values of 0.5. All problems are initialized with an even distribution of material, and convergence is achieved as when the largest change in the design variables between iterations is less than 0.01.

3.6.1 Cantilever Beam

The cantilever beam problem in Figure 3.1(a) has a design domain of 100 by 30 units. For all the cases in this problem, the CoV of the Young's modulus random field is 15%, while the correlation lengths are varied from long to short. The parameters in the minimum weight RTO problems are imposed with maximum robust compliance $c_{\max} = 350$ and $\kappa = 6$, hence having a high emphasis on reducing the variance of the structural behavior.

The first case uses a long correlation length random field with $(l_x, l_y) = (50, 15)$, half the lengths of the domain. To discretize it with the truncated KLE scheme, 2000 expansion terms are used to ensure that the truncation energy error (Equation (2.20)) is below 0.1%. The MCTO design is in Figure 3.2(a). The design has horizontal outer flanges that are thick near the fixed boundary, and join at the load point. This adds bending stiffness to the structure. Between the flanges are oblique members that form crosses, which act as the bracing system to separate the flanges and carry the transverse shear force.

The ground truth c_V and the PDF of compliance of the MCTO design is computed using a MC UQ employing 10,000 random samples of compliance. Using the MCTO design as a reference structure, the approximation of its c_V and PDF of compliance are also computed employing the NE with various orders using the same pool of samples. Their comparisons are reported in Figure 3.2(b) and Figure 3.2(c). This analysis is useful to assess the accuracy of the NE scheme. For computing the perturbation matrix, the $\alpha\bar{\mathbf{K}}$ approximation is used instead of the exact $\mathbf{\Delta K}$. This leads to error in the output, as the robust compliance computed from the perturbation series of NE using this approximation is different from c_V. The same can be said

(a) MCTO minimum volume design.

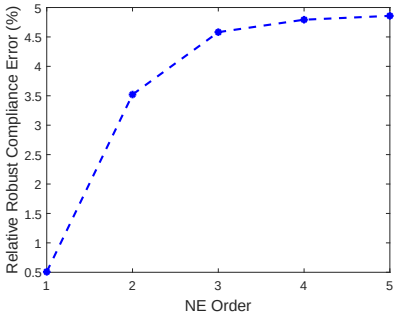

(b) Relative error of the NE UQ estimation of c_V for the MCTO design for various expansion orders.

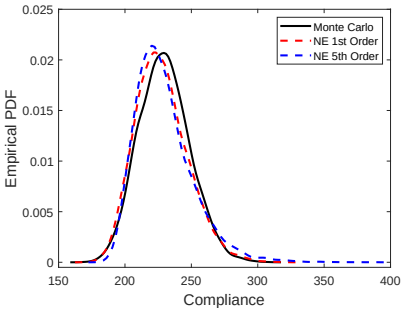

(c) PDF of the compliance of the MCTO design estimated by the MC and NE UQ schemes.

Figure 3.2 Cantilever beam designed using MCTO with $c_{\max} = 350$ and $\kappa = 6$ for c_R. Using a lognormal Young's modulus random field with CoV $= 15\%$ and $(l_x, l_y) = (50, 15)$, discretized by KLE with 2000 expansion terms. Based on the MCTO design layout, the accuracy of NE UQ scheme is assessed.

for samples of compliance. Since the NE scheme is convergent under appropriate conditions, by observing the convergent behavior with higher NE orders the effect of the approximation error can be studied. In Figure 3.2(b), the error asymptotically approaches a maximum with the increase in the order of NE, which is a reflection of the convergence behavior of the NE UQ scheme. The values of α are not sufficiently high to violate the convergence criterion (sampled α values are within $[-1, 1]$), hence leading to higher order terms having negligible magnitudes. This shows that the NE approximation of c_R converges to a value that is a constant offset and greater than the ground truth c_V. The PDFs of compliance illustrate that the central shapes of the distributions computed from different schemes are very similar, but the higher order NE schemes result in a longer tail. This corresponds to the increase in the error in estimation of c_R for higher NE order and shows that the majority of the error is attributable to the higher order statistics. These graphs show that for random fields with long correlation lengths, this approximation of the perturbation matrix leads to lower error in the estimation of robust compliance for lower expansion order. The advantage of this approach is its computational efficiency, as the randomness of the system is compressed into α. This efficiency is demonstrated in the optimization results.

NETO with 1st, 2nd, and 4th order expansions is applied to the same RTO problem. The resulting designs are shown in Figure 3.3. Qualitatively, the outer flanges of the NETO designs are similar to that of the MCTO design in Figure 3.2(a). However,

the number of internal cross braces varies. The quantitative assessments of the four RTO designs are reported in Table 3.1. The volume of the 1st order NETO design is the lowest, while those of the MCTO and 4th order NETO designs are the highest. All of the designs have c_V below 350, hence satisfying the performance constraint. Assessing the structures purely on volume, the 1st order NETO design is the best as it is the lightest and sufficiently robust in stiffness. However, it is evident that the higher volume structures have appreciably lower c_V. This is partially due to the inverse relation between volume and structural stiffness. Also, c_E is very close to 350 for all four algorithms because of the $c_{\max} = 350$ constraint. In all designs, this constraint is activated to minimize the volume. The robust stiffness per unit volume (S_V) has similar values for all robust structures. Hence, the quality of the four designs is similar.

(a) NETO 1st order design. **(b)** NETO 2nd order design. **(c)** NETO 4th order design.

Figure 3.3 NETO designs for the RTO problem described in Figure 3.2.

Table 3.1 Optimization results of various algorithms for the RTO problem described in Figure 3.2.

Method	v_f	c_V	c_E	S_V	Relative c_R Error (%)	CPU Time Per Iteration	Iterations
MCTO	0.499	344.05	350.01	5.82e-3	1.73	97.2	234
NETO-1st	0.492	348.88	350.03	5.82e-3	0.331	0.232	181
NETO-2nd	0.493	348.64	350.03	5.82e-3	0.399	0.258	213
NETO-4th	0.499	344.93	349.99	5.80e-3	1.47	0.241	197

The error in c_R shown in Table 3.1 is the highest for the MCTO method and the lowest for the 1st order NETO. In this problem, the number of samples used in MCTO is insufficient for a highly accurate statistical estimation. However, the accuracy of MCTO scales with the inverse square root of the number of samples. Hence, reducing the MCTO error requires significantly more samples. NETO experiences an increase in the error with higher expansion orders, converging to an asymptote. This trend is consistent with the behavior observed in Figure 3.2(b). This behavior may change

depending on the problem configuration, such as changes in the parameters of the random field. The main advantage of the NETO algorithm is the computational efficiency, as the CPU time required per iteration is about 500 times greater for MCTO than NETO. The number of optimization iterations required is similar for all algorithms, suggesting that NETO does not suffer from ill-convergence issues.

The next case has a Young's modulus random field with moderate correlation lengths of $(l_x, l_y) = (20, 5)$. Again, 2000 expansion terms are used in the truncated KLE representation. The minimum volume design by MCTO is shown in Figure 3.4(a), while the NETO designs are shown in Figure 3.5. The general structural shapes of these designs again consist of outer flanges made up of thicker members, alongside inner oblique members forming cross braces. The number of the inner braces is the same for all designs, but the shapes of the braces differ.

(a) MCTO minimum volume design.

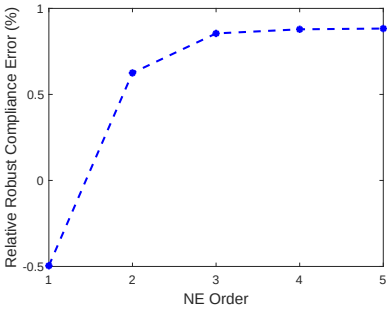

(b) Relative error of the NE UQ estimation of c_V for the MCTO design for various expansion orders.

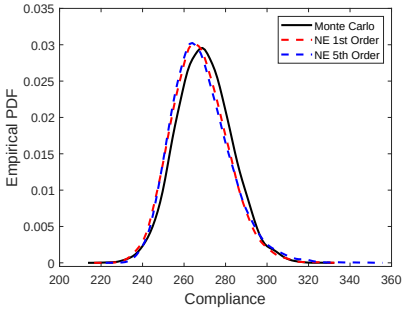

(c) PDF of the compliance of the MCTO design estimated by the MC and NE UQ schemes.

Figure 3.4 Cantilever beam designed using MCTO with $c_{\max} = 350$ and $\kappa = 6$ for c_R. Using a lognormal Young's modulus random field with CoV = 15% and $(l_x, l_y) = (20, 5)$, discretized by KLE with 2000 expansion terms. Based on the MCTO design layout, the accuracy of NE UQ scheme is assessed.

(a) NETO 1st order design.

(b) NETO 2nd order design.

(c) NETO 4th order design.

Figure 3.5 NETO designs for the RTO problem described in Figure 3.4.

The accuracy of the NE UQ scheme is depicted in Figures 3.4(b) and 3.4(c). Again, this is based on computing the random compliance of the MCTO design in

Figure 3.4(a). The 1st order NE scheme underestimates c_R while the 2nd order NE scheme overestimates it, and the magnitude of the errors are similar. Higher order NE schemes result in further overestimation and higher errors. The PDFs of compliance show that the higher order NE results in a longer tail in the high value region, hence causing higher estimation error, similar to the previous case. However, the central bell shapes of the PDFs estimated by 1st order and 5th order NE match with the PDF estimated by MC. Compared to the case with $(l_x, l_y) = (50, 15)$, the support for the PDF of compliance is smaller in range and the position of the maximum is at a lower compliance. These are expected since having longer correlation lengths while maintaining the same random field CoV leads to higher mean and variance in the output compliance. Also, α is again bounded between -1 and 1, leading to convergence in the NE with the relative error in c_R reaching a plateau for higher orders. This again shows that approximating the $\mathbf{\Delta K}$ in NE leads to a constant error when the order of NE is sufficiently high.

The numerical assessments of the four RTO designs are reported in Table 3.2. The 1st order NETO design has the lowest volume fraction, but it also has the highest c_V. In fact, the value violates the constraint, meaning that the behavior of this structure does not satisfy the required compliance. This is caused by the high estimation error of the 1st order NETO scheme, as it has ten times more estimation error in c_R compared to the other three methods. The other RTO designs all have similar design volumes, while satisfying the constraint of c_R. Their level of accuracy in the approximation of c_R is also very high, as all three methods result in less than 0.2% relative error. This suggests that as the correlation lengths decrease, the higher order NE schemes provide a better approximation. Interestingly, referring to S_V, the 1st order NETO, despite having high error in the c_R estimation, is highest. The S_V of the MCTO, 2nd order NETO, and 4th order NETO designs are similar. The compliance estimation error of the 1st order NE UQ did not cause deterioration of the gradient leading to a low quality local minimum. Hence, the design still has a similar performance as other robust designs. Finally, the MCTO algorithm required about 400 times more CPU time per iteration compared to the NETO methods. The aggregation of these time savings over hundreds of optimization iterations leads to significant computational benefits.

The last cantilever design case is for very short correlation lengths of $(l_x, l_y) = (5, 5)$ for the Young's modulus random field. Due to the slow decay of KLE eigenvalues, 10,000 expansion terms are kept during truncation. This case corresponds to very high stochastic dimensionality. Even if the KLE truncation criterion is relaxed

Table 3.2 Optimization results of various algorithms for the RTO problem described in Figure 3.4.

Method	v_f	c_V	c_E	S_V	Relative c_R Error (%)	CPU Time Per Iteration	Iterations
MCTO	0.411	349.34	350.01	6.96e-3	0.193	86.2	203
NETO-1st	0.401	355.93	350.09	7.00e-3	1.64	0.232	191
NETO-2nd	0.408	350.72	350.03	6.98e-3	0.199	0.246	186
NETO-4th	0.409	350.66	349.98	6.97e-3	0.193	0.239	209

to account for 90% of the random field energy, about 2900 expansion terms are required. The robust design from MCTO is shown in Figure 3.6(a), while the NETO designs are shown in Figure 3.7. All four geometries are similar. For this case, the relative robust compliance error in Figure 3.6(b) is convergent and the higher order NE schemes led to a reduction in the error. In contrast to the case of long correlation lengths, increasing the order of NE is beneficial for accuracy. The offset in error caused by the perturbation approximation leads to an underestimation of the robust compliance. In addition, the support ranges of the PDFs of compliance in Figure 3.6(c) are significantly smaller than the ranges for long correlation lengths, which reflects the reduction in variation of the structural performance. For short correlation lengths, the NE approximation of the PDF of compliance is skewed down compared to the PDF from the MC scheme. Hence, even though the shape of the central bell curve is well represented by the NE scheme, the peak of the PDF is shifted to a lower compliance, which is the main source of statistical error.

The quantitative data of the optimization output and performances of the algorithms are in Table 3.3. The final volume fraction of all four robust designs is similar to within 0.8%, hence the optimality of the structures is comparable. Examining the volumes of the robust designs as a function of the correlation lengths, it is observed that as the correlation lengths decrease, the amount of material required to satisfy the constraint on robust compliance decreases. For instance, the case with $(l_x, l_y) = (50, 15)$ led to designs with volume fractions close to 0.5, while the designs from the case with $(l_x, l_y) = (5, 5)$ have volume fractions close to 0.36. This is an expected trend that is explained by considering the statistics of compliance. For a set amount of material and a consistent CoV, as the correlation lengths decrease, the uncertainty of both the random field and the structural behavior also decreases, leading to a lower c_V. Conversely, for a specified constraint on c_R, less material is required in

(a) MCTO minimum volume design.

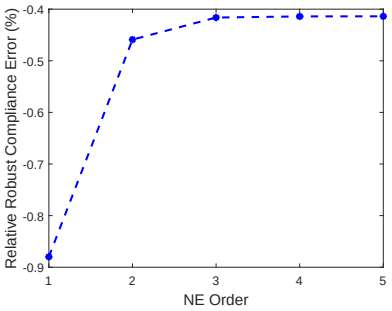

(b) Relative error of the NE UQ estimation of c_V for the MCTO design for various expansion orders.

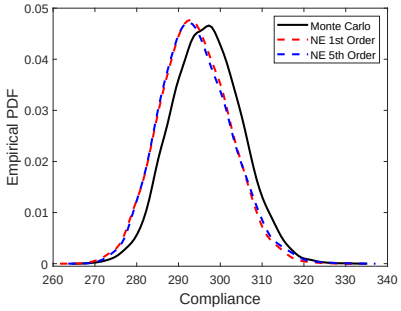

(c) PDF of the compliance of the MCTO design estimated by the MC and NE UQ schemes.

Figure 3.6 Cantilever beam designed using MCTO with $c_{\max} = 350$ and $\kappa = 6$ for c_R. Using a lognormal Young's modulus random field with CoV = 15% and $(l_x, l_y) = (5, 5)$, discretized by KLE with 10,000 expansion terms. Based on the MCTO design layout, the accuracy of NE UQ scheme is assessed.

(a) NETO 1st order design.

(b) NETO 2nd order design.

(c) NETO 4th order design.

Figure 3.7 NETO designs for the RTO problem described in Figure 3.6.

the robust designs. MCTO overestimates the ground truth robust compliance, c_V, of its design, while the NETO algorithms slightly underestimate the c_V corresponding to their designs. Hence, the NETO designs all marginally violate the constraint of $c_{\max} = 350$, by less than 1%.

For all four algorithms, c_E is about 350, meaning that the constraints are active for all cases. The estimation error of c_R is the highest for the MCTO scheme at over 1%. All of the NETO schemes have an error of less than 1%, with the 2nd and 4th order having lower errors compared to the 1st order. This trend matches the error convergence behavior observed in Figure 3.6(b), affirming that for the case of very short correlation lengths, using a higher expansion order in NE results in an improvement in the accuracy of the estimation of the c_R. This is in contrast with the case of long correlation lengths. Last, the CPU times per iteration required by the NETO algorithms are orders of magnitude less than for MCTO, while the total number of optimization iterations is comparable for all cases. This significant difference in computational efficiency is a major advantage of NETO.

Table 3.3 Optimization results of various algorithms for the RTO problem described in Figure 3.6.

Method	v_f	c_V	c_E	S_V	Relative c_R Error (%)	CPU Time Per Iteration	Iterations
MCTO	0.366	346.39	350.02	7.88e-3	1.05	55.9	216
NETO-1st	0.363	352.85	350.05	7.81e-3	0.793	0.246	264
NETO-2nd	0.364	350.13	350.01	7.85e-3	0.036	0.246	200
NETO-4th	0.364	351.15	349.94	7.83e-3	0.346	0.241	215

3.6.2 Simply Supported Bridge

The second problem is the design of a simply supported bridge on a domain of 80 by 40 units, as shown in Figure 3.1(b). For the RTO problem, $c_{\max} = 20$ and $\kappa = 4$ are enforced. Multiple sources of uncertainty are considered, as both Young's modulus and Poisson's ratio are modeled as lognormal random fields with correlation lengths of $(l_x, l_y) = (50, 25)$. The CoV are 10% and 15%, for the modulus and the Poisson's ratio, respectively. The truncated KLE scheme is employed to discretize both random fields with 1000 expansion variables. Since it is a multivariate random field, the total number of stochastic dimensions is a sum of the individual expansion variables. Hence, as with short correlation lengths, the stochastic dimensions are high. The NE approximation combines the randomness of both properties into various orders of α. It acts as a dimension reduction technique to mitigate high dimensionality.

The MCTO design and its associated compliance statistics computed using the NE scheme are shown in Figure 3.8. Qualitatively, the robust design has a thick outer arch with thinner straight members connecting the arch with the point of load application. The straight members are distributed at different oblique angles and are mainly subject to tension, while the thick arch is subject to compression. The correlation lengths are over half of the domain edge lengths. Hence, the behaviors of the relative error in c_R and the compliance PDFs estimated by NE are consistent with long correlation lengths considered in other problem. That is, NE generally results in an overestimation of c_V, and the error is higher for higher order NE, but approaches an asymptotic maximum. The shape of the compliance PDF from NE matches that from Monte Carlo, but the higher order NE leads to a longer tail.

The RTO designs from first, second, and fourth order NETO are shown in Figure 3.9. The general layout is similar to the MCTO design, but the number of inner members varies. The numerical assessments are provided in Table 3.4. All of the

(a) MCTO minimum volume design.

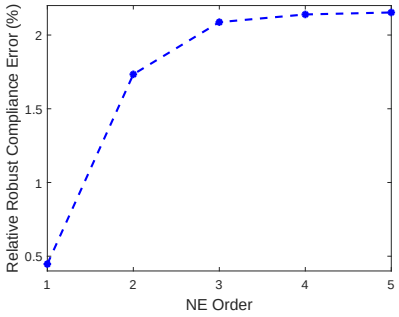

(b) Relative error of the NE UQ estimation of c_V for the MCTO design for various expansion orders.

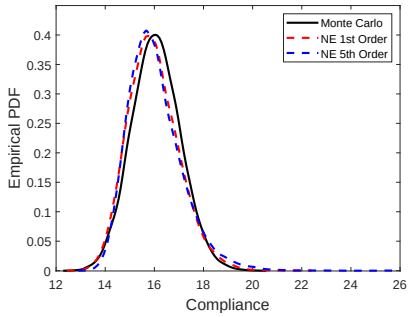

(c) PDF of the compliance of the MCTO design estimated by the MC and NE UQ schemes.

Figure 3.8 Simply supported bridge designed using MCTO with $c_{\max} = 20$ and $\kappa = 4$ for RTO. Lognormal Young's modulus with CoV $= 10\%$ and $(l_x, l_y) = (50, 25)$ and lognormal Poisson's ratio with CoV $= 15\%$ and $(l_x, l_y) = (50, 25)$ are used. Based on the properties of the MCTO design, the accuracy of NE UQ scheme is assessed.

(a) NETO 1st order design.

(b) NETO 2nd order design.

(c) NETO 4th order design.

Figure 3.9 NETO designs for the RTO problem described in Figure 3.8.

designs satisfy the $c_{\max} = 20$ constraint according to c_V. The NETO methods all overestimated c_V, leading to slight overdesign of the structures. The MCTO had the lowest relative error in c_R, which allows it to have higher c_V and remove more material. The accuracy of first order NETO is the highest and is similar to MCTO. This is consistent with the behavior seen in Figure 3.8(b). The stiffness per volume is very similar for all designs. This again demonstrates that despite the differences in the algorithmic performance, the quality of the structures is very similar. The CPU time per iteration shows that the MCTO is over 400 times slower than NETO, showing that the efficiency of NETO is maintained for multiple sources of stochastic uncertainty.

Table 3.4 Optimization results of various algorithms for the RTO problem described in Figure 3.8.

Method	v_f	c_V	c_E	S_V	Relative c_R Error (%)	CPU Time Per Iteration	Iterations
MCTO	0.331	20.013	19.999	0.151	0.0678	161	175
NETO-1st	0.333	19.972	20.000	0.151	0.143	0.361	185
NETO-2nd	0.335	19.751	20.000	0.151	1.26	0.354	188
NETO-4th	0.339	19.677	19.999	0.150	1.63	0.370	190

3.7 Conclusion

In this chapter, the NETO algorithm is developed, which employs a novel approximate NE as the UQ module. A dimension reduction approach is applied to the NE scheme where the randomness in the system is jointed accounted for by the powers of the random variable α, which does not explicitly depend on the parametrization of the input uncertainty and hence is efficient under high stochastic dimensions. In RTO, the c_R objective and its gradients have closed form expressions that depend on $\mathbb{E}[\alpha^q]$ and $\mathbb{E}\left[\alpha^q \frac{\partial \alpha}{\partial \rho_e}\right]$, and hence the computation is very efficient. The $\mathbb{E}[\alpha^q]$ and $\mathbb{E}\left[\alpha^q \frac{\partial \alpha}{\partial \rho_e}\right]$ are computed using sampling method. However, they require statistics of variables that depend on the stiffness matrix, and constructing many samples of the stiffness matrix each iteration is costly. Hence, a novel storage and update scheme is developed, which decomposes these variables into stochastic components and deterministic design variable scaling. Samples of the stochastic components are precomputed and stored, while the scaling is updated through RTO. The product of these two components enables rapid computation of the statistics of the matrix variables following design variable updates since only scalar arithmetic is required rather than matrix assembly.

The NETO algorithm is applied to two numerical cases of volume minimization under a c_R constraint, where material uncertainty with short correlation lengths and multi-source uncertainties are considered. Compared to the standard MCTO employing 1000 random samples, the NETO is nearly 400 times faster for all cases. The relative errors of the approximation of c_R using NE are less than 2% and depend on the characteristics of the random field, which is slightly higher compared to MCTO. Regardless, the NETO designs demonstrated similar levels of optimality as the MCTO designs by assessing the stiffness per volume metric. These cases demonstrate the efficacy of NETO in generating high quality uncertainty aware designs while providing a substantial reduction in computational cost compared to MCTO.

Chapter 4

Multi-fidelity Monte Carlo for Robust Optimization

Algorithms for robust topology optimization (RTO) are typically a nested loop [71, 44], where the inner loop consists of an uncertainty quantification (UQ) scheme for estimating the statistics of the quantity of interest (QOI), while the outer loop is comprised of sensitivity analysis and design updates. To improve the quality of RTO, either process could be targeted. In this thesis, the focus is on improving the inner loop UQ procedure, since having an accurate estimation of the statistics leads to high quality gradients in optimization. The uncertainty of interest in this thesis is the material variability introduced by additive manufacturing. These uncertainties are typically modeled as random fields with short correlation lengths approximated by the Karhunen-Loève Expansion (KLE). This tends to result in very high stochastic dimensions and hence, the Monte Carlo (MC) scheme is typically applied in the inner loop due to its insensitivity to the dimension of the problem [72, 73].

A few definitions are needed. A parameter is a constant scalar value that describes the statistic of a population, such as the mean or the variance. The values of parameters are unknown since it is normally impossible to evaluate the entire population. An estimator is a mathematical expression used to estimate the value of a population parameter, given a set of samples. Estimators are derived with specific properties, such as being unbiased. For a sample set input, evaluating the estimator is one realization of its value, and also an approximation of the population parameter. The estimator is a random variable since it changes according to the input sample set. For notation, if a population parameter is Q, then the estimator is $\widehat{Q}$.

In the regular MC scheme, estimators are employed to approximate population parameters such as the mean and the variance. These estimators use samples of QOI

evaluated from a high-fidelity model (HFM). A metric for assessing the quality of these estimators is the mean squared error (MSE), which is an L^2 measure defined as the average squared deviation of the statistic estimated by the estimator compared to the true parameter. The MSE provides guidance on the number of samples to use in computing the MC estimators. For a regular MC scheme, the MSE decreases with $\frac{1}{\sqrt{n_s}}$, with n_s being the number of random samples employed. However, this is a slow convergence rate, and many variance reduction techniques have been considered in the literature to accelerate MC. One type of approach is to improve the sampling procedure, leading to schemes such as quasi-MC [74, 75], importance sampling [76, 77], and Latin-Hypercube sampling [78, 79]. Another type of approach employs low-fidelity models (LFMs) that approximate the HFM and improve the parameter estimations by combining samples from the LFMs and HFM. The associated schemes include multilevel Monte Carlo (MLMC) [71, 72, 80, 81, 82], multi-index Monte Carlo (MIMC) [83], and multi-fidelity Monte Carlo (MFMC) [37, 84, 85, 86, 87].

The MFMC scheme is more flexible than MLMC and MIMC since it does not necessitate a strict model hierarchy of the LFMs, and only requires that the LFM be cheap to evaluate and have good correlation with the HFM [84, 87]. Consequently, MFMC can be employed for a wider variety of LFMs and also in the absence of LFM error bounds [73]. Hence, MFMC is applied in this work as the UQ scheme for RTO. To estimate a parameter, MFMC primarily relies on evaluating the LFM, with occasional recourse to the HFM for accuracy adjustment. Since evaluating the LFM is much cheaper, the reduced querying of the HFM allows more samples of the LFM to be computed, leading to a reduction in the MSE while using effectively the same amount of HFM evaluations compared to the regular MC scheme. In other words, the accuracy of the estimation is improved while the cost is maintained.

The objective function of RTO problems focusing on compliance consists of a linear combination of the mean (μ_c) and the standard deviation (σ_c) of compliance, which is denoted as robust compliance (c_R). Hence, the application of MFMC to RTO requires estimators of these parameters and their associated MSE expressions in order to control the approximation accuracy. There are many MFMC and MLMC strategies developed for the optimal estimation of a parameter [37, 72, 73, 80, 84, 85, 87, 88]. These strategies have been deployed in various practical problems, such as structural analysis [89, 90, 91, 92], engineering simulations [93, 94, 95, 96, 97], and optimization under uncertainty [43, 44, 98, 99]. However, the majority of existing approaches target parameters in the form of a single statistical moment, and methodologies focusing on

more complex statistics are rarely investigated [71, 73]. For application in robust optimization, the objective is typically a linear combination of functions of statistical moments of the QOI, for example c_R. The existing approaches focus on one moment, which may not minimize the MSE of the robust objective.

The main contribution of this chapter is to develop appropriate MFMC strategies addressing the optimal estimation of the parameter of QOI in the form of a robust objective for optimization procedures. The next section introduces the general framework of MFMC, in addition to providing the detailed ingredients required in MFMC.

4.1 General Framework of Multifidelity Monte Carlo

In this section, the MFMC framework for estimating a statistical parameter is described, consisting of three ingredients. The first is the expression of the MFMC estimator and its associated MSE. Since MFMC combines LFM and HFM samples, the second ingredient is control variate coefficients that relate these two sets of samples and minimize the MSE. The third is a sample allocation strategy to specify the number of HFM and LFM samples, denoted by n_s and m_s, required to minimize the MSE.

4.1.1 Control Variate in Monte Carlo

The principle of the MFMC approach is to reduce the MSE of an estimator through the introduction of a control variate, which is a random variable that can be cheaply or easily evaluated and has a known population parameter. The estimate of a population parameter Q_Γ for a random variable Γ is the unbiased estimator $\hat{Q}_\Gamma$, such that $\mathbb{E}\left[\hat{Q}_\Gamma\right] = Q_\Gamma$. The MSE of this estimator is the same as its variance, denoted by the operator $\mathbb{V}[\cdot]$, hence $\text{MSE}[\hat{Q}_\Gamma] = \mathbb{V}[\hat{Q}_\Gamma]$. For a control variate random variable γ, if the same population parameter, Q_γ, for the control variate is known and is estimated with the unbiased estimator $\hat{Q}_\gamma$, the control variate augmented estimator for Q_Γ is:

$$\hat{Q}_\Gamma^{CV} = \hat{Q}_\Gamma + \alpha(Q_\gamma - \hat{Q}_\gamma).$$

The control variate coefficient, α, is a constant, and this new estimator maintains the mean convergence property of $\mathbb{E}\left[\hat{Q}_\Gamma^{CV}\right] = Q_\Gamma$, and hence it is also unbiased. The MSE of the new estimator is its variance:

$$\text{MSE}[\hat{Q}_\Gamma^{CV}] = \mathbb{E}\left[(\hat{Q}_\Gamma^{CV} - Q_\Gamma)^2\right] = \mathbb{V}[\hat{Q}_\Gamma^{CV}] = \mathbb{V}[\hat{Q}_\Gamma] + \alpha^2\mathbb{V}[\hat{Q}_\gamma] - 2\alpha \cdot \text{Cov}[\hat{Q}_\Gamma, \hat{Q}_\gamma],$$

where $\mathrm{Cov}[\cdot]$ is the covariance operator. Setting the constant $\alpha = \frac{\mathrm{Cov}[\hat{Q}_\Gamma, \hat{Q}_\gamma]}{\mathbb{V}[\hat{Q}_\gamma]}$ minimizes the MSE. Employing the Pearson correlation coefficient relation [100], the covariance is re-expressed as $\mathrm{Cov}[\hat{Q}_\Gamma, \hat{Q}_\gamma] = \mathrm{Corr}[\hat{Q}_\Gamma, \hat{Q}_\gamma]\sqrt{\mathbb{V}[\hat{Q}_\Gamma]\mathbb{V}[\hat{Q}_\gamma]}$. Hence, the MSE is rewritten using the correlation and the expression for optimal α as:

$$\mathrm{MSE}[\hat{Q}_\Gamma^{CV}] = (1 - \mathrm{Corr}^2[\hat{Q}_\Gamma, \hat{Q}_\gamma])\mathbb{V}[\hat{Q}_\Gamma].$$

If the estimators of the control variate and the variable of interest are strongly positively correlated, then $(1 - \mathrm{Corr}^2[\hat{Q}_\Gamma, \hat{Q}_\gamma]) \sim 0$. Consequently, the $\hat{Q}_\Gamma^{CV}$ estimator leads to a significant reduction in MSE in comparison with the original estimator, which has an MSE of $\mathbb{V}[\hat{Q}_\Gamma]$. Provided the control variate γ is cheap to evaluate, the additional effort in computing its realizations is negligible compared with the cost of obtaining samples of Γ. Hence, the reduction in MSE is achieved without any penalty in cost. For the case of the multi-fidelity Monte Carlo scheme, the estimators of HFM and LFM are all Monte Carlo estimators.

In practical engineering applications, the Γ is equivalent to the output of interest, evaluated from the HFM such as a finite element model, while the γ control variate is the output from the LFM that closely resembles the HFM, such as a reduced basis model. The parameter Q is a parameter of interest, such as the mean or variance. Typically, knowing the exact population parameters of the LFM is impractical for realistic problems. Hence, a common approach in MFMC is that given $\hat{Q}_\Gamma$ and $\hat{Q}_\gamma$, which are Monte Carlo estimators computed using n_s samples, the parameter Q_γ is approximated with a MC estimator using m_s samples, requiring $m_s > n_s$ [37, 85, 87]. Hence, Q_γ is approximated at a much higher accuracy compared to the other terms. Since the multifidelity estimator involves the same MC estimators evaluated using different sample sizes, for clarity the number of samples required for an estimator will be denoted in the superscript (for example, $\widehat{Q_\gamma}^{m_s}$ and $\widehat{Q_\gamma}^{n_s}$). With this approximation, the MFMC estimator is:

$$\hat{Q}_\Gamma^{MF} = \widehat{Q_\Gamma}^{n_s} + \alpha(\widehat{Q_\gamma}^{m_s} - \widehat{Q_\gamma}^{n_s}), \quad m_s > n_s.$$

Since the individual estimators are unbiased, the $\hat{Q}_\Gamma^{MF}$ estimator is also unbiased, meaning $\mathbb{E}\left[\hat{Q}_\Gamma^{MF}\right] = Q_\Gamma$. Hence, even in the absence of error bounds and error estimators for the LFM, the MFMC estimator is unbiased and leads to computational benefits if the correlation between the HFM and the LFM is high. In addition, the n_s samples are a subset of the m_s samples [37, 85, 87] and hence the covariance between

$\widehat{Q_\gamma}^{m_s}$ and $\widehat{Q_\Gamma}^{n_s}$ is non-zero, meaning that these estimators are correlated.

Ultimately, MFMC augments the standard MC scheme by introducing control variate random variables. The MFMC scheme requires additional variables, including control variate coefficients and sample numbers for models of different fidelities.

4.1.2 Optimal Control Variate Coefficient and Sample Allocation

The MFMC scheme requires variables α, n_s and m_s. Typically, these variables are either selected to minimize the MSE of the estimator of interest given a limited computational budget [37, 85, 86, 87, 101], or they are selected so that the MSE is below a desired threshold [71, 72, 80, 81, 82]. In this work, the first scenario is considered.

Suppose the parameter of interest is Q_Γ and the MFMC estimator is $\hat{Q}_\Gamma^{MF}$. Since the cost of evaluating the HFM is higher than the LFM, a normalizing factor is defined as: $w_c = \frac{\text{Computational Cost of HFM}}{\text{Computational Cost of LFM}} > 1$. This ratio allows the budget to be expressed as the number of HFM evaluations. For a budget P_b, which is equivalent to P_b HFM solves, the variables are selected through an optimization problem:

$$\begin{aligned} \min_{\alpha, n_s, m_s} \quad & \text{MSE}[\hat{Q}_\Gamma^{MF}], \\ \text{s.t.} \quad & : n_s + \frac{m_s}{w_c} \leq P_b; \\ & : m_s > n_s \geq n_0. \end{aligned} \tag{4.1}$$

The minimum sample requirement is n_0. To solve this optimization problem, a closed form expression for the MSE as a function of α, n_s, and m_s is required. In application to optimization, at each iteration, a small set of solutions sampled from the HFM and the LFM are computed as the pilot samples, and these are used to evaluate the MSE [37, 85, 87]. Hence, the expression for MSE must be in a form that is amenable to evaluation with this pilot sample set. Denote this pilot sample size as n_{plt}. It is smaller than the final required samples, that is, $m_s > n_s \geq n_{plt}$. With the above ingredients, Equation (4.1) is solved numerically, which provides the stationary points for all of the variables. The m_s and n_s are discrete integers and hence in numerical optimization, they are relaxed to become continuous variables. After finding their optima, the values are rounded to the nearest integer.

For estimating the statistical raw moments or central moments, the solution to Equation (4.1) is well-established [37, 86, 87]. However, there are very limited inves-

tigations for Q_Γ in the form of a linear combination of mean and standard deviation parameters. Hence, the development of novel MFMC strategies targeting optimal estimation of a robust objective is the goal of this chapter. Several key ingredients presented in upcoming sections are summarized below.

- A closed form approximation, $\text{MSE}[\widehat{c_R}]_{\mu\sigma}$, and two upper bounds, $\text{MSE}[\widehat{c_R}]_{\text{p}}^{\text{ub}}$ and $\text{MSE}[\widehat{c_R}]_{\text{cs}}^{\text{ub}}$, of the MSE of $\hat{Q}_\Gamma^{MF}$ in the form of a linear combination of mean and standard deviation estimators are derived in Theorem 1. These expressions are used as the optimization objectives in Equation (4.1), which corresponds to the novel MFMC strategies for optimal estimation of a robust objective.

- The MFMC variance estimator employed is from Qian et al. [85]. The closed form expression for the optimal α that minimizes the MSE of this estimator is presented in Lemma 2.

- Using the MFMC estimators, approximations of the confidence intervals of the mean and variance are developed using Lemma 3, Lemma 4, and Corollary 4.1, which are useful for statistical inference in post-processing.

- Unbiased estimators for various parameters are derived in Lemmata 5, 6, 7, 8, 9, 10, 11, and 12. These estimators enable the closed form expressions of $\text{MSE}[\widehat{c_R}]_{\mu\sigma}$, $\text{MSE}[\widehat{c_R}]_{\text{p}}^{\text{ub}}$ and $\text{MSE}[\widehat{c_R}]_{\text{cs}}^{\text{ub}}$ to be computed for the MFMC and MC estimators given n_{plt} pilot samples of HFM and LFM outputs. This is of great importance for practical optimization settings.

- An analytical approximation for the solution to Equation (4.1) with the $\text{MSE}[\widehat{c_R}]_{\text{cs}}^{\text{ub}}$ upper bound as the optimization objective is developed in Lemma 13.

4.2 Estimators for the MFMC Scheme

Estimating the robust compliance requires estimators for both the mean and standard deviation. In this section, the MFMC estimators for the mean, variance, and standard deviation are described. The closed form expressions of the MSEs of these estimators are provided, alongside unbiased estimators of high order parameters which enables these MSEs to be computed with n_{plt} pilot samples of HFM and LFM. Also, the strategies for determining α, n_s, and m_s which lead to the optimal estimation of these parameters are discussed. The approximation of confidence intervals for the mean and variance are presented.

For notation, the number of samples required is specified in the superscript of the estimator. Since models of different fidelity are used, subscripts are used to distinguish them, with "h" representing the HFM evaluation of compliance and "l" representing the LFM evaluation of compliance. Also, each MFMC estimator is composed of MC estimators. The expressions for MC estimators and their MSEs are summarized in Appendix A.1 as supplementary information.

4.2.1 Mean, Variance and Standard Deviation

The MFMC mean estimator from Ng and Willcox [37] is employed, which is a composite of unbiased MC mean estimators based on the HFM and the LFM outputs ($\boldsymbol{c_h}$ and $\boldsymbol{c_l}$):

$$\begin{aligned}\widehat{\mu_{c,MF}} &= \widehat{\mu_{h,MC}}^{n_s} + \alpha_\mu(\widehat{\mu_{l,MC}}^{m_s} - \widehat{\mu_{l,MC}}^{n_s}),\\ &= \frac{1}{n_s}\sum_{i=1}^{n_s} c_{h,i} + \alpha_\mu\left(\frac{1}{m_s}\sum_{j=1}^{m_s} c_{l,j} - \frac{1}{n_s}\sum_{k=1}^{n_s} c_{l,k}\right).\end{aligned} \tag{4.2}$$

Here, α_μ is the control variate coefficient for the MFMC mean estimator. Explicitly evaluating this estimator with the compliance samples leads to one instance of an approximation of μ_c, that is, $\widehat{\mu_{c,MF}}(\boldsymbol{c}) \approx \mu_c$. The MFMC variance estimator of Qian et al. [85] is employed, denoted as $\widehat{\sigma^2_{c,MF}}$. It is also composed of unbiased MC variance estimators based on the HFM and LFM outputs:

$$\begin{aligned}\widehat{\sigma^2_{c,MF}} &= \widehat{\sigma^2_{h,MC}}^{n_s} + \alpha_\sigma\left(\widehat{\sigma^2_{l,MC}}^{m_s} - \widehat{\sigma^2_{l,MC}}^{n_s}\right),\\ &= \frac{1}{n_s-1}\sum_{i=1}^{n_s}(c_{h,i} - \widehat{\mu_{h,MC}}^{n_s})^2\\ &\quad + \alpha_\sigma\left(\frac{1}{m_s-1}\sum_{j=1}^{m_s}(c_{l,j} - \widehat{\mu_{l,MC}}^{m_s})^2 - \frac{1}{n_s-1}\sum_{k=1}^{n_s}(c_{l,k} - \widehat{\mu_{l,MC}}^{n_s})^2\right).\end{aligned} \tag{4.3}$$

The α_σ is the control variate coefficient for the variance estimator. The MFMC estimators for mean and variance are unbiased, meaning that $\mathbb{E}\left[\widehat{\mu_{c,MF}}\right] = \mu_h = \mu_c$ and $\mathbb{E}\left[\widehat{\sigma^2_{c,MF}}\right] = \sigma^2_h = \sigma^2_c$.

For estimating the standard deviation parameter σ_c, in general, without *a priori* knowledge of the distribution of the compliance, it is difficult to obtain an unbiased estimator due to the nonlinear square root function. Hence, the square root of the variance estimator, which is a biased estimator of σ_c is used:

$$\widehat{\sigma_{c,MF}} = \sqrt{\widehat{\sigma^2_{c,MF}}}. \tag{4.4}$$

The bias of this estimator is provided in Lemma 14 in Appendix A.1.2.

4.2.2 Mean Squared Errors

Assuming the values of the variables α_μ, α_σ, n_s, and m_s are known, the expressions for the MSE of the mean, variance, and standard deviation estimators are discussed. MSE is an L^2 assessment of the difference between the true parameter and the approximation of the estimator. The unbiased estimator $\widehat{\mu_{c,MF}}$ has a MSE of [37]:

$$\text{MSE}[\widehat{\mu_{c,MF}}] = \frac{1}{n_s}\left[\sigma_h^2 + \left(1 - \frac{n_s}{m_s}\right)\left(\alpha_\mu^2\sigma_l^2 - 2\alpha_\mu \text{Cov}[c_h, c_l]\right)\right], \tag{4.5}$$

where $\sigma_h^2 = \sigma_c^2$ is the variance parameter for the compliance calculated using the HFM, σ_l^2 is the variance parameter for the compliance calculated using the LFM, and $\text{Cov}[c_h, c_l]$ is the covariance parameter of the two compliance calculations.

The MSE of the unbiased variance estimator is [85]:

$$\begin{aligned}\text{MSE}[\widehat{\sigma_{c,MF}^2}] = &\frac{1}{n_s}(\delta_h - \frac{n_s-3}{n_s-1}\sigma_h^4) + \alpha_\sigma^2\left(\frac{1}{n_s}(\delta_l - \frac{n_s-3}{n_s-1}\sigma_l^4) - \frac{1}{m_s}(\delta_l - \frac{m_s-3}{m_s-1}\sigma_l^4)\right) \\ &+ 2\alpha_\sigma\left[\frac{1}{m_s}\left(\text{Cov}[\vartheta_h, \vartheta_l] + \frac{2}{m_s-1}\text{Cov}[c_h, c_l]^2\right)\right. \\ &\left. - \frac{1}{n_s}\left(\text{Cov}[\vartheta_h, \vartheta_l] + \frac{2}{n_s-1}\text{Cov}[c_h, c_l]^2\right)\right],\end{aligned} \tag{4.6}$$

where δ_h and δ_l are the 4th central moment parameters of the compliance calculated using the HFM and LFM. The random variable ϑ_h is $\vartheta_h = (c_h - \mu_h)^2$, with $\mu_h = \mu_c$ the mean of the compliance calculated from the HFM. Similarly, $\vartheta_l = (c_l - \mu_l)^2$, with μ_l the mean of the compliance computed from the LFM (different from μ_c), and $\text{Cov}[\vartheta_h, \vartheta_l]$ is the covariance of ϑ_h and ϑ_l. The means of ϑ_h and ϑ_l by definition lead to the variances $\sigma_h^2 = \sigma_c^2$ and σ_l^2. The variances of ϑ_h and ϑ_l are additionally defined as $\tau_h = \mathbb{V}[\vartheta_h]$ and $\tau_l = \mathbb{V}[\vartheta_l]$.

For the MSE of the biased $\widehat{\sigma_{c,MF}}$ estimator , the result from Lemma 14 in Appendix A.1.2 is directly applicable by replacing MSE $\left[\widehat{\sigma_c^2}\right]$ with MSE$[\widehat{\sigma_{c,MF}^2}]$.

4.2.3 Optimal Strategy for MFMC Mean

For an efficient MFMC scheme, α_μ, n_s, and m_s are chosen to minimize the MSE of the estimator through the optimization in Equation (4.1). For the case of the mean

estimator ($\hat{Q}_\Gamma^{MF} = \widehat{\mu_{c,MF}}$), the expressions of optimal variables are developed in Ng and Willcox [37] and summarized in Lemma 1. Their approach applies to the mean of any raw or central statistical moment estimators.

Lemma 1. *Given random variable of interest Γ, whose mean (μ_Γ) is a statistical moment of c_h computed from the HFM, and control variate random variable γ, whose mean (μ_γ) is a statistical moment of c_l computed from the LFM, the unbiased MFMC estimator of μ_Γ is:*

$$\widehat{\mu_{\Gamma,MF}} = \widehat{\mu_{\Gamma,MC}}^{n_s} + \alpha(\widehat{\mu_{\gamma,MC}}^{m_s} - \widehat{\mu_{\gamma,MC}}^{n_s}), \quad m_s > n_s,$$

where α is the control variate constant, and $\widehat{\mu_{\Gamma,MC}}^{n_s}$ is the MC mean estimator of μ_Γ using n_s HFM samples, $\widehat{\mu_{\gamma,MC}}^{m_s}$ is the MC mean estimator of μ_γ using m_s LFM samples, and similar definitions apply to $\widehat{\mu_{\gamma,MC}}^{n_s}$.

Given a total computational budget $P_b = n_s + \frac{m_s}{w_c}$ and defining $r_m = \frac{m_s}{n_s}$, the MSE of this MFMC estimator is:

$$MSE\left[\widehat{\mu}_\Gamma^{MF}\right] = \frac{1}{P_b}(1 + \frac{r_m}{w_c})\left[\mathbb{V}[\Gamma] + \frac{r_m - 1}{r_m}(\alpha^2\mathbb{V}[\gamma] - 2\alpha Cov[\Gamma, \gamma])\right].$$

The MSE is minimized, solving Equation 4.1, when:

$$\alpha = \frac{Cov[\Gamma, \gamma]}{\mathbb{V}[\gamma]}, \quad and \;\; r_m = \sqrt{\frac{w_c Corr[\Gamma, \gamma]^2}{1 - Corr[\Gamma, \gamma]^2}}$$

where $Corr[\Gamma, \gamma]^2 = \frac{Cov[\Gamma,\gamma]^2}{(\mathbb{V}[\Gamma]\mathbb{V}[\gamma])}$.

Proof of Lemma 1: Refer to Ng and Willcox [37] or Peherstorfer et al. [86]. □

This lemma applies directly to the MFMC mean estimator in Equation (4.2) by substituting $\widehat{\mu_{\Gamma,MF}} = \widehat{\mu_{c,MF}}$, $\Gamma = c_h$ and $\gamma = c_l$. The MSE minimization leads to:

$$\alpha_\mu^* = \frac{\mathrm{Cov}[c_h, c_l]}{\sigma_l^2}, \quad \text{and} \;\; r_m = \sqrt{\frac{w_c \mathrm{Corr}[c_h, c_l]^2}{1 - \mathrm{Corr}[c_h, c_l]^2}}. \tag{4.7}$$

4.2.4 Optimal Strategy for MFMC Variance

To determine the optimal variables associated with the MFMC variance estimator employed in this work (Equation (4.6)), Lemma 1 is not directly applicable. The reason is that the variance (σ_h^2) is the second central moment parameter, hence leading

to $\Gamma = \vartheta_h = (c_h - \mu_h)^2$, $\gamma = \vartheta_l = (c_l - \mu_l)^2$, and $\widehat{\mu_{\Gamma,MF}} = \widehat{\mu_{\vartheta_h,MF}}$ in Lemma 1. The random variables ϑ_h and ϑ_l are defined in Equation (4.6). However, $\widehat{\mu_{\vartheta_h,MF}}$ is not practically computable, as the parameters μ_h and μ_l are not known, and are approximated by estimators $\widehat{\mu_{h,MC}}^{n_s}$, $\widehat{\mu_{l,MC}}^{m_s}$, and $\widehat{\mu_{l,MC}}^{n_s}$. Consequently, the expression for the MSE and the solution to the optimization problem in Equation 4.1 change. For this case, the closed form of the optimal α_σ is developed in the following lemma.

Lemma 2. *For the MFMC variance estimator $\widehat{\sigma^2_{c,MF}}$ in Equation* (4.3)*, the optimal α_σ that minimizes its MSE (see Equation* (4.6)*) is:*

$$\alpha^*_\sigma = \frac{\frac{1}{n_s}\left(Cov[\vartheta_h, \vartheta_l] + \frac{2}{n_s - 1} Cov[c_h, c_l]^2\right) - \frac{1}{m_s}\left(Cov[\vartheta_h, \vartheta_l] + \frac{2}{m_s - 1} Cov[c_h, c_l]^2\right)}{\frac{1}{n_s}(\delta_l - \frac{n_s - 3}{n_s - 1}\sigma_l^4) - \frac{1}{m_s}(\delta_l - \frac{m_s - 3}{m_s - 1}\sigma_l^4)}. \tag{4.8}$$

Proof of Lemma 2: See Appendix A.2. □

The α^*_σ also minimizes the MSE of the standard deviation estimator $\widehat{\sigma_{c,MF}}$ according to Lemma 14. Due to the complexity of MSE$[\widehat{\sigma^2_{c,MF}}]$, numerical methods are required to find the optimal n_s and m_s.

4.2.5 Approximation of Confidence Intervals

A useful attribute of MC estimators in statistical inference is that they can be used to calculated approximate confidence intervals, which provide bounds for the true values of the parameters. In this section, the CI approximation is extended for the case of MFMC estimators by employing limiting distribution approximations.

The approximate CI for the MFMC estimator of a generic statistical raw or central moment, as defined in Lemma 1, is developed. For notations, convergence in distribution is $\xrightarrow{\text{d}}$, a normal distribution characterized by mean μ and variance σ^2 is $\mathcal{N}(\mu, \sigma^2)$

Lemma 3. *Assuming Γ and γ are second order random variables, given the unbiased MFMC estimator $\widehat{\mu_{\Gamma,MF}}$ from Lemma 1 for the approximation of the statistical moment μ_Γ with an MSE of MSE $\left[\widehat{\mu_{\Gamma,MF}}\right]$ and assuming at least one of the following pairs of random variables are jointly normal:*

1. *the random variables Γ and γ;*
2. *the random variables $\widehat{\mu_{\Gamma,MC}}^{n_s}$ and $\widehat{\mu_{\gamma,MC}}^{m_s} - \widehat{\mu_{\gamma,MC}}^{n_s}$;*

3. the random variables $\widehat{\mu_{\gamma,MC}}^{m_s}$ *and* $\widehat{\mu_{\Gamma,MC}}^{n_s} - \alpha\widehat{\mu_{\gamma,MC}}^{n_s}$.

Then, the limiting distribution of the error of the estimator is normal:

$$\lim_{n_s\to\infty}\lim_{m_s\to\infty}\left(\widehat{\mu_{\Gamma,MF}} - \mu_\Gamma\right) \xrightarrow{d} \mathcal{N}(0, MSE\left[\widehat{\mu_{\Gamma,MF}}\right]),$$

and hence, the confidence interval for confidence level P_{CI} *is approximately:*

$$Pr\big(\mu_\Gamma \in \left[\widehat{\mu_{\Gamma,MF}} - z_{P_{CI}} MSE\left[\widehat{\mu_{\Gamma,MF}}\right], \widehat{\mu_{\Gamma,MF}} + z_{P_{CI}} MSE\left[\widehat{\mu_{\Gamma,MF}}\right]\right]\big) \approx P_{CI},$$

where $z_{P_{CI}}$ *depends on* P_{CI}*. Note that* $\mathbb{V}\left[\widehat{\mu_{\Gamma,MF}}\right] = MSE\left[\widehat{\mu_{\Gamma,MF}}\right]$ *due to the unbiasedness of the MFMC estimator.*

Proof of Lemma 3: See Appendix A.2.2. □

The desired probability of the confidence interval is P_{CI} and $z_{P_{CI}}$ is a parameter that depends on the value P_{CI} and the distribution. For example, a $P_{CI} = 99\%$ in normal distribution leads to $z_{99\%} \approx 2.575$, and a $P_{CI} = 90\%$ CI in normal distribution leads to $z_{90\%} \approx 1.645$. These CIs can also be considered as random variables since the bounds are based on estimators, which vary from sample set to sample set. What the CI reflects is that if several sample sets and the corresponding CIs are computed, approximately $P_{CI}\%$ of the CIs contain the true parameter.

The third assumption in Lemma 3 is typically directly applicable to multi-level Monte Carlo schemes. In MFMC, the n_s samples are a subset of the m_s samples, hence necessitating this assumption. In MLMC, the n_s and m_s samples are independent, meaning that $\widehat{\mu_{\gamma,MC}}^{m_s}$ and $\widehat{\mu_{\Gamma,MC}}^{n_s} - \alpha\widehat{\mu_{\gamma,MC}}^{n_s}$ are independent normal random variables by construction. Hence, the third assumption holds trivially for MLMC.

Lemma 3 is useful for describing the distribution and confidence interval associated with the $\widehat{\mu_{c,MF}}$ estimator. However, as the variance estimator $\widehat{\mu_{\vartheta_h,MF}}$ in Lemma 3 is not practically computable, a separate lemma is required to relate the limiting distribution of $\widehat{\mu_{\vartheta_h,MF}}$ with $\widehat{\sigma^2_{c,MF}}$.

Lemma 4. *Assuming* c_h *and* c_l *are second order random variables, and* α_σ *is a bounded constant, the MFMC variance estimator,* $\widehat{\sigma^2_{c,MF}}$*, defined in Equation* (4.6)*, has a limiting distribution that follows the distribution of* $\widehat{\mu_{\vartheta_h,MF}}$*:*

$$\lim_{n_s\to\infty}\lim_{m_s\to\infty}\widehat{\sigma^2_{c,MF}} \xrightarrow{d} \widehat{\mu_{\vartheta_h,MF}},$$

where $\xrightarrow{d}$ *denotes convergence in distribution, and*

$$\widehat{\mu_{\vartheta_h,MF}} = \widehat{\mu_{\vartheta_h,MC}}^{n_s} + \alpha_\sigma(\widehat{\mu_{\vartheta_l,MC}}^{m_s} - \widehat{\mu_{\vartheta_l,MC}}^{n_s}),$$

with $\vartheta_h = (c_h - \mu_h)^2$*, and* $\vartheta_l = (c_l - \mu_l)^2$*.*

Proof of Lemma 4: See Appendix A.2.3. □

With the assistance of Lemma 3 and Lemma 4, the following corollary summarizes the estimations of confidence intervals for the mean and variance parameters, employing the MFMC mean (Equation (4.2) and variance (Equation (4.3)) estimators.

Corollary 4.1. *Assuming the same premise as Lemma 3, the* P_{CI} *confidence interval for* $\widehat{\mu_{c,MF}}$ *estimation of* μ_h *is approximately:*

$$Pr\big(\mu_h \in \big[\widehat{\mu_{c,MF}} - z_{P_{CI}} MSE[\widehat{\mu_{c,MF}}], \widehat{\mu_{c,MF}} + z_{P_{CI}} MSE[\widehat{\mu_{c,MF}}]\big]\big) \approx P_{CI},$$

and the P_{CI} *confidence interval for* $\widehat{\sigma^2_{c,MF}}$ *estimation of* σ_h^2 *is approximately:*

$$Pr\Big(\sigma_h^2 \in \Big[\widehat{\sigma^2_{c,MF}} - z_{P_{CI}} MSE[\widehat{\sigma^2_{c,MF}}], \widehat{\sigma^2_{c,MF}} + z_{P_{CI}} MSE[\widehat{\sigma^2_{c,MF}}]\Big]\Big) \approx P_{CI}.$$

Proof of Corollary 4.1: For the CI associated with μ_h, Lemma 3 can be directly applied with $\Gamma = c_h$ and $\gamma = c_l$.

For the case of $\widehat{\sigma^2_{c,MF}}$, using Lemma 4, the limiting distribution of $\widehat{\sigma^2_{c,MF}}$ is approximately the same as that of $\widehat{\mu_{\vartheta_h,MF}}$. Hence:

$$\begin{aligned}
\lim_{n_s\to\infty}\lim_{m_s\to\infty}\left(\widehat{\sigma^2_{c,MF}} - \sigma_h^2\right) &= \lim_{n_s\to\infty}\lim_{m_s\to\infty}\left((\widehat{\sigma^2_{c,MF}} - \widehat{\mu_{\vartheta_h,MF}}) + (\widehat{\mu_{\vartheta_h,MF}} - \sigma_h^2)\right), \\
&\xrightarrow{\text{d}} \lim_{n_s\to\infty}\lim_{m_s\to\infty}(\widehat{\mu_{\vartheta_h,MF}} - \sigma_h^2), \\
&\sim \mathcal{N}(0, \text{MSE}\left[\widehat{\mu_{\vartheta_h,MF}}\right]).
\end{aligned}$$

The third line is from the application of Lemma 3 to $\widehat{\mu_{\vartheta_h,MF}}$. Approximating MSE $\left[\widehat{\mu_{\vartheta_h,MF}}\right]$ with MSE$[\widehat{\mu_{c,MF}}]$, the CI associated with σ_h^2 is deduced. □

In practical problems, the assumptions required by Lemma 3 do not need to hold exactly. As long as they are approximately true, the confidence interval provides a reasonable approximation as long as P_{CI} is not too demanding.

4.2.6 Practical MSE Computations

Computing the MSE of the MFMC estimators as well as α_μ^* and α_σ^* involves complex population parameters, including: σ_h^2, σ_l^2, δ_h, δ_l, σ_h^4, σ_l^4, σ_h^3, $\text{Cov}[c_h, c_l]$, $\text{Cov}[c_h, c_l]^2$, and $\text{Cov}[\vartheta_h, \vartheta_l]$. In optimization applications, a pilot sample set consisting of n_{plt} HFM and LFM samples are available for approximating these quantities. Hence, unbiased estimators of these parameters that can be computed with a pilot sample set are required.

For the unbiased estimation of the central moment parameters σ_h^2, σ_l^2, δ_h, and δ_l, their estimators are well-established, and are summarized in Corollary 15.1 in Appendix A.2.5.

For the unbiased estimation of σ_h^4 and σ_l^4, consider the general form of σ_c^4. Although σ_c^4 could be estimated with $(\widehat{\sigma_c^2})^2$, this is a biased estimation even if $\widehat{\sigma_c^2}$ is an unbiased estimator of σ_c^2. In general, the product of unbiased estimators does not lead to a new unbiased estimator, meaning that $\mathbb{E}\left[(\widehat{\sigma_c^2})^2\right] \neq \sigma_c^4$. Hence, an unbiased MC estimator of σ_c^4 is developed in Lemma 5.

Lemma 5. *Given n_s MC samples as well as the unbiased MC sample variance estimator $\widehat{\sigma_{c,MC}^2}$ and the unbiased MC fourth central moment estimator $\widehat{\delta}_c$, an unbiased MC estimator for the square of the population variance, σ_c^4, is given as:*

$$\widehat{\sigma_c^4} = \frac{n_s(n_s-1)}{n_s^2-2n_s+3}(\widehat{\sigma_{c,MC}^2})^2 - \frac{n_s-1}{n_s^2-2n_s+3}\widehat{\delta}_c. \tag{4.9}$$

Proof of Lemma 5: See Appendix A.2.4. □

Using Lemma 5, the unbiased estimators of σ_h^4 and σ_l^4 are provided in Corollary 5.1.

Corollary 5.1. *Given n_{plt} pilot samples of c_h evaluated from the HFM and c_l evaluated from the LFM, the unbiased estimators of σ_h^4 and σ_l^4 are:*

$$\widehat{\sigma_h^4} = \frac{n_{plt}(n_{plt}-1)}{n_{plt}^2-2n_{plt}+3}\left(\widehat{\sigma_h^2}\right)^2 - \frac{n_{plt}-1}{n_{plt}^2-2n_{plt}+3}\widehat{\delta_h}; \tag{4.10}$$

$$\widehat{\sigma_l^4} = \frac{n_{plt}(n_{plt}-1)}{n_{plt}^2-2n_{plt}+3}\left(\widehat{\sigma_l^2}\right)^2 - \frac{n_{plt}-1}{n_{plt}^2-2n_{plt}+3}\widehat{\delta_l}. \tag{4.11}$$

Proof of Corollary 5.1: The $\widehat{\sigma_h^4}$ and $\widehat{\sigma_l^4}$ are derived following the result of Lemma 5, replacing n_s with n_{plt}, and the individual estimators with HFM or LFM estimators. □

For σ_h^3, it is difficult to derive a general unbiased estimator due to issues associated with the square root. Given the n_{plt} pilot samples, it is estimated using:

$$\sigma_h^3 \approx \widehat{\sigma_h^3} = \widehat{\sigma_h^2}^{3/2},$$

where $\widehat{\sigma_h^2}$ is the MC estimator given by Equation (A.10).

Before deriving the unbiased estimators for the covariance parameters $\mathrm{Cov}[c_h, c_l]$, $\mathrm{Cov}[c_h, c_l]^2$, and $\mathrm{Cov}[\vartheta_h, \vartheta_l]$, Lemmata 6 and 7 are first presented to simplify the process. These two lemmata provide general expressions for the unbiased MC estimators of a generic product between two or three parameters.

Lemma 6. *Given two random variables of interest A and B, and n_s MC samples. The unbiased MC estimators of their mean $\mu_A = \mathbb{E}[A]$ and $\mu_B = \mathbb{E}[B]$ is $\widehat{\mu_A} = \frac{1}{n_s}\sum_{i=1}^{n_s} A_i$ and $\widehat{\mu_B} = \frac{1}{n_s}\sum_{i=1}^{n_s} B_i$. The unbiased MC estimators of their product $\mu_{AB} = \mathbb{E}[AB]$ is $\widehat{\mu_{AB}} = \frac{1}{n_s}\sum_{i=1}^{n_s} A_i B_i$. An unbiased MC estimator for approximating the product parameter $\mu_A\mu_B = \mathbb{E}[A]\mathbb{E}[B]$ is given as:*

$$\widehat{\mu_A\mu_B} = \frac{1}{n_s - 1}\left(n_s\widehat{\mu_A}\widehat{\mu_B} - \widehat{\mu_{AB}}\right). \tag{4.12}$$

Proof of Lemma 6: See Appendix A.2.6. □

Lemma 7. *Given three random variables of interest A, B and C, as well as n_s MC samples, the unbiased MC estimators of their mean $\mu_A = \mathbb{E}[A]$, $\mu_B = \mathbb{E}[B]$, and $\mu_C = \mathbb{E}[C]$ are $\widehat{\mu_A} = \frac{1}{n_s}\sum_{i=1}^{n_s} A_i$, $\widehat{\mu_B} = \frac{1}{n_s}\sum_{i=1}^{n_s} B_i$, and $\widehat{\mu_C} = \frac{1}{n_s}\sum_{i=1}^{n_s} C_i$. The unbiased MC estimators of the pairwise products $\mu_{AB}\mu_C = \mathbb{E}[AB]\mathbb{E}[C]$, $\mu_{AC}\mu_B = \mathbb{E}[AC]\mathbb{E}[B]$, and $\mu_{BC}\mu_A = \mathbb{E}[BC]\mathbb{E}[A]$, are provided by Lemma 6 as $\widehat{\mu_{AB}\mu_C}$, $\widehat{\mu_{AC}\mu_B}$, and $\widehat{\mu_{BC}\mu_A}$. The unbiased MC estimator of the triple product of the random variables $\mu_{ABC} = \mathbb{E}[ABC]$ is $\widehat{\mu_{ABC}} = \frac{1}{n_s}\sum_{i=1}^{n_s} A_i B_i C_i$. An unbiased MC estimator for approximating the product parameter $\mu_A\mu_B\mu_C = \mathbb{E}[A]\mathbb{E}[B]\mathbb{E}[C]$ is given as:*

$$\widehat{\mu_A\mu_B\mu_C} = \frac{1}{(n_s-1)(n_s-2)}\left(n_s^2\widehat{\mu_A}\widehat{\mu_B}\widehat{\mu_C} - \widehat{\mu_{ABC}} - (n_s-1)(\widehat{\mu_{AB}\mu_C} + \widehat{\mu_{AC}\mu_B} + \widehat{\mu_{BC}\mu_A})\right) \tag{4.13}$$

Proof of Lemma 7: See Appendix A.2.7. □

Remark 1. *Using the result of Lemma 6 and replacing random variables A and B appropriately leads to the following unbiased estimators: $\widehat{\mu_{h^2}\mu_h}$ obtained from $A = c_h^2$ and $B = c_h$; $\widehat{\mu_{l^2}\mu_l}$ obtained from $A = c_l^2$ and $B = c_l$; $\widehat{\mu_{hl}^2}$ obtained from $A = B = c_h c_l$; $\widehat{\mu_{h^2}\mu_{l^2}}$ obtained from $A = c_h^2$ and $B = c_l^2$; $\widehat{\mu_{h^2 l}\mu_l}$ obtained from $A = c_h^2 c_l$ and $B = c_l$;*

$\widehat{\mu_{hl^2}\mu_h}$ obtained from $A = c_h c_l^2$ and $B = c_h$; $\widehat{\mu_{l^2}\mu_h}$ obtained from $A = c_l^2$ and $B = c_h$; $\widehat{\mu_{hl}\mu_l}$ obtained from $A = c_h c_l$ and $B = c_l$; $\widehat{\mu_{h^2}\mu_l}$ obtained from $A = c_h^2$ and $B = c_l$; and $\widehat{\mu_{hl}\mu_h}$ obtained from $A = c_h c_l$ and $B = c_h$.

Using the result of Lemma 7 as well as the pre, replacing A, B and C appropriately leads to following unbiased estimators: $\widehat{\mu_h^3}$ obtained from $A = B = C = c_h$ $\widehat{\mu_l^3}$ obtained from $A = B = C = c_l$ $\widehat{\mu_{hl}\mu_h\mu_l}$ obtained from $A = c_h c_l$, $B = c_h$, and $C = c_l$; $\widehat{\mu_{h^2}\mu_l^2}$ obtained from $A = c_h^2$, $B = c_l$, and $C = c_l$; $\widehat{\mu_{l^2}\mu_h^2}$ obtained from $A = c_l^2$, $B = c_h$, and $C = c_h$; $\widehat{\mu_h\mu_l\mu_l}$ obtained from $A = c_h$, $B = c_l$, and $C = c_l$; and $\widehat{\mu_l\mu_h\mu_h}$ obtained from $A = c_l$, $B = c_h$, and $C = c_h$.

The lemma presented below is for estimating the parameter $\mu_h^2\mu_l^2$, which leads to a fourth order estimator, as it is the product of four individual parameters.

Lemma 8. *Given n_{plt} pilot samples of c_h from evaluation of HFM and c_l from evaluation of LFM, as well as unbiased MC estimators $\widehat{\mu_h} = \frac{1}{n_{plt}}\sum_{i=1}^{n_{plt}} c_{h,i}$, $\widehat{\mu_l} = \frac{1}{n_{plt}}\sum_{i=1}^{n_{plt}} c_{l,i}$, $\widehat{\mu_{h^2l^2}} = \frac{1}{n_{plt}}\sum_{i=1}^{n_{plt}} c_{h,i}^2 c_{l,i}^2$, an unbiased MC estimator for approximating $\mu_h^2\mu_l^2$ is:*

$$\begin{aligned}\widehat{\mu_h^2\mu_l^2} = \frac{1}{(n_{plt}-2)(n_{plt}-3)}\Bigg(&\frac{n_{plt}^3}{n_{plt}-1}\widehat{\mu_h}^2\widehat{\mu_l}^2 - \frac{1}{n_{plt}-1}\widehat{\mu_{h^2l^2}} - 2\widehat{\mu_{h^2l}\mu_l} \\ &- 2\widehat{\mu_{hl^2}\mu_h} - 2\widehat{\mu_{hl}^2} - \widehat{\mu_{h^2}\mu_{l^2}} - (n_{plt}-2)\widehat{\mu_{h^2}\mu_l^2} \\ &- (n_{plt}-2)\widehat{\mu_{l^2}\mu_h^2} - 4(n_{plt}-2)\widehat{\mu_{hl}\mu_h\mu_l}\Bigg),\end{aligned} \tag{4.14}$$

where the expressions for $\widehat{\mu_{h^2l}\mu_l}$, $\widehat{\mu_{hl^2}\mu_h}$, $\widehat{\mu_{hl}^2}$, $\widehat{\mu_{h^2}\mu_{l^2}}$, $\widehat{\mu_{h^2}\mu_l^2}$, $\widehat{\mu_{l^2}\mu_h^2}$, and $\widehat{\mu_{hl}\mu_h\mu_l}$ are discussed in Remark 1.

Proof of Lemma 8: See Appendix A.2.9. □

The unbiased estimator for $\mathrm{Cov}[c_h, c_l]$ is shown in Corollary 8.1 below. This corollary makes use of Lemma 16 in Appendix A.2.8, whose result provides a general unbiased estimator for a generic $\mathrm{Cov}[\cdot,\cdot]$ parameter.

Corollary 8.1. *Given n_{plt} pilot samples of c_h evaluated from the HFM and c_l evaluated from the LFM, as well as unbiased MC estimators $\widehat{\mu_h} = \frac{1}{n_{plt}}\sum_{i=1}^{n_{plt}} c_{h,i}$, $\widehat{\mu_l} = \frac{1}{n_{plt}}\sum_{i=1}^{n_{plt}} c_{l,i}$, and $\widehat{\mu_{hl}} = \frac{1}{n_{plt}}\sum_{i=1}^{n_{plt}} c_{h,i}c_{l,i}$, an unbiased estimator for $Cov[c_h, c_l]$ is:*

$$\widehat{Cov[c_h, c_l]} = \frac{1}{n_{plt}-1}\left(n_{plt}\widehat{\mu_h}\widehat{\mu_l} - \widehat{\mu_{hl}}\right), \tag{4.15}$$

Proof of Corollary 8.1: Using the result of Lemma 16, replacing the random variables A and B with c_h and c_l leads to the estimator for $\mathrm{Cov}[c_h, c_l]$. □

The unbiased estimators for $\text{Cov}[c_h, c_l]^2$ and $\text{Cov}[\vartheta_h, \vartheta_l]$, which are high order statistics are derived in the following lemmata.

Lemma 9. *Given n_{plt} pilot samples of c_h evaluated from the HFM and c_l evaluated from the LFM and using the unbiased estimators discussed in Remark 1 and Lemma 8, an unbiased estimator for $Cov[c_h, c_l]^2$ is:*

$$\widehat{Cov[c_h, c_l]}^2 = \widehat{\mu_{hl}^2} - 2\widehat{\mu_{hl}\mu_h\mu_l} + \widehat{\mu_h^2\mu_l^2}. \tag{4.16}$$

Proof of Lemma 9: Expanding based on the definition of $\text{Cov}[c_h, c_l]^2$:

$$\text{Cov}[c_h, c_l]^2 = (\mathbb{E}[c_h c_l] - \mathbb{E}[c_h]\mathbb{E}[c_l])^2 = \mathbb{E}[c_h c_l]^2 - 2\mathbb{E}[c_h c_l]\mathbb{E}[c_h]\mathbb{E}[c_l] + \mathbb{E}[c_h]^2\mathbb{E}[c_l]^2.$$

Noting that $\mathbb{E}[c_h c_l]^2 = \mu_{hl}^2$, $\mathbb{E}[c_h c_l]\mathbb{E}[c_h]\mathbb{E}[c_l] = \mu_{hl}\mu_h\mu_l$, and $\mathbb{E}[c_h]^2\mathbb{E}[c_l]^2 = \mu_h^2\mu_l^2$, these parameters are replaced by their unbiased estimators discussed in Remark 1. This leads to the expression for $\widehat{\text{Cov}[c_h, c_l]}^2$ in Equation (4.16). This estimator is unbiased since taking the expected value of the right hand side of Equation (4.16) leads to $\text{Cov}[c_h, c_l]^2$, as shown above. □

Lemma 10. *Given n_{plt} pilot samples of c_h evaluated from the HFM and c_l evaluated from the LFM, and using the unbiased estimators discussed in Remark 1 and Lemma 8, an unbiased estimator for $Cov[\vartheta_h, \vartheta_l]$ is:*

$$\widehat{Cov[\vartheta_h, \vartheta_l]} = \widehat{Cov[c_h^2, c_l^2]} - 2\mu_l\widehat{Cov[c_h^2, c_l]} - 2\mu_h\widehat{Cov[c_h, c_l^2]} + 4\mu_h\mu_l\widehat{Cov[c_h, c_l]}, \tag{4.17}$$

where

$$\widehat{Cov[c_h^2, c_l^2]} = \frac{n_{plt}}{n_{plt} - 1}\left(\widehat{\mu_{h^2l^2}} - \widehat{\mu_{h^2}}\widehat{\mu_{l^2}}\right). \tag{4.18}$$

$$\mu_l\widehat{Cov[c_h^2, c_l]} = \widehat{\mu_{h^2l}\mu_l} - \widehat{\mu_{h^2}\mu_l^2}, \tag{4.19}$$

$$\mu_h\widehat{Cov[c_h, c_l^2]} = \widehat{\mu_{hl^2}\mu_h} - \widehat{\mu_{l^2}\mu_h^2}, \tag{4.20}$$

and

$$\mu_h\mu_l\widehat{Cov[c_h, c_l]} = \widehat{\mu_{hl}\mu_h\mu_l} - \widehat{\mu_h^2\mu_l^2}. \tag{4.21}$$

Proof of Lemma 10: See Appendix A.2.10. □

4.3 Robust Compliance Estimator

In the previous sections, the unbiased estimators and their MSEs for approximating the mean, variance, and standard deviation are presented for both MC and MFMC schemes. For robust topology optimization, the quantity of interest is the robust compliance, which is a linear combination of the mean and standard deviation of compliance. For MFMC and MLMC schemes, the optimal estimation strategies for this QOI and approximations for its MSE are not well-established in the literature. Existing estimates target a single statistical moment, so MFMC and MLMC schemes focusing on complex QOIs are rarely explored. For example, Menhorn et al. [71] devised strategies for QOI in robust optimization but for the MLMC scheme, while Ayoul-Guilmard et al. [73] formulated estimation strategies for conditional-value-at-risk quantities, again only for MLMC applications.

The goal of this section is to investigate strategies for calculating optimal MFMC estimators for the robust compliance, which requires approximation of its MSE. This work focuses on the scenario where the computational budget is fixed, and the MSE of the estimator is minimized. The robust compliance estimator is a weighted sum of the mean and standard deviation estimators. For the standard MC scheme, it is:

$$\widehat{c_{R,MC}} = \widehat{\mu_{c,MC}} + \kappa\widehat{\sigma_{c,MC}}. \tag{4.22}$$

For the MFMC scheme, it is:

$$\widehat{c_{R,MF}} = \widehat{\mu_{c,MF}} + \kappa\widehat{\sigma_{c,MF}}. \tag{4.23}$$

4.3.1 Mean Squared Error of a Robust Compliance Estimator

For a robust compliance estimator ($\widehat{c_R}$) formulated as a weighted sum of mean and standard deviation estimators, this section presents one novel upper bound for the MSE of $\widehat{c_R}$, one novel approximation of the MSE of $\widehat{c_R}$, and an alternative upper bound for the MSE of $\widehat{c_R}$ that was developed by Menhorn et al. [71] for MLMC.

This work focuses on the MSE of the estimator, unlike other literature on MLMC and MFMC, which focuses on reducing the variance of the estimators [71, 87]. The majority of literature considers variance reduction since MFMC and MLMC estimators developed targeting single statistical moments are typically unbiased, hence their MSEs are equivalent to their variances. However, the standard deviation estimator

is biased, hence $\widehat{c_R}$ is also biased, and it is more appropriate to consider MSE, which is a combination of the bias and variance of the estimator. The MSE estimates for a generic $\widehat{c_R}$ estimator are presented in Theorem 1.

Theorem 1. *Given an unbiased mean estimator $\widehat{\mu}_c$ and an unbiased variance estimator $\widehat{\sigma}_c^2$, the estimator for the robust compliance (c_R) is:*

$$\widehat{c_R} = \widehat{\mu}_c + \kappa\sqrt{\widehat{\sigma}_c^2}. \tag{4.24}$$

An upper bound for the MSE of $\widehat{c_R}$, denoted as $MSE[\widehat{c_R}]_{cs}^{ub}$, is:

$$MSE[\widehat{c_R}] \leq MSE[\widehat{c_R}]_{cs}^{ub} = (1 + \kappa\frac{\sigma_c}{\mu_c})MSE[\widehat{\mu}_c] + \left(\frac{\kappa^2}{4\sigma_c^2} + \frac{\kappa\mu_c}{4\sigma_c^3}\right) MSE\left[\widehat{\sigma}_c^2\right]. \tag{4.25}$$

An alternative upper bound for the MSE of $\widehat{c_R}$, denoted as $MSE[\widehat{c_R}]_p^{ub}$, is:

$$MSE[\widehat{c_R}] \leq MSE[\widehat{c_R}]_p^{ub} = MSE[\widehat{\mu}_c] + \frac{\kappa^2}{4\sigma_c^2}MSE\left[\widehat{\sigma}_c^2\right] + \frac{\kappa}{\sigma_c}\sqrt{MSE[\widehat{\mu}_c]MSE\left[\widehat{\sigma}_c^2\right]}. \tag{4.26}$$

An estimation for this MSE, denoted as $MSE[\widehat{c_R}]_{\mu\sigma}$, is:

$$MSE[\widehat{c_R}] \approx MSE[\widehat{c_R}]_{\mu\sigma} = MSE[\widehat{\mu}_c] + \frac{\kappa^2}{4\sigma_c^2}MSE\left[\widehat{\sigma}_c^2\right] - \kappa\mu_c\sigma_c + \frac{\kappa}{\sigma_c}\mathbb{E}\left[\widehat{\mu}_c\widehat{\sigma}_c^2\right]. \tag{4.27}$$

Proof of Theorem 1: See Appendix A.3.1. □

The $\mathrm{MSE}[\widehat{c_R}]_{\mathrm{p}}^{\mathrm{ub}}$ bound is derived by Menhorn et al. [71] in the context of MLMC. Their derivation uses the Pearson correlation relation and is based on variance reduction of $\widehat{c_R}$. This thesis is based on the reduction of MSE, as both the $\mathrm{MSE}[\widehat{c_R}]_{\mathrm{p}}^{\mathrm{ub}}$ and $\mathrm{MSE}[\widehat{c_R}]_{\mathrm{cs}}^{\mathrm{ub}}$ bounds are formulated with the Cauchy-Schwarz inequality. The subscript *cs* refers to the application of Cauchy-Schwarz in deriving $\mathrm{MSE}[\widehat{c_R}]_{\mathrm{cs}}^{\mathrm{ub}}$, the subscript *p* refers to the alternative derivation of $\mathrm{MSE}[\widehat{c_R}]_{\mathrm{p}}^{\mathrm{ub}}$ using the Pearson correlation relation, and the subscript $\mu\sigma$ refers to the product of moments required in the expression of $\mathrm{MSE}[\widehat{c_R}]_{\mu\sigma}$.

The closed form expression of MSE is necessary for quality control of the estimator, and for MFMC it is used as an objective function to select several variables through the minimization procedure of Equation (4.1). In Theorem 1, $\mathrm{MSE}[\widehat{c_R}]_{\mu\sigma}$ provides a direct estimation of the MSE and when possible it should be used as the objective function. However, $\mathrm{MSE}[\widehat{c_R}]_{\mu\sigma}$ depends on products of raw moments that may be difficult to compute with high accuracy using a small set of pilot samples. The

upper bounds $\text{MSE}[\widehat{c_R}]_{\text{cs}}^{\text{ub}}$ and $\text{MSE}[\widehat{c_R}]_{\text{p}}^{\text{ub}}$ only depend on the MSEs of mean and variance estimators, which have small magnitudes and can be computed with reasonable accuracy using pilot samples. Hence, they are alternative objective functions for the selection of MFMC variables. Since the upper bounds are not direct approximations of the MSE, minimizing the bounds will reduce the MSE, but may not minimize the MSE. The two upper bounds exploit different correlation structures of the estimators, and hence their efficacy depends on the details of a particular problem.

4.3.2 Computation of MSE for MC Robust Compliance

To compute the expressions in Theorem 1 for the case of MC robust compliance, in addition to the MSEs of mean and variance estimators, the parameter $\mathbb{E}\left[\widehat{\mu}_c\widehat{\sigma}_c^2\right]$ is required. This is an expected value of the product of two estimators, which for the case of the MC scheme is $\mathbb{E}\left[\widehat{\mu_{c,MC}}\widehat{\sigma_{c,MC}^2}\right]$. Bootstrapping methods using multiple sets of samples can be used to compute this value. However, this requires multiple unique evaluations of each estimator. For optimization problems, typically, only one set of MC samples is available per iteration, and bootstrapping cannot be employed to approximate this parameter. To alleviate this, algebraic manipulations are done to re-express $\mathbb{E}\left[\widehat{\mu_{c,MC}}\widehat{\sigma_{c,MC}^2}\right]$ in terms of statistics that can be estimated using one set of MC samples. Lemma 11 provides the expended expression of the expected value of terms with the general form $\widehat{\mu_{A,MC}}^{n_A}\widehat{\sigma_{B,MC}^2}^{n_B}$, which can be applied for the case of $\mathbb{E}\left[\widehat{\mu_{c,MC}}\widehat{\sigma_{c,MC}^2}\right]$.

Lemma 11. *Given two random variables A and B, as well as the unbiased MC mean estimator $\widehat{\mu_{A,MC}}^{n_A}$ for A using n_A samples and the unbiased MC variance estimator $\widehat{\sigma_{B,MC}^2}^{n_B}$ for B using n_B samples. Assuming the individual samples are independent, then the expected value of $\widehat{\mu_{A,MC}}^{n_A}\widehat{\sigma_{B,MC}^2}^{n_B}$ is:*

$$\begin{aligned}\mathbb{E}\left[\widehat{\mu_{A,MC}}^{n_A}\widehat{\sigma_{B,MC}^2}^{n_B}\right] = \frac{1}{q}\mathbb{E}\left[AB^2\right] + \frac{q-1}{q}\mathbb{E}[A]\mathbb{E}\left[B^2\right] \\ - \frac{2}{q}\mathbb{E}[AB]\mathbb{E}[B] - \frac{q-2}{q}\mathbb{E}[A]\mathbb{E}[B]^2,\end{aligned} \tag{4.28}$$

where $q = \max(n_A, n_B)$.

Proof of Lemma 11: See Appendix A.3.2. □

Using Lemma 11, the complete unbiased estimator for $\mathbb{E}\left[\widehat{\mu_{c,MC}}\widehat{\sigma_{c,MC}^2}\right]$ is provided in Corollary 11.1 below.

Corollary 11.1. *An unbiased estimator for* $\mathbb{E}\left[\widehat{\mu_{c,MC}}\widehat{\sigma^2_{c,MC}}\right]$ *is:*

$$\mathbb{E}\left[\widehat{\widehat{\mu_{c,MC}}\widehat{\sigma^2_{c,MC}}}\right] = \frac{1}{n_s}\widehat{\mu_{c^3}} + \frac{n_s-3}{n_s}\widehat{\mu_{c^2}\mu_c} - \frac{n_s-2}{n_s}\widehat{\mu^3_c}. \tag{4.29}$$

Proof of Corollary 11.1: Using the result of Lemma 11 and substituting $n_A = n_B = n_s$ and $A = B = c$ leads to

$$\mathbb{E}\left[\widehat{\mu_{c,MC}}\widehat{\sigma^2_{c,MC}}\right] = \frac{1}{n_s}\mu_{c^3} + \frac{n_s-3}{n_s}\mu_{c^2}\mu_c - \frac{n_s-2}{n_s}\mu^3_c.$$

The unbiased MC estimators $\widehat{\mu_{c^3}}$, $\widehat{\mu_{c^2}\mu_c}$ and $\widehat{\mu^3_c}$ are discussed in Remark 2. Substituting these estimators for their corresponding parameters in the above expression leads to Equation (4.29). □

4.3.3 Computation of MSE for MFMC Robust Compliance

Similarly, to compute the expressions in Theorem 1 for the case of MFMC robust compliance, $\mathbb{E}\left[\widehat{\mu_{c,MF}}\widehat{\sigma^2_{c,MF}}\right]$ is required. Even though this parameter can be approximated using a bootstrap approach, for the purpose of optimization which has one set of samples for each iteration, an alternative formulation is required. The approach is to expand $\mathbb{E}\left[\widehat{\mu_{c,MF}}\widehat{\sigma^2_{c,MF}}\right]$ to individual parameters that can be approximated using one set of pilot samples of compliance evaluated from the HFM and LFM. When the individual parameters are approximated with their estimators, an unbiased estimator for $\mathbb{E}\left[\widehat{\mu_{c,MF}}\widehat{\sigma^2_{c,MF}}\right]$ is obtained.

Given constants α_μ and α_σ, expand $\mathbb{E}\left[\widehat{\mu_{c,MF}}\widehat{\sigma^2_{c,MF}}\right]$ as:

$$\begin{aligned}
\mathbb{E}\left[\widehat{\mu_{c,MF}}\widehat{\sigma^2_{c,MF}}\right] &= \mathbb{E}\left[\left(\widehat{\mu_{h,MC}}^{n_s} + \alpha_\mu(\widehat{\mu_{l,MC}}^{m_s} - \widehat{\mu_{l,MC}}^{n_s})\right)\left(\widehat{\sigma^2_{h,MC}}^{n_s} + \alpha_\sigma(\widehat{\sigma^2_{l,MC}}^{m_s} - \widehat{\sigma^2_{l,MC}}^{n_s})\right)\right], \\
&= \mathbb{E}\left[\widehat{\mu_{h,MC}}^{n_s}\widehat{\sigma^2_{h,MC}}^{n_s}\right] + \alpha_\sigma\mathbb{E}\left[\widehat{\mu_{h,MC}}^{n_s}\widehat{\sigma^2_{l,MC}}^{m_s}\right] - \alpha_\sigma\mathbb{E}\left[\widehat{\mu_{h,MC}}^{n_s}\widehat{\sigma^2_{l,MC}}^{n_s}\right] \\
&\quad + \alpha_\mu\mathbb{E}\left[\widehat{\mu_{l,MC}}^{m_s}\widehat{\sigma^2_{h,MC}}^{n_s}\right] + \alpha_\mu\alpha_\sigma\mathbb{E}\left[\widehat{\mu_{l,MC}}^{m_s}\widehat{\sigma^2_{l,MC}}^{m_s}\right] \\
&\quad - \alpha_\mu\alpha_\sigma\mathbb{E}\left[\widehat{\mu_{l,MC}}^{m_s}\widehat{\sigma^2_{l,MC}}^{n_s}\right] - \alpha_\mu\mathbb{E}\left[\widehat{\mu_{l,MC}}^{n_s}\widehat{\sigma^2_{h,MC}}^{n_s}\right] \\
&\quad - \alpha_\mu\alpha_\sigma\mathbb{E}\left[\widehat{\mu_{l,MC}}^{n_s}\widehat{\sigma^2_{l,MC}}^{m_s}\right] + \alpha_\mu\alpha_\sigma\mathbb{E}\left[\widehat{\mu_{l,MC}}^{n_s}\widehat{\sigma^2_{l,MC}}^{n_s}\right].
\end{aligned} \tag{4.30}$$

The expression above consists of the expected value of terms with the general form $\widehat{\mu_{A,MC}}^{n_A}\widehat{\sigma^2_{B,MC}}^{n_B}$, and its expanded expression is provided in Lemma 11, where the random variables A and B correspond to either c_h or c_l, while n_A and n_B corresponds

to either the n_s or m_s independent samples used in the MC scheme. The expanded expression of $\widehat{\mu_{A,MC}}^{n_A}\widehat{\sigma^2_{B,MC}}^{n_B}$ is in Lemma 11, which helps to derive unbiased estimators for variants of the $\widehat{\mu_{A,MC}}^{n_A}\widehat{\sigma^2_{B,MC}}^{n_B}$ terms in Equation (4.30), and they are discussed in Remark 2.

Remark 2. *Given n_{plt} pilot samples of c_h from evaluation of the HFM and c_l from evaluation of the LFM, combining the result of Lemma 11 and the unbiased estimators discussed in Remark 1, the unbiased estimators for the parameters: $\mathbb{E}\left[\widehat{\mu_{h,MC}}^{n_s}\widehat{\sigma^2_{h,MC}}^{n_s}\right]$, $\mathbb{E}\left[\widehat{\mu_{h,MC}}^{n_s}\widehat{\sigma^2_{l,MC}}^{m_s}\right]$, $\mathbb{E}\left[\widehat{\mu_{h,MC}}^{n_s}\widehat{\sigma^2_{l,MC}}^{n_s}\right]$, $\mathbb{E}\left[\widehat{\mu_{l,MC}}^{m_s}\widehat{\sigma^2_{h,MC}}^{n_s}\right]$, $\mathbb{E}\left[\widehat{\mu_{l,MC}}^{n_s}\widehat{\sigma^2_{h,MC}}^{n_s}\right]$, $\mathbb{E}\left[\widehat{\mu_{l,MC}}^{m_s}\widehat{\sigma^2_{l,MC}}^{m_s}\right]$, and $\mathbb{E}\left[\widehat{\mu_{l,MC}}^{n_s}\widehat{\sigma^2_{l,MC}}^{n_s}\right]$ are obtained. For brevity, the full expressions are not shown.*

All the ingredients for constructing an unbiased estimator for $\mathbb{E}\left[\widehat{\mu_{c,MF}}\widehat{\sigma^2_{c,MF}}\right]$ are available:

Lemma 12. *Given constants α_μ and α_σ and n_{plt} pilot samples of c_h evaluated from the HFM and c_l evaluated from the LFM, an unbiased estimator for $\mathbb{E}\left[\widehat{\mu_{c,MF}}\widehat{\sigma^2_{c,MF}}\right]$ is:*

$$\begin{aligned}\mathbb{E}\left[\widehat{\mu_{c,MF}}\widehat{\sigma^2_{c,MF}}\right] = {} & \mathbb{E}\left[\widehat{\mu_{h,MC}}^{n_s}\widehat{\sigma^2_{h,MC}}^{n_s}\right] + \alpha_\sigma\mathbb{E}\left[\widehat{\mu_{h,MC}}^{n_s}\widehat{\sigma^2_{l,MC}}^{m_s}\right] - \alpha_\sigma\mathbb{E}\left[\widehat{\mu_{h,MC}}^{n_s}\widehat{\sigma^2_{l,MC}}^{n_s}\right] \\ & + \alpha_\mu\mathbb{E}\left[\widehat{\mu_{l,MC}}^{m_s}\widehat{\sigma^2_{h,MC}}^{n_s}\right] + \alpha_\mu\alpha_\sigma\mathbb{E}\left[\widehat{\mu_{l,MC}}^{m_s}\widehat{\sigma^2_{l,MC}}^{m_s}\right] \\ & - \alpha_\mu\alpha_\sigma\mathbb{E}\left[\widehat{\mu_{l,MC}}^{m_s}\widehat{\sigma^2_{l,MC}}^{n_s}\right] - \alpha_\mu\mathbb{E}\left[\widehat{\mu_{l,MC}}^{n_s}\widehat{\sigma^2_{h,MC}}^{n_s}\right] \\ & - \alpha_\mu\alpha_\sigma\mathbb{E}\left[\widehat{\mu_{l,MC}}^{n_s}\widehat{\sigma^2_{l,MC}}^{m_s}\right] + \alpha_\mu\alpha_\sigma\mathbb{E}\left[\widehat{\mu_{l,MC}}^{n_s}\widehat{\sigma^2_{l,MC}}^{n_s}\right].\end{aligned} \tag{4.31}$$

Proof of Lemma 12: Using the expanded form of $\mathbb{E}\left[\widehat{\mu_{c,MF}}\widehat{\sigma^2_{c,MF}}\right]$ in Equation (4.30), and substituting the expected value parameters in the right hand side of the equation with their respective unbiased estimators discussed in Remark 2, the unbiased estimator $\mathbb{E}\left[\widehat{\mu_{c,MF}}\widehat{\sigma^2_{c,MF}}\right]$ is obtained. □

Ultimately, given n_{plt} pilot samples, and constants α_μ, α_σ, n_s, and m_s, all the expressions required by the MFMC scheme for computing the robust compliance estimator and its MSE approximations are available. The n_{plt} samples used to compute the unbiased estimators are decided based on required statistical confidence and are generally set heuristically, typically more than 30.

4.3.4 Optimal Control Variate Coefficients and Sample Allocation

For the MFMC scheme, the goal is to minimize the MSE of a robust compliance estimator while respecting a total available computational budget. Hence, the final ingredients is are the optimal values of α_μ, α_σ, n_s, and m_s. This is achieved by solving the optimization problem in Equation (4.1) using one of the expressions in Theorem 1 as the objective function.

For the cases where the upper bounds $\text{MSE}[\widehat{c_R}]_{\text{p}}^{\text{ub,MF}}$ and $\text{MSE}[\widehat{c_R}]_{\text{cs}}^{\text{ub,MF}}$ are used as the objective function, the optimal α_μ^* and α_σ^* developed in Equations (4.7) and (4.8) also minimize these upper bounds, regardless of the values of n_s and m_s, as long as $m_s > n_s$ is satisfied. In terms of sample allocation, an exact analytical expression for the optimal r_m is difficult to derive due to the complexity of the expressions, and hence numerical optimization methods are used to determine n_s and m_s.

The $\text{MSE}[\widehat{c_R}]_{\mu\sigma}^{\text{MF}}$ approximates the exact MSE of $\widehat{c_{R,MF}}$. However, its complicated expression means that α_μ^* and α_σ^* are not guaranteed to be the optimal coefficients. For this case, the values of α_μ, α_σ,n_s and m_s all are determined by numerical optimization to minimize $\text{MSE}[\widehat{c_R}]_{\mu\sigma}^{\text{MF}}$.

The costs of evaluating the HFM and LFM depend on the problem, and they are measured in real time to ensure consistency. In this work, since n_{plt} pilot samples are used to compute the required estimators, the costs are measured using an average of the n_{plt} computational times and n_{plt} is a lower bound for the samples, that is, $m_s > n_s > n_{plt}$, since it is a sunk cost.

Analytical Sample Allocation Strategy

An analytical approximation for the optimal sample allocation is developed for the case where minimizing $\text{MSE}[\widehat{c_R}]_{\text{cs}}^{\text{ub}}$ is the goal of the optimization in Equation (4.1), based on limiting distribution approximations. Since $\widehat{\sigma_{c,MF}^2}$ and $\widehat{\mu_{\vartheta_h,MF}}$ are both unbiased estimators, their MSEs are equivalent to their variances. Lemma 4 demonstrates that their limiting distributions are approximately the same, and consequently, the MSE of $\widehat{\sigma_{c,MF}^2}$ can be approximated by the MSE of $\widehat{\mu_{\vartheta_h,MF}}$. Hence, the allocation scheme for n_s and m_s values in Lemma 1 that minimizes the MSE of $\widehat{\mu_{\vartheta_h,MF}}$ also approximately minimizes the MSE of $\widehat{\sigma_{c,MF}^2}$.

The last ingredient required to formulate an approximation of the optimal sample allocation to minimize $\text{MSE}[\widehat{c_R}]_{\text{cs}}^{\text{ub}}$ is obtained by noting that $\text{MSE}[\widehat{c_R}]_{\text{cs}}^{\text{ub}}$ (Equation (4.25)) has a general form of $\text{MSE}[\widehat{c_R}]_{\text{cs}}^{\text{ub}} = \chi_1 \text{MSE}[\widehat{\mu_c}] + \chi_2 \text{MSE}\left[\widehat{\sigma_c^2}\right]$, where

$\chi_1 > 0$ and $\chi_2 > 0$ are constants. This is a linear combination of the MSEs of the MFMC estimators of the first raw and second central statistical moments. The following lemma extends Lemma 1 for this case.

Lemma 13. *Let c_h and ϑ_h be random variables whose means are statistical moment parameters μ_h and σ_h^2 of compliance from the HFM, and let c_l and ϑ_l be control variate random variables whose means are the statistical moment parameters μ_l and σ_l^2 of compliance from the LFM. Following Lemma 1, the unbiased MFMC estimator of μ_h is:*

$$\widehat{\mu_{c,MF}} = \widehat{\mu_{h,MC}}^{n_s} + \alpha_\mu(\widehat{\mu_{l,MC}}^{m_s} - \widehat{\mu_{h,MC}}^{n_s}), \quad m_s > n_s,$$

and the unbiased MFMC estimator for σ_h^2 is:

$$\widehat{\mu_{\vartheta_h,MF}} = \widehat{\mu_{\vartheta_h,MC}}^{n_s} + \alpha_\sigma(\widehat{\mu_{\vartheta_l,MC}}^{m_s} - \widehat{\mu_{\vartheta_l,MC}}^{n_s}), \quad m_s > n_s,$$

where α_μ and α_σ are the control variate coefficients. Let a linear combination of the MSEs of estimators be:

$$\chi_1 MSE\left[\widehat{\mu_{c,MF}}\right] + \chi_2 MSE\left[\widehat{\mu_{\vartheta_h,MF}}\right],$$

where $\chi_1 > 0$ and $\chi_2 > 0$ are constants. Given a computational budget $P_b = n_s + w_c m_s$ and define $r_m = \frac{m_s}{n_s}$, this linear combination of MSE is minimized when:

$$\begin{aligned} &\alpha_\mu = \frac{Cov[\vartheta_h, \vartheta_l]}{\mathbb{V}[\vartheta_l]}; \;\; \alpha_\sigma = \frac{Cov[c_h, c_l]}{\mathbb{V}[c_l]}, \;\; and \\ &r_m = r_m^* = \sqrt{\frac{w_c(\chi_1 Corr[c_h, c_l]^2 \sigma_h^2 + \chi_2 Corr[\vartheta_h, \vartheta_l]^2 \tau_h)}{\chi_1 \sigma_h^2 (1 - Corr[c_h, c_l]^2) + \chi_2 \tau_h (1 - Corr[\vartheta_h, \vartheta_l]^2)}}. \end{aligned} \tag{4.32}$$

where τ_h is the variance of ϑ_h.

Proof of Lemma 13: See Appendix A.3.3. □

To summarize, an approximate analytical optimal sample allocation strategy is developed for minimizing the $\text{MSE}[\widehat{c_R}]_{\text{cs}}^{\text{ub,MF}}$ bound of the MFMC robust compliance estimator. The optimal control variate coefficients (α_μ^* and α_σ^*) follow Equations (4.7) and (4.8), while the allocation of HFM and LFM samples follows the expression for the sample ratio (r_m^*) developed in Lemma 13.

4.4 Conclusion

This chapter develops MFMC strategies for the optimal estimation of a robust objective during optimization. The robust objective is a weighted sum of the mean and standard deviation of a QOI, and having an accurate estimation of the robust objective ensures high quality gradients in optimization.

MFMC employs estimators to approximate the robust objective, and the quality of the estimator is measured by its MSE. A bifidelity scheme is developed in this chapter where samples evaluated from a HFM and a LFM are used to construct the estimators. The estimators require control variate coefficients to relate the outputs of the two models and sample allocation strategies to specify the number of samples required from the two models. These variables are selected through an optimization problem to minimize the MSE of the MFMC estimator.

For very high dimensional uncertainties, only MC is applicable. The MSE of a MC estimator decreases with $1/\sqrt{n_s}$, which is very inefficient. MFMC is a variance reduction technique and if the outputs from the HFM and LFM have a good correlation, then under the same computational budget, the MFMC estimator has a lower MSE than the MC estimator. However, existing MFMC approaches select the variables based on the optimal estimation of a single statistical moment, which does not result in the minimal MSE of the estimator of the robust objective. Hence, this work develops two upper bounds and an approximation for the MSE of the robust objective, which is used as the optimization objectives to obtain the variables required in the MFMC scheme. These optimization problems correspond to different novel MFMC strategies for the optimal estimation of the robust objective under a limited computational budget and are solved numerically. An analytical approximation of the solution to one of the strategies is also developed. The variables required by the MFMC scheme selected through these strategies enable more significant MSE reduction compared to the standard MC and MFMC schemes targeting a single moment.

In optimization, only one set of samples is available for each iteration. Hence, to compute the MSE in the optimization strategy required by the MFMC, many unbiased estimators are developed with closed form equations, which are evaluated using only a small sample set of the outputs from the HFM and LFM. These estimators permit the optimization problem in MFMC to be solved each iteration, which enables the application of MFMC in optimization. Furthermore, novel approximations for the confidence intervals of the mean and variance employing the MFMC estimators are developed, which are useful for statistical inference.

Chapter 5

Multi-fidelity Monte Carlo Robust Topology Optimization

In this chapter, the multi-fidelity Monte Carlo (MFMC) strategies developed in Chapter 4 are applied to robust topology optimization (RTO) problems. As mentioned in Section 2.7, this thesis focus the type of RTO framework that relies on having a reliable and efficient uncertainty quantification (UQ) scheme to ensure the design gradients are of good quality. For material uncertainty represented by high dimensional stochastic surrogates, MC-based RTO is used to generate accurate estimations of the statistics of the quantity of interest (QOI). The accuracy of the estimations of statistics can be appraised using the mean squared error (MSE) metric. For the standard MC scheme using n_s samples, the MSE decreases with $\frac{1}{\sqrt{n_s}}$, which is inefficient. The MFMC scheme improves on the standard MC by combining evaluations of a high fidelity model (HFM) and low fidelity models (LFM) to achieve reduction in the MSE of an estimate of a statistic using the same computational budget. Only De et al. [35], Hamdia et al. [43], and Hyun et al. [44] have investigated the application of MFMC and multilevel Monte Carlo (MLMC) to RTO. Their LFMs are based on coarsening the mesh of the finite element (FE) model. For input uncertainty modeled by random fields with short correlation lengths and approximated using Karhunen–Loève expansion (KLE), a coarsened FE mesh could result in aliasing of the KLE surrogate. Also, the MSE reduction frameworks employed in these works focus on a single statistical moment, rather than the robust objective, a combination of mean and standard deviation.

Hence, the contribution of this work is twofold. The first is incorporating the MFMC UQ strategies developed in Chapter 4 into the RTO framework. Since these strategies focus on the optimal estimation of the robust objective with a limited

computational budget, they produce more accurate estimations than the MC scheme and other MFMC schemes that target a single moment. The second is developing a MFMC-based RTO algorithm employing the reduced basis (RB) scheme as the LFM. The RB model does not interact with the spatial discretization of the problem, and hence is more appropriate for problems with short correlation lengths.

In this chapter, the full finite element (FE) model corresponds to the HFM, which employs the bilinear quadrilateral element with a plane stress constitutive model. The governing equation is the linear elasticity model. With the FE discretization, this leads to the linear system $\mathbf{Ku} = \mathbf{F}$, where $\mathbf{K}$ is the FE stiffness matrix, $\mathbf{F}$ is the load vector, and $\mathbf{u}$ is the displacement vector. The RB scheme is generated using an on-the-fly procedure, which is employed in data assimilation problems [94] and to accelerate deterministic topology optimization (DTO) [102, 103, 104]. One bottleneck arising from the application of RB in TO is the lack of accurate *a priori* error bounds or *a posteriori* error estimates for the RB model. Typical applications of the RB scheme require these error measures to search through the input parameter space and construct an efficient basis, in addition to ensuring the RB solution does not significantly deviate from the output of HFM [105, 106, 107, 108, 109, 110]. In general, the error estimates of RB require an approximation of the inverse of the coercivity constant of the system [105, 108, 109, 110]. However, with the application of Solid Isotropic Material with Penalization (SIMP) or other element removal procedures, the stiffness matrix of a topology-optimized structure is very ill-conditioned, and hence the coercivity constant tends towards zero. For problems that require an estimation of the accuracy of the output statistics, the direct RB approach is not desirable. Conveniently, MFMC does not necessitate error bounds for RB, making RB a plausible LFM.

5.1 Statistical Gradients

For application of MFMC in RTO, the gradients of the mean and variance estimators are required. This work uses a bifidelity approach, where the HFM corresponds to the full FE model, while the LFM corresponds to the RB model. The displacement and compliance from HFM are $\mathbf{u} = \mathbf{K}^{-1}\mathbf{F}$ and $c_h = \mathbf{F}^T\mathbf{u}$. Denote $\mathbf{\Phi}$ as the basis from the RB scheme, the RB coefficient vector is $\boldsymbol{\eta} = (\mathbf{\Phi}^T\mathbf{K}\mathbf{\Phi})^{-1}(\mathbf{\Phi}^T\mathbf{F})$, the LFM displacement is $\tilde{\mathbf{u}} = \mathbf{\Phi}\boldsymbol{\eta}$, and the LFM compliance is $c_l = \mathbf{F}^T\tilde{\mathbf{u}}$. The sample-wise compliance derivative vector with respect to the element density vector $\boldsymbol{\rho}$ is $\frac{\partial c_h}{\partial \boldsymbol{\rho}} = -\mathbf{u}^T\frac{\partial \mathbf{K}^{-1}}{\partial \boldsymbol{\rho}}\mathbf{u}$ for HFM, and $\frac{\partial c_l}{\partial \boldsymbol{\rho}} = -\tilde{\mathbf{u}}^T\frac{\partial \mathbf{K}^{-1}}{\partial \boldsymbol{\rho}}\tilde{\mathbf{u}}$ for LFM.

The gradients for the MFMC mean and variance estimators are:

$$\begin{aligned}\frac{\partial\widehat{\mu_{c,MF}}}{\partial\boldsymbol{\rho}} &= \frac{\partial\widehat{\mu_{h,MC}}^{n_s}}{\partial\boldsymbol{\rho}} + \alpha_\mu\left(\frac{\partial\widehat{\mu_{l,MC}}^{m_s}}{\partial\boldsymbol{\rho}} - \frac{\partial\widehat{\mu_{l,MC}}^{n_s}}{\partial\boldsymbol{\rho}}\right),\\ &= \frac{1}{n_s}\sum_{i=1}^{n_s}\frac{\partial c_{h,i}}{\partial\boldsymbol{\rho}} + \alpha_\mu\left(\frac{1}{m_s}\sum_{j=1}^{m_s}\frac{\partial c_{l,j}}{\partial\boldsymbol{\rho}} - \frac{1}{n_s}\sum_{k=1}^{n_s}\frac{\partial c_{l,k}}{\partial\boldsymbol{\rho}}\right);\end{aligned}$$

and

$$\begin{aligned}\frac{\partial\widehat{\sigma^2_{c,MF}}}{\partial\boldsymbol{\rho}} &= \frac{2}{n_s-1}\sum_{i=1}^{n_s}(c_{h,i} - \widehat{\mu_{h,MC}}^{n_s})(\frac{\partial c_{h,i}}{\partial\boldsymbol{\rho}} - \frac{\partial\widehat{\mu_{h,MC}}^{n_s}}{\partial\boldsymbol{\rho}})\\ &\quad+\alpha_\sigma\Bigg(\frac{2}{m_s-1}\sum_{j=1}^{m_s}(c_{l,j} - \widehat{\mu_{l,MC}}^{m_s})(\frac{\partial c_{l,j}}{\partial\boldsymbol{\rho}} - \frac{\partial\widehat{\mu_{l,MC}}^{m_s}}{\partial\boldsymbol{\rho}})\\ &\quad-\frac{2}{n_s-1}\sum_{k=1}^{n_s}(c_{l,k} - \widehat{\mu_{l,MC}}^{n_s})(\frac{\partial c_{l,k}}{\partial\boldsymbol{\rho}} - \frac{\partial\widehat{\mu_{l,MC}}^{n_s}}{\partial\boldsymbol{\rho}})\Bigg).\end{aligned}$$

Hence, the gradient for the MFMC robust compliance is:

$$\frac{\partial\widehat{c_{R,MF}}}{\partial\boldsymbol{\rho}} = \frac{\partial\widehat{\mu_{c,MF}}}{\partial\boldsymbol{\rho}} + \frac{\kappa}{2\widehat{\sigma_{c,MF}}}\frac{\partial\widehat{\sigma^2_{c,MF}}}{\partial\boldsymbol{\rho}}, \tag{5.1}$$

where $\widehat{\sigma_{c,MF}} = \sqrt{\widehat{\sigma^2_{c,MF}}}$.

5.2 Robust Topology Optimization Algorithm

There are four free variables in the bi-fidelity MFMC framework, namely the control variate coefficients α_μ and α_σ, and sample sizes n_s and m_s. Four variants of the MFMC UQ schemes are developed. They differ depending on the choices of the free variables. The "CSn" scheme denotes when $\text{MSE}[\widehat{c_R}]^{\text{ub}}_{\text{cs}}$ is minimized by using α^*_μ and α^*_σ, defined in Equation (4.7) and (4.8) in Chapter 4, and n_s and m_s are numerically optimized. The "Pn" scheme denotes when $\text{MSE}[\widehat{c_R}]^{\text{ub}}_{\text{p}}$ is minimized by using α^*_μ and α^*_σ and n_s and m_s are numerically optimized. The "CSt" scheme denotes when $\text{MSE}[\widehat{c_R}]^{\text{ub}}_{\text{cs}}$ is minimized by using α^*_μ and α^*_σ and theoretical optimal sample ratio r^*_m. The "EVan" denotes when $\text{MSE}[\widehat{c_R}]_{\mu\sigma}$ is minimized by numerically optimizing all four variables.

For application in RTO, the sensitivities of the approximate robust compliance calculated by MFMC are derived in Equation (5.1), which are computed once the four variables are known. The MFMC UQ schemes also require the computational

costs associated with the HFM and LFM. Since the target application is optimization, the cost of evaluating the HFM is defined as the CPU time required to build the FE system, solve the FE problem, compute the sample-wise compliance, and compute the sample-wise sensitivities. The cost of evaluating the LFM is defined the same way, except it is based on the RB model instead. These costs are measured in real time during optimization. Specifically, at the beginning of each iteration, the computation of n_{plt} pilot samples is timed, and the averaged values determine the costs.

The LFM employed is the RB scheme. The RB is constructed using the on-the-fly procedure, meaning that it is from solutions along the optimization trajectory. Specifically, the first RTO iteration uses the full Monte Carlo procedure based on the P_b cost constraint. The resulting displacement solutions are orthogonalized by singular value decomposition (SVD) and the first n_b left singular vectors are retained, forming the initial RB basis. The value of n_b is the desired RB size, and its value has an impact on the computational cost of the LFM as well as the statistical correlation between the HFM and LFM solutions, which in turn affects the efficacy of the MFMC scheme. In the succeeding iterations, the basis is updated at the end of each optimization iteration using the n_s HFM model solutions, and then truncated to n_b columns using SVD.

There are occasions when the LFM is a poor representation of the HFM. This occurs when their statistical correlation is low, which means that they behave like independent random variables. In this case, it is undesirable to continue with the MFMC scheme. Instead, returning to the full MC procedure is beneficial. To provide a threshold for this condition, a heuristic approach is taken, where from the statistics computed from the n_{plt} pilot samples the resulting model correlation parameters $\text{Corr}[c_h, c_l]$ and $\text{Corr}[\vartheta_h, \vartheta_l]$ are assessed, as well as the optimal values of n_s and m_s. If the correlations are low, or if m_s is approximately equal to (or lower than) n_s, the optimization iteration reverts to a full MC scheme. In numerical cases considered, this very rarely occurs.

The general multi-fidelity Monte Carlo robust topology optimization (MFTO) procedure is Algorithm 2. The Method of Moving Asymptotes (MMA) updates the design variables. The stopping criteria are when either the maximum change in the design variables is less than 1%, or the maximum number of optimization iterations (k_{max}) is attained. For the naming convention, the specific UQ scheme applied is added with a dash. For example, the "CSn" MFMC UQ scheme applied to MFTO leads to "MFTO-CSn."

Algorithm 6: MFTO algorithm

Input: Sample set $\{\boldsymbol{\xi}_i\}$, P_b computational budget, n_{plt} pilot size, and n_b RB size.
Input: Initialize $\tilde{\boldsymbol{\rho}}$, loop $k = 1$
while $\|\tilde{\boldsymbol{\rho}}_k - \tilde{\boldsymbol{\rho}}_{k-1}\|_\infty > 0.01$ and $k < k_{max}$ **do**
→ Filter $\tilde{\boldsymbol{\rho}}_k$ to $\boldsymbol{\rho}_k$ with Equation (2.6) and (2.7)
if $k = 1$ **then**
→ MC iteration, store all $\mathbf{u}(\boldsymbol{\xi}_i)$.
else
for $i = 1 : n_{plt}$ **do**
→ compute and time HFM samples $\mathbf{u}(\boldsymbol{\xi}_i)$ and $\frac{\partial c_h(\boldsymbol{\xi}_i)}{\partial \boldsymbol{\rho}}$
→ compute and time LFM samples $\tilde{\mathbf{u}}(\boldsymbol{\xi}_i)$ and $\frac{\partial c_l(\boldsymbol{\xi}_i)}{\partial \boldsymbol{\rho}}$
end for
→ use the n_{plt} samples to compute unbiased estimators.
→ Find the optimal values of α_μ, α_σ, n_s, and m_s.
→ Compute the MSE estimates of optimization statistics.
if $\mathrm{Corr}[c_h, c_l] << 1$ or $\mathrm{Corr}[\vartheta_h, \vartheta_l] << 1$ or $m_s \approx n_s$ **then**
→ Recourse to MC iteration, store all $\mathbf{u}(\boldsymbol{\xi}_i)$.
→ Compute $\widehat{c_R}$ and $\frac{\partial \widehat{c_R}}{\partial \boldsymbol{\rho}}$ using MC estimator.
else
for $i = n_{plt} + 1 : n_s$ **do**
→ compute HFM samples $\mathbf{u}(\boldsymbol{\xi}_i)$ and $\frac{\partial c_h(\boldsymbol{\xi}_i)}{\partial \boldsymbol{\rho}}$.
end for
for $i = n_{plt} + 1 : m_s$ **do**
→ compute LFM samples $\tilde{\mathbf{u}}(\boldsymbol{\xi}_i)$ and $\frac{\partial c_l(\boldsymbol{\xi}_i)}{\partial \boldsymbol{\rho}}$.
end for
→ Compute $\widehat{c_R}$ and $\frac{\partial \widehat{c_R}}{\partial \boldsymbol{\rho}}$ using MFMC estimator.
end if
end if
→ Using the new $\mathbf{u}$, update to $\boldsymbol{\Phi}_{k+1}$ via SVD and truncate at n_b size.
→ update to $\tilde{\boldsymbol{\rho}}_{k+1}$ using MMA.
end while

5.3 Numerical Results

The MFTO schemes are applied to two two-dimensional robust compliance minimization problems with a volume constraint subject to uncertainty in the material properties. One is an MBB (Messerschmitt-Bölkow-Blohm) beam problem with pointwise loading as shown in Figure 5.1(a), and the other is a carrier plate problem with distributed loading as shown in Figure 5.1(b). For both problems, Young's modulus is uncertain, and it is modeled using homogeneous lognormal random fields with a two-dimensional exponential correlation function. The Karhunen–Loève expansion

(KLE) is employed to represent the random fields and for sufficient accuracy the KLE is required to capture over 95% of the random field energy. These test problems specifically focus on very short correlation lengths, as both problems involve correlation lengths of $(l_x, l_y) = (5, 5)$ units. Satisfying the threshold for the MBB problem requires to 2500 random variables (ξ_m), and for the carrier plate problem 3200 random variables. Both problems have very high stochastic dimensionality, and only the Monte Carlo family of methods is applicable. The variability of a homogeneous random field is captured through its covariance CoV, which is the ratio of the standard deviation of the random field to the mean. For both problems, the mean is set to one, while CoV is set to 35%. Hence, these random fields have short correlation lengths and high variance, which is representative of typical material uncertainties caused by additive manufacturing.

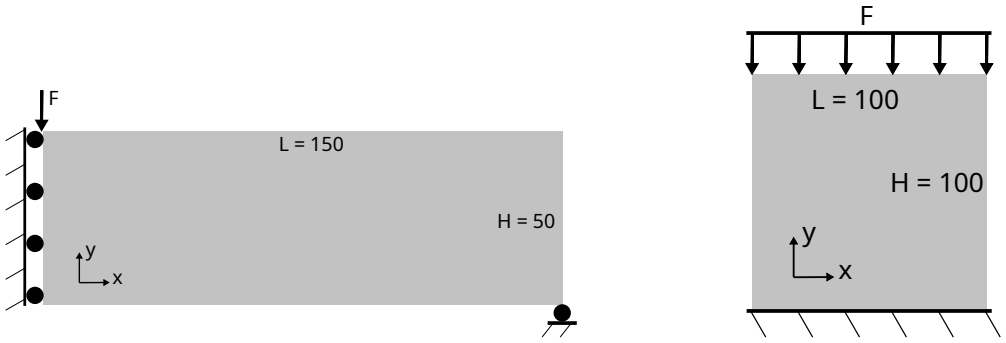

(a) MBB beam. **(b)** Carrier plate.

Figure 5.1 Design domain of the MBB beam and carrier plate, with applied loading and boundary conditions.

Several RTO parameters are constant for both problems. The weight factor κ in c_R is set to 4 ($\kappa = 4$), while in the SIMP scheme, penalization $p = 3$ and minimum density $\rho_{min} = 10^{-3}$ are imposed. For the regularization filter, $r_f = 1.5$ is set for all cases, equivalent to 1.5 times the element edge length. The Heaviside projection filter in Equation (2.7) is applied with a continuation scheme on β, so that β starts with a value of 1 and doubles every 40 iterations until a maximum of 16, which is maintained until convergence. In addition, the `asyinit` and the `move` parameter in MMA remain as the default values of 0.5. All calculations are initialized with an even distribution of material. For the parameters in MFTO, the computational budget is $P_b = 500$, meaning that 500 HFM samples are affordable for each optimization iteration. The n_b is 50, and n_{plt} is 50 for computing the initial estimators of statistical parameters.

The MCTO algorithm is a benchmark for comparison for the results of both

problems. The number of samples used in MCTO is 500, which is equivalent to P_b in MFTO. The deterministic TO (DTO) design is computed, where Young's modulus is constant with a value of one. The result of DTO represents optimization without awareness of uncertainty, and it is contrasted with the outputs of RTO algorithms. To assess the numerical properties and the efficacy of the MFTO and MCTO algorithms, several strategies are employed, and they are discussed in detail in the following subsection.

5.3.1 Assessment Methodologies

The robust optimization algorithms follow a nested loop structure, where the inner loop is responsible for the accurate estimation of statistics, while the outer loop is tasked with design updates. This work improves the inner loop UQ procedure. Several assessment methods are described which are used at RTO iterations of interest.

Bootstrap Cross-Validation

Given the KLE surrogate of the random field truncated to M expansion variables, a pool of $n_p = 20,000$ independent random samples of the expansion variables $\boldsymbol{\xi}_i = \{\xi_m\}_i, m = 1, \cdots, M; i = 1, \cdots, n_p$ is generated. For a material distribution $\boldsymbol{\rho}$ from any optimization iteration, n_p of corresponding HFM compliance realizations are computed using the $\boldsymbol{\xi}_i$ samples, leading to $c_{h,i}, i = 1, \cdots, n_p$. In addition, given the basis from the RB scheme, $\boldsymbol{\Phi}$, the corresponding n_p of LFM compliance realizations are computed for the MFTO algorithms at the given iteration, leading to $c_{l,i}, i = 1, \cdots, n_p$.

With this pool of compliance samples, the population parameters are computed by employing an MC UQ scheme that uses all $n_p = 20,000$ samples. Parameters including μ_h, σ_h^2, μ_l, and σ_l^2 are computed with high accuracy using MC estimators due to the large sample size. These are ground truths of the mean and variance of compliance evaluated from the HFM and LFM for the given material distribution.

Since the ground truth values of the parameters are available, bootstrapping provides an alternative approximation of the properties of estimators. Closed form expressions of the MSEs of various estimators are provided in Chapter 4. The bootstrap procedure is used as a means to cross-validate these expressions and as a neutral way to assess the quality of the estimators. For bootstrapping [111, 112], given n_p compliances calucalted using the HFM and LFM, define a desired multi-fidelity (MF) sample set consisting of a sample set calculated with the HFM with the size of $N_B^h < n_p$,

and a sample set calculated with the LFM with the size of $N_B^l < n_p$. Draw with replacement $\mathcal{B}$ sets of these MF sample sets. Each MF sample set is a bootstrap set, which consists of HFM sample sets $\boldsymbol{c_h}^k = \{c_{h,i}\}_k; i = 1, \cdots, N_B^h; k = 1, \cdots, \mathcal{B}$, as well as LFM sample sets with the same structure except with N_B^l. For each MF sample set, quantities related to the estimators are evaluated, which leads to $\mathcal{B}$ realizations. Each of these realizations is called a bootstrap replicate. Given an estimator $\hat{Q}$ and $\mathcal{B}$ bootstrap replicates, the approximation of its MSE is

$$\mathrm{MSE}\left[\hat{Q}\right]^B \overset{\mathrm{def}}{=} \frac{1}{\mathcal{B}} \sum_{k=1}^{\mathcal{B}} \left(\hat{Q}_k - Q\right)^2,$$

where Q is the true population parameter, obtained using n_p samples.

To provide an interpretation of the estimator error in relation to the magnitude of the parameters in an L^2 sense, the ratio of the bootstrap MSE approximations with the parameter values is reported: $\frac{\mathrm{MSE}\left[\hat{Q}\right]^B}{Q^2}$, which is denoted by Δ_Q. When Q is not available, it is replaced by the L^2 norm of the estimator, leading to

$$\Delta_Q \overset{\mathrm{def}}{=} \frac{\mathrm{MSE}\left[\hat{Q}\right]^B}{\mathbb{E}\left[\hat{Q}^2\right]} = \frac{\mathbb{E}\left[(\hat{Q} - Q)^2\right]}{\mathbb{E}\left[\hat{Q}^2\right]} \approx \frac{\mathrm{MSE}\left[\hat{Q}\right]^B}{Q^2}.$$

In this work, the difference from the approximation is negligible.

For MC or MFMC estimators, closed form expressions for MSE are in Chapter 4 employing unbiased estimators. Using these expressions and the MF sample sets, $\mathcal{B}$ bootstrap replicates of the MSEs of the estimators are evaluated. The $\mathcal{B}$ replicates are averaged to reduce the statistical noise induced by variation in sample sets. This is the bootstrap smoothing or bagging procedure. For a generic estimator $\hat{Q}$, each bootstrap replicate of the MSE is $\mathrm{MSE}\left[\hat{Q}\right]_k$ and hence, this procedure is defined as

$$\mathbb{E}_B\left[\mathrm{MSE}\left[\hat{Q}\right]\right] \overset{\mathrm{def}}{=} \frac{1}{\mathcal{B}} \sum_{k=1}^{\mathcal{B}} \mathrm{MSE}\left[\hat{Q}\right]_k.$$

This averaged value, $\mathbb{E}_B\left[\mathrm{MSE}\left[\hat{Q}\right]\right]$, is defined as the predicted MSE of the estimator and is compared with the bootstrap estimation of the MSE $\left[\hat{Q}\right]^B$ to assess the accuracy of the closed form expressions for MSE.

In addition, using $\mathrm{MSE}\left[\hat{Q}\right]_k$, the $\mathcal{B}$ bootstrap replicates of the MSE, the confidence interval (CI) approximations constructed using mean and variance estimators

are cross-validated. To approximate the P_{CI} confidence interval bound of Q using $\hat{Q}$, the general form is:

$$\Pr\Big(Q \in \Big[\hat{Q} - z_{P_{CI}}\text{MSE}\left[\hat{Q}\right], \hat{Q} + z_{P_{CI}}\text{MSE}\left[\hat{Q}\right]\Big]\Big) \approx P_{CI}.$$

The estimation of the confidence interval is random, since the value of the bounds changes depending on the realization of $\hat{Q}$ and its MSE. Using the $\mathcal{B}$ bootstrap replicates, $\mathcal{B}$ of these confidence intervals are computed. Since the true parameter, Q is also known, the cross-validated confidence level of the bounds is given as:

$$P_{CI}^{B} \overset{\text{def}}{=} \frac{\#\text{ of times } Q \in \left[\hat{Q}_k - z_{P_{CI}}\text{MSE}\left[\hat{Q}\right]_k, \hat{Q}_k + z_{P_{CI}}\text{MSE}\left[\hat{Q}\right]_k\right]}{\mathcal{B}}.$$

For the MC estimators, given $\boldsymbol{\rho}$ for an MCTO iteration, the sample set calculated using the LFM in each MF bootstrap sample set is null, meaning $N_B^l = 0$, and the sample set $\boldsymbol{c_h}$ evaluated using the HFM has size $N_B^h = P_b = 500$, which corresponds to the size of the MC scheme used in optimization. The $\mathcal{B}$ bootstrap replicates enable the computation of the MSE and CI related to the estimators $\widehat{\mu_{c,MC}}$ and $\widehat{\sigma^2_{c,MC}}$. For the robust compliance estimator $\widehat{c_{R,MC}}$, in addition to MSE $\left[\widehat{c_{R,MC}}\right]^B$, the $\mathbb{E}_B[\cdot]$ average of the upper bounds and MSE estimation from Theorem 1 are computed.

For the MFMC estimators, given $\boldsymbol{\rho}$ for an MFTO iteration, two MF bootstrap sample sets are defined. The first consists of $\boldsymbol{c_h}$ calculated using the HFM with a size of $N_B^h = n_s$ and $\boldsymbol{c_l}$ evaluated using the LFM with a size of $N_B^l = m_s$. The n_s and m_s are the sample allocations from the MFMC strategy at that iteration. The underlying KLE samples $\boldsymbol{\xi}$ for the n_s samples are reused by the first n_s of the m_s samples, while the remaining $m_s - n_s$ samples are independently generated. The MSE $\left[\hat{Q}\right]^B$ related to the mean, variance, and robust compliance estimators are evaluated using these MF sample sets. The second MF bootstrap sample set is defined with both the sample sets evaluated using the HFM and LFM having sizes of $N_B^h = N_B^l = n_{plt}$. This corresponds to the number of pilot samples used in the MFTO algorithms, and assesses the accuracy of the MSE expressions in a realistic optimization setting. The $\mathbb{E}_B\Big[\text{MSE}\left[\hat{Q}\right]\Big]$ and CI related to $\widehat{\mu_{c,MF}}$ and $\widehat{\sigma^2_{c,MF}}$ are computed with the bootstrap procedure. For the $\widehat{c_{R,MF}}$ estimator, depending on the variant of the MFTO scheme, the $\mathbb{E}_B[\cdot]$ average of the corresponding MSE upper bound or estimation is computed.

Comparison Between MFMC and Standard MC

To demonstrate the effectiveness of MFMC compared to standard MC, additional analyses are conducted. Given $\boldsymbol{\rho}$ at an MFTO iteration, using $N_B^h = P_b = 500$, the computational budget constraint, the bootstrapping analysis of an equivalent cost MC scheme is carried out. The MSEs of MC estimators from bootstrap approximations (e.g. MSE $\left[\widehat{c_{R,MC}}\right]^B$) are reported and compared with the results of MFMC. The difference between MSE $\left[\widehat{c_{R,MC}}\right]^B$ and MSE $\left[\widehat{c_{R,MF}}\right]^B$ assesses the effectiveness of estimating c_R using the MFMC scheme compared to the standard MC scheme given the same computational budget.

An equivalent sample analysis is also presented. From the bootstrap computation, the MSE $\left[\widehat{c_{R,MF}}\right]^B$ is obtained for the MFMC estimator. The numerical results show that the MSE$[\widehat{c_R}]_{\mu\sigma}$ is an accurate approximation of the actual MSE$[\widehat{c_R}]$ using P_b samples. Hence, employing MSE $\left[\widehat{c_{R,MF}}\right]^B$ as a threshold and considering MSE$[\widehat{c_R}]_{\mu\sigma}$ as the expression for the MSE of the MC estimator with the number of MC samples a free variable, the equivalent samples required by the MC estimator to achieve this threshold is computed and denoted as $n_{c_R}^{eq,B}$. This is a root-finding problem solved numerically. To ensure accurate statistics, for computing the unbiased estimators required in the expression of MSE$[\widehat{c_R}]_{\mu\sigma}$ for the MC scheme, all $n_p = 20,000$ HFM samples are used. The value of $n_{c_R}^{eq,B}$ represents the approximate number of MC samples required to achieve the exact MSE of the MFMC estimator.

Comparison Between MFMC Strategies

In MFMC schemes, the control variate coefficients and sample allocation sizes are free variables, and there are many strategies for selecting their values to minimize the MSE of the estimator. The majority of existing MFMC strategies minimize the MSE of a single raw or central statistical moment. For RTO applications, it is possible to use an MFMC strategy that targets the optimal estimation of either the mean or the variance. However, the robust compliance objective is more complex as it is a linear combination of the mean and standard deviation. The strategies targeting a single parameter are not optimal for robust compliance. Since the strategies developed in this work are specifically intended for robust compliance, comparisons between MFMC schemes in this work and the MFMC schemes that target a single statistical moment, which is what is available in the literature, are reported.

First, the estimators and the MFMC strategies focusing on optimal estimation of mean or variance are defined. Denote the MFMC strategy focusing on optimal

estimation of mean as the MF-μ^* scheme, and the MFMC strategy targeting variance as the MF-σ^* scheme. For both cases, the expressions of the mean estimator, variance estimator, and robust compliance follow Equations (4.2), (4.3), and (4.23). Also, both cases employ the optimal control variate coefficients defined in Equations (4.7) and (4.8). For finding the sample allocation, the MF-μ^* scheme follows the strategy in Lemma 1, while the MF-σ^* scheme employs a numerical optimization.

To this end, given $\boldsymbol{\rho}$ at an MFTO iteration and n_{plt} pilot samples of HFM and LFM, the control variate coefficients and sample allocation for the MF-μ^* and MF-σ^* strategies are computed, giving rise to the estimators associated with these two schemes. Denote the robust compliance estimator for the MF-μ^* scheme as $\widehat{c_{R,\mu^*}}$ and for the MF-σ^* scheme as $\widehat{c_{R,\sigma^*}}$. The same bootstrap computations described previously are applied to these two estimators, and their approximated MSEs are denoted as MSE $\left[\widehat{c_{R,\mu^*}}\right]^B$ and MSE $\left[\widehat{c_{R,\sigma^*}}\right]^B$. These MSEs are compared with the value of MSE $\left[\widehat{c_{R,MF}}\right]^B$, which is the MSE of the estimator of robust compliance determined using MFMC.

5.3.2 MBB Beam

The spatial domain of the MBB beam problem is in Figure 5.1(a). It is 150 units wide and 50 units high. The applied force is a point load, $F = 1$, on the top left corner of the domain in the negative y direction, while the displacement boundary conditions are zero horizontal displacement on the left edge, and zero vertical displacement on the bottom right corner. The volume constraint is 50% of the design domain, which is equivalent to 3750 units squared. For a constant unit value Young's modulus, the DTO design is shown in Figure 5.2(a). The statistics of the DTO design, shown in brackets in the subcaption, are computed using 20,000 samples of the Young's modulus. Since the resulting beam is subject to bending load, the design has thick horizontal members at the bottom and top edges of the domain. In the middle of the domain, two thick oblique members connect the top member with the bottom member.

To demonstrate the characteristics of a random field with short correlation lengths, these samples are aggregated to compute the mean and variance of the modulus at the centroid of each element, and the result is illustrated in Figure 5.3. Both of these statistics exhibit changes with small length scales across the domain. This leads to regions of relatively high or low modulus that have small areas.

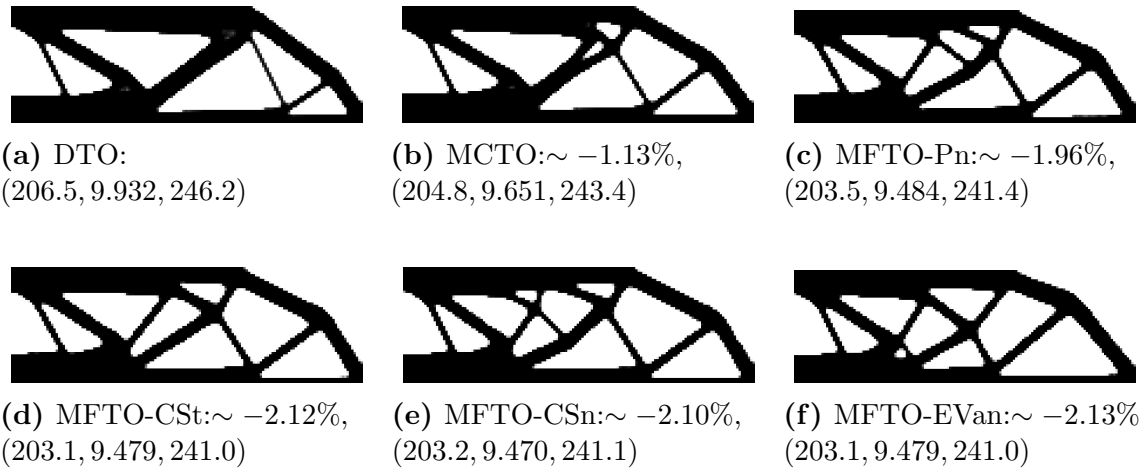

(a) DTO: $(206.5, 9.932, 246.2)$

(b) MCTO:$\sim -1.13\%$, $(204.8, 9.651, 243.4)$

(c) MFTO-Pn:$\sim -1.96\%$, $(203.5, 9.484, 241.4)$

(d) MFTO-CSt:$\sim -2.12\%$, $(203.1, 9.479, 241.0)$

(e) MFTO-CSn:$\sim -2.10\%$, $(203.2, 9.470, 241.1)$

(f) MFTO-EVan:$\sim -2.13\%$, $(203.1, 9.479, 241.0)$

Figure 5.2 Structural designs for the MBB problem produced by DTO and different RTO algorithms with $\kappa = 4$. The subcaption details their ground truth statistics in brackets: (μ_c, σ_c, c_R). For the RTO algorithms, the difference in c_R between the RTO design and DTO design is also reported as a percentage. Note that a negative difference means a reduction in c_R.

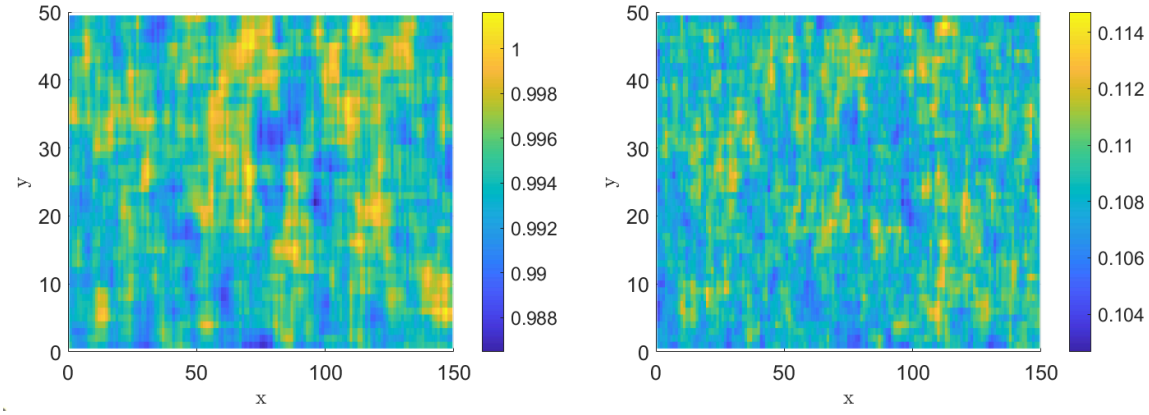

(a) Mean of the sampled modulus.

(b) Variance of the sampled modulus.

Figure 5.3 Mean and variance of the Young's modulus at the centroid of elements over the domain of the MBB beam, computed using the 20,000 random samples.

MBB RTO Designs

In Figure 5.2, the designs produced by different RTO algorithms for the MBB beam problem are shown, with their statistical parameters. In general, they have varying topologies due to differences in the oblique members in the middle of the domain. The c_R of the RTO designs are all similar to within 1%, hence showing that for problems with short correlation lengths, various local minima of similar quality exist. The posi-

tion of the thicker members on the top and bottom edges as well as the left side of the domain in the RTO designs are generally the same because this feature is paramount in reducing the c_R of the designs. The presence of small changes in modulus shown in Figure 5.3 does not have a significant influence on this. More importantly, these RTO designs all have lower c_R than the DTO design, by at least 1%. This demonstrates the effectiveness of these uncertainty-aware algorithms. The MFTO algorithms produce designs that have a lower c_R than MCTO, with the MFTO-EVan design having the lowest value. Hence, in terms of robust optimization, the MFTO algorithms using on-the-fly RB perform better than the benchmark MCTO using equivalent computational cost.

The MSE estimates of $\widehat{c_R}$ are used to assess the quality of the inner loop UQ procedure and to minimize the MSE for the case of MFMC estimators. To shed light on the performance of the MFMC and MC estimators through the optimization, the bootstrapping investigation is done at the 5th, 40th, and 200th iterations of the RTO processes. These iterations are selected because they are representative of various stages of the optimization. The material distributions from the MFTO-Pn algorithm corresponding to these iterations are shown in Figure 5.4. The 5th iteration is early in the optimization, where only a vague outline of structural members is established and the majority of the domain is grey, indicating intermediate densities. The 40th iteration represents the intermediate stage of optimization, where a topology is visible before large β, including small members with intermediate densities that are removed in subsequent iterations. The 200th iteration shown in Figure 5.4(c) corresponds to the final stage of optimization, where $\beta = 16$ is a maximum, leading to sharp contrast between the solid and void regions with fewer oblique members. The $\boldsymbol{\rho}$ at the 200th iteration is very similar to the final MFTO-Pn design, apart from minor adjustments.

(a) MFTO-Pn 5th iteration. **(b)** MFTO-Pn 40th iteration. **(c)** MFTO-Pn 200th iteration.

Figure 5.4 MFTO-Pn material distribution ($\boldsymbol{\rho}$) at intermediate iterations for MBB problem.

Analyses of MC Estimators

The results from bootstrap analyses of the MC estimators are shown in Table 5.1. The of Δ_μ show that the relative ratio of the L^2 error of the mean estimator compared to the squared value of the mean is consistently of order 10^{-6} throughout optimization. For variance, Δ_{σ^2} is consistently of order 10^{-3}. This is because accurate approximations of higher order statistics are much more difficult, even if their magnitudes are no higher than lower order statistics. On the other hand, the ratio associated with $\widehat{c_{R,MC}}$ in the Δ_{c_R} column is of order 10^{-5} throughout, which is lower than that of Δ_{σ^2}, but higher than Δ_μ. Focusing on the MSE of mean would lead to a very optimistic error expectation, while the MSE of variance is overly pessimistic. Hence, it is important to focus on the MSE of the objective of interest.

Table 5.1 Bootstrap analysis results of the MC estimators using $\boldsymbol{\rho}$ at different optimization iterations of MCTO.

MCTO	MSE $\left[\widehat{c_{R,MC}}\right]^B$	$\mathbb{E}_B\left[\text{MSE}[\widehat{c_R}]_{\text{p}}^{\text{ub,MC}}\right]$	$\mathbb{E}_B\left[\text{MSE}[\widehat{c_R}]_{\text{cs}}^{\text{ub,MC}}\right]$	$\mathbb{E}_B\left[\text{MSE}[\widehat{c_R}]_{\mu\sigma}^{\text{MC}}\right]$	Δ_μ	Δ_{σ^2}	Δ_{c_R}
Iter 5	4.51	7.38	28.3	4.53	3.59e-6	3.72e-3	2.34e-5
Iter 40	2.09	3.33	11.7	2.05	4.67e-6	4.14e-3	2.95e-5
Iter 200	1.65	2.72	9.57	1.67	4.76e-6	3.64e-3	2.78e-5

Since the estimation of the MSE and the confidence interval associated with the MC mean and variance estimators are well-established, the focus is on the robust compliance estimator. Observing the data in the MSE $\left[\widehat{c_{R,MC}}\right]^B$ column, the MSE of $\widehat{c_{R,MC}}$ decreases as optimization proceeds. Since Δ_{c_R} exhibits little variation, this is caused by a decrease in the robust compliance. Two upper bounds and an approximation of the MSE of $\widehat{c_{R,MC}}$ are developed in Theorem 1. The bootstrap averages of their approximations are shown in the columns $\mathbb{E}_B\left[\text{MSE}[\widehat{c_R}]_{\text{p}}^{\text{ub,MC}}\right]$, $\mathbb{E}_B\left[\text{MSE}[\widehat{c_R}]_{\text{cs}}^{\text{ub,MC}}\right]$, and $\mathbb{E}_B\left[\text{MSE}[\widehat{c_R}]_{\mu\sigma}^{\text{MC}}\right]$. For the MC scheme, the upper bounds $\text{MSE}[\widehat{c_R}]_{\text{cs}}^{\text{ub}}$ and $\text{MSE}[\widehat{c_R}]_{\text{p}}^{\text{ub}}$ are higher than the bootstrap computation MSE $\left[\widehat{c_{R,MC}}\right]^B$. For this problem, $\text{MSE}[\widehat{c_R}]_{\text{p}}^{\text{ub}}$ is a tighter bound than $\text{MSE}[\widehat{c_R}]_{\text{cs}}^{\text{ub}}$. The $\text{MSE}[\widehat{c_R}]_{\mu\sigma}$ approximation leads to very similar values to MSE $\left[\widehat{c_{R,MC}}\right]^B$ for the three iterations examined. This demonstrates the ability of $\text{MSE}[\widehat{c_R}]_{\mu\sigma}$ to approximate the exact MSE of the c_R estimator for the MC scheme. These results add confidence to the prediction in Theorem 1. The MSEs for estimators of c_R decrease as the optimization progresses, which is a desirable behavior.

Behaviors of MFMC Variables

To investigate the MFTO algorithms, the behaviors of several parameters are presented. The graphs are based on the optimization results from MFTO-Pn, which is representative of other MFTO variants for this analysis.

The enabler of the MFMC scheme is the control variate random variable that statistically resembles the random variable of interest. In this work, the control variate is the on-the-fly RB (the LFM) output, and the random variable of interest is the FE model (the HFM) output. The estimated correlation coefficients for the first order and second order statistics between these two models through optimization are shown in Figure 5.5(a). The c_h and c_l are associated with the μ_h and μ_l estimations, while ϑ_h and ϑ_l are associated with σ_h^2 and σ_l^2 estimations. The graphs show that apart from the first few iterations, the statistical correlation between HFM and LFM is close to one. Such a strong positive correlation means that despite the lack of exact error computation associated with the RB output, the response of the RB follows that of the FE very well. This shows that the on-the-fly RB surrogate is an effective control variate in approximating the behavior of the FE solution in RTO problems, adding confidence to the practical applicability of the MFTO algorithms.

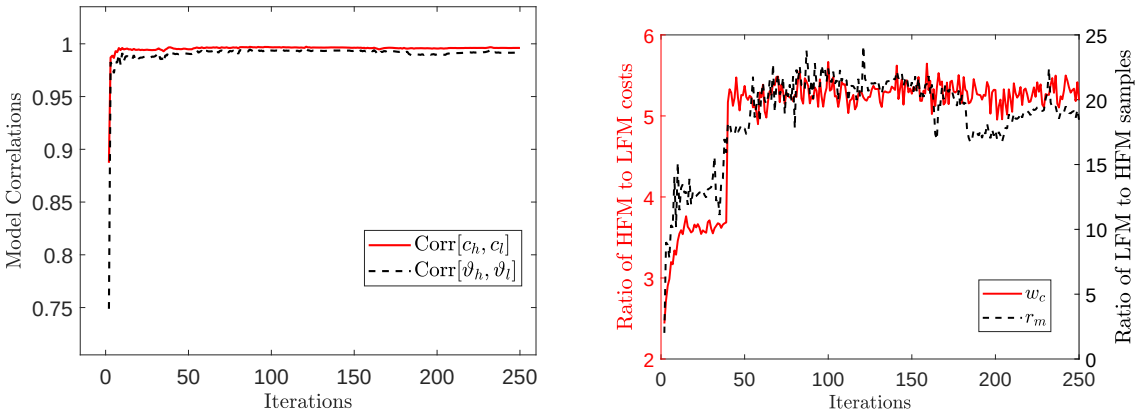

(a) The correlation of first and second order outputs from the HFM and LFM.

(b) Model cost ratio w_c and optimized sample allocation ratio r_m.

Figure 5.5 Behavior of various parameters from the MFTO-Pn algorithm over the first 250 MFTO-Pn iterations for the MBB beam problem.

The second requirement to make MFTO a feasible approach is the low computational cost associated with the LFM. In Figure 5.5(b), the ratio of the cost of FEM to RB, shown in red, is plotted for the first 250 iterations. The value of w_c starts at around 2, exhibits a plateau at about 3.5, before increasing to about 5.5. In the

initial phase of the optimization, the densities of selected elements are reduced to approach a local minimum, which changes the initial even distribution of material into a feasible structure with void regions. The wide range in element densities leads to ill-conditioning of the FE stiffness matrix ($\mathbf{K}$), increasing the cost of solving the FE model. This causes the initial rise in w_c. The increase in w_c at around iteration 40 is caused by the increase in β, which further drives the density to either 0 or 1. Consequently, $\mathbf{K}$ becomes nearly positive semi-definite, and solving the FE problem increases significantly in cost. In contrast, the vectors in the basis matrix ($\mathbf{\Phi}$) of the RB scheme are orthonormal. The reduced order stiffness matrix, $\mathbf{\Phi}^T\mathbf{K}\mathbf{\Phi}$, does not suffer from ill-conditioning and the associated cost does not increase despite changes in the element densities. Overall, this shows that the RB model is appreciably cheaper than the FE model, especially for distributions of density that have high solid-void contrast as are expected in topology optimization.

The optimized sample allocation ratio for MFTO-Pn shown in Figure 5.5(b) in black follows the trend of w_c. Figure 5.5(a) shows a strong correlation between the HFM and LFM at all iterations, and hence the other strong influence on sample allocation is the contrast in computational cost. The high value of w_c means that the MFMC relies mainly on the LFM, with occasional recourse to the HFM. Alongside the strong correlation of the LFM with the HFM, these are desired behaviors for MFMC and hence encourage its use in RTO problems.

Since bootstrapping requires computing n_p HFM and LFM compliances using $\boldsymbol{\rho}$ from iterations of interest, the kernel density approximation method is applied to estimate their probability density functions (PDF) using these compliance samples. These are shown in Figure 5.6(a). The progression of the shape of the PDFs through optimization provides a visual interpretation of the RTO procedure. The PDF at the 5th iteration has a large mean and variance. As optimization progresses to the 40th and 200th iterations, the variance decreases leading to a sharper peak of the PDF, and the mean also decreases. These behaviors correspond to the reduction in the robust compliance. In general, the mean and variance of the LFM PDFs are slightly lower than those of the HFM PDFs. The shapes of these PDFs resemble bell curves, so Gaussian distributions approximate them. Hence, the assumption in Lemma 3 is satisfied, allowing confidence interval approximations of the mean and variance estimators to be computed.

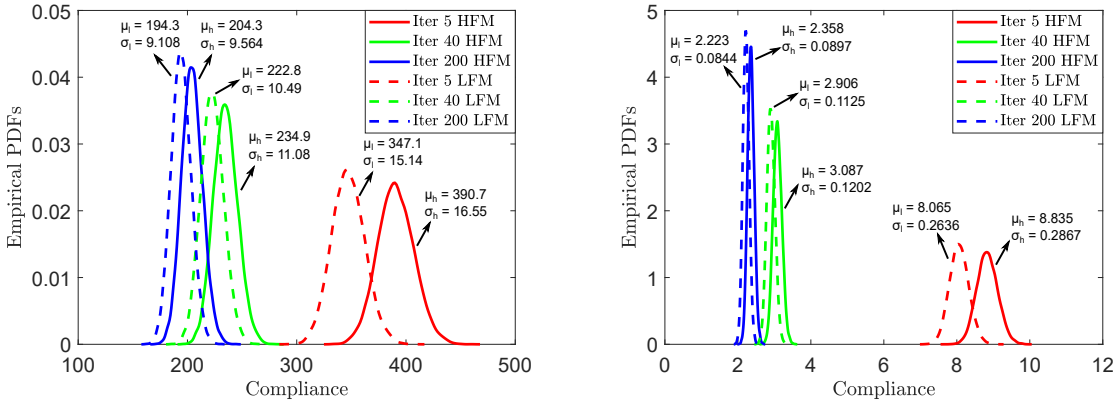

(a) Case of MFTO-Pn for the MBB beam. **(b)** Case of MFTO-CSt for the carrier plate.

Figure 5.6 Approximated probability density function of the HFM and LFM compliances at intermediate iterations of MFMC algorithms using n_p samples.

Analyses of MFMC Mean and Variance Estimators

The results of bootstrap analyses of the MFMC mean and variance estimators for MFTO-Pn are in Tables 5.2 and 5.3.

Table 5.2 Bootstrap analysis results of the MFMC mean estimator using $\boldsymbol{\rho}$ at different optimization iterations of MFTO-Pn.

MFTO-Pn	MSE $\left[\widehat{\mu_{c,MF}}\right]^B$	$\mathbb{E}_B\left[\text{MSE}[\widehat{\mu_{c,MF}}]\right]$	$P^B_{90\%}$	$P^B_{99\%}$	Δ_μ
Iter 5	0.325	0.346	90.2%	99.4%	2.13e-6
Iter 40	0.0858	0.0872	88.8%	99.2%	1.55e-6
Iter 200	0.0571	0.0596	89.8%	99.0%	1.37e-6

Table 5.3 Bootstrap analysis results of the MFMC variance estimator using $\boldsymbol{\rho}$ at different optimization iterations of MFTO-Pn.

MFTO-Pn	MSE $\left[\widehat{\sigma^2_{c,MF}}\right]^B$	$\mathbb{E}_B\left[\text{MSE}[\widehat{\sigma^2_{c,MF}}]\right]$	$P^B_{90\%}$	$P^B_{99\%}$	Δ_{σ^2}
Iter 5	255.	256.	91.6%	99.2%	3.40e-3
Iter 40	31.4	32.2	90.4%	98.4%	2.08e-3
Iter 200	16.2	15.7	89.0%	99.2%	1.94e-3

Comparing the bootstrap computations of the MSE of the estimators, MSE $\left[\widehat{\mu_{c,MF}}\right]^B$ and MSE $\left[\widehat{\sigma^2_{c,MF}}\right]^B$, with the average of their approximations, $\mathbb{E}_B\left[\text{MSE}[\widehat{\mu_{c,MF}}]\right]$ and $\mathbb{E}_B\left[\text{MSE}[\widehat{\sigma^2_{c,MF}}]\right]$, the values are very similar for all cases. This indicates that the

closed form expressions for estimating the MSE of $\widehat{\mu_{c,MF}}$ and $\widehat{\sigma^2_{c,MF}}$ employing various unbiased estimators approximate their values accurately. Figure 5.6(a) shows that the HFM and LFM outputs have PDFs with Gaussian shape. Hence, the assumption of Lemma 3 is satisfied, and the confidence interval bounds for μ_c and σ_c^2 are approximated with the MFMC estimators for the 90% and 99% confidence levels. The verification of this is in columns $P^B_{90\%}$ and $P^B_{99\%}$ for the mean and variance. The data confirm that among the $\mathcal{B}$ replicates of confidence intervals, the percentage of intervals that contain the actual value of the parameter is appropriate for the imposed confidence level. Hence, the result adds confidence to Corollary 4.1. The magnitude of the MSEs decreases through optimization, and so does their ratio with the square of the parameter value, shown in columns Δ_μ and Δ_{σ^2}. The Δ_{σ^2} is three orders of magnitude greater than Δ_μ.

Analyses of MFMC Robust Compliance Estimator

This section examines the bootstrap analyses of the MFMC robust compliance estimators ($\widehat{c_{R,MF}}$) from the four MFTO variants. The goal is to minimize the MSE of $\widehat{c_{R,MF}}$. The MFTO variants differ by the strategies used to determine the variables: α_μ, α_σ, n_s, and m_s. To assess the efficacy of these strategies, comparisons with the MC estimator as well as MFMC estimators that target only the optimal estimation of either the mean (MF-μ^*) or the variance (MF-σ^*) are reported.

For the MFTO-Pn variant, the results are in Table 5.4. For this algorithm, the strategy is to select the MFMC variables by minimizing $\mathrm{MSE}[\widehat{c_R}]^{\mathrm{ub}}_{\mathrm{p}}$, an upper bound of the MSE. The average of the $\mathcal{B}$ replicates of this upper bound estimation is in the $\mathbb{E}_B\left[\mathrm{MSE}[\widehat{c_R}]^{\mathrm{ub,MF}}_{\mathrm{p}}\right]$ column. It exceeds the bootstrap estimation in MSE $\left[\widehat{c_{R,MF}}\right]^B$, and it decreases during optimization. Hence, $\mathrm{MSE}[\widehat{c_R}]^{\mathrm{ub,MF}}_{\mathrm{p}}$ computed using unbiased estimators is a feasible bound and a good indicator of the behavior of the expected L^2 error of the MFMC robust compliance estimator. The Δ_{c_R} values, although not shown, are for these three iterations, 2.08×10^{-5}, 1.48×10^{-5}, and 1.41×10^{-5}. Hence, Δ_{c_R} is between Δ_μ and Δ_{σ^2}, shown in Tables 5.2 and 5.3. This is similar to MCTO, again showing that the focus must be on the error of the actual objective.

The MSE $\left[\widehat{c_{R,MF}}\right]^B$ is less than MSE $\left[\widehat{c_{R,MC}}\right]^B$ at all iterations, by between 20% and 60%. This confirms the capability of MFMC to obtain lower errors in the estimation of the objective while using the same computational budget compared to standard MC. This effect is more apparent as the optimization progresses. The $n^{eq,B}_{c_R}$ is the number of samples required for the standard MC estimator to achieve the MSE $\left[\widehat{c_{R,MF}}\right]^B$ threshold. The values of $n^{eq,B}_{c_R}$ exhibit an increasing trend, and they

Table 5.4 Bootstrap analysis results of the robust compliance estimator using $\boldsymbol{\rho}$ at different optimization iterations of MFTO-Pn.

MFTO-Pn	MSE $\left[\widehat{c_{R,MF}}\right]^B$	$\mathbb{E}_B\left[\text{MSE}[\widehat{c_R}]_{\text{p}}^{\text{ub,MF}}\right]$	MSE $\left[\widehat{c_{R,MC}}\right]^B$	$n_{c_R}^{eq,B}$	MSE $\left[\widehat{c_{R,\mu^*}}\right]^B$	MSE $\left[\widehat{c_{R,\sigma^*}}\right]^B$
Iter 5	4.33	6.30	5.47	593	5.85	4.28
Iter 40	1.15	1.70	2.40	1010	1.62	1.13
Iter 200	0.828	1.13	1.73	1052	1.01	0.827

suggest that about double the computational cost is required to achieve the same MSE if the regular MC scheme is used instead.

To compare the MFTO-Pn strategy with the MF-μ^* and MF-σ^* strategies with the same computational budgets, the MSE of their robust compliance estimators, $\widehat{c_{R,\mu^*}}$ and $\widehat{c_{R,\sigma^*}}$, are presented in the MSE $\left[\widehat{c_{R,\mu^*}}\right]^B$ and MSE $\left[\widehat{c_{R,\sigma^*}}\right]^B$ columns. For all iterations, MSE $\left[\widehat{c_{R,MF}}\right]^B$ is lower than MSE $\left[\widehat{c_{R,\mu^*}}\right]^B$, and approximately the same as MSE $\left[\widehat{c_{R,\sigma^*}}\right]^B$. Hence, for the MBB beam problem, the MFMC strategy focusing on the optimal estimation of mean leads to a poor robust compliance estimator. For this problem, controlling the MSE of the variance is more demanding and is paramount to the accuracy of robust compliance. The MFMC-Pn strategy here performed similar to the MF-σ^* strategy.

The bootstrap computations associated with the MFTO-CSt scheme are in Table 5.5. For the CSt scheme, the sample allocation and control variate coefficients are selected to minimize the $\text{MSE}[\widehat{c_R}]_{\text{cs}}^{\text{ub}}$ upper bound. The $\mathbb{E}_B\left[\text{MSE}[\widehat{c_R}]_{\text{cs}}^{\text{ub,MF}}\right]$ corresponds to the average of $\text{MSE}[\widehat{c_R}]_{\text{cs}}^{\text{ub,MF}}$ from $\mathcal{B}$ bootstrap replicates. Comparatively, $\mathbb{E}_B\left[\text{MSE}[\widehat{c_R}]_{\text{cs}}^{\text{ub,MF}}\right]$ is higher than MSE $\left[\widehat{c_{R,MF}}\right]^B$, which is the bootstrap estimation of the exact MSE of $\widehat{c_{R,MF}}$. Compared to $\text{MSE}[\widehat{c_R}]_{\text{p}}^{\text{ub}}$ in the MFTO-Pn case, $\text{MSE}[\widehat{c_R}]_{\text{cs}}^{\text{ub}}$ is a looser upper bound in this problem, but $\text{MSE}[\widehat{c_R}]_{\text{cs}}^{\text{ub}}$ has similar behavior as the exact MSE of the estimator.

Table 5.5 Bootstrap analysis results of the robust compliance estimator using $\boldsymbol{\rho}$ at different optimization iterations of MFTO-CSt.

MFTO-CSt	MSE $\left[\widehat{c_{R,MF}}\right]^B$	$\mathbb{E}_B\left[\text{MSE}[\widehat{c_R}]_{\text{cs}}^{\text{ub,MF}}\right]$	MSE $\left[\widehat{c_{R,MC}}\right]^B$	$n_{c_R}^{eq,B}$	MSE $\left[\widehat{c_{R,\mu^*}}\right]^B$	MSE $\left[\widehat{c_{R,\sigma^*}}\right]^B$
Iter 5	3.66	22.8	5.23	741	4.65	3.68
Iter 40	0.949	5.98	2.53	1282	1.28	0.955
Iter 200	0.807	4.11	1.92	1196	1.06	0.818

Comparison of MSE $\left[\widehat{c_{R,MF}}\right]^B$ with MSE $\left[\widehat{c_{R,MC}}\right]^B$ demonstrates that the $\widehat{c_{R,MF}}$ leads to significantly lower MSE than the regular MC estimator. The same conclusion

is also reached at by looking at the equivalent MC sample metric $n_{c_R}^{eq,B}$. The improvement shown for the MFTO-CSt case is greater than for the MFTO-Pn case. The MSE of MF-μ^* and MF-σ^* formulated by optimal mean or variance estimation strategies are reported in MSE $\left[\widehat{c_{R,\mu^*}}\right]^B$ and MSE $\left[\widehat{c_{R,\sigma^*}}\right]^B$. Compared to MSE $\left[\widehat{c_{R,MF}}\right]^B$, both of these estimators have a higher L^2 error, with the $\widehat{c_{R,\mu^*}}$ estimator from MF-μ^* strategy being the worst. This demonstrates that minimizing the MSE$[\widehat{c_R}]_{\text{cs}}^{\text{ub}}$ upper bound is an effective approach to selecting MFMC variables that lead to optimal estimation of c_R. The MFMC-CSt strategy accounts for the error from the estimation of mean and standard deviation estimation, in addition to considering their interactions. Hence, the resultant $\widehat{c_{R,MF}}$ is more accurate than if only one of the statistical moments is considered.

The MFTO-CSn variant also selects the MFMC variables by minimizing the MSE$[\widehat{c_R}]_{\text{cs}}^{\text{ub}}$ upper bound. The previous CSt scheme employs the approximate optimal r_m^* from Lemma 13 based on limiting distribution approximations, whereas the CSn scheme numerically optimizes the sample allocation variables. To compare these two approaches, through the course of MFTO-CSn optimization, the approximate r_m^* at each iteration is computed. Both r_m are graphed in Figure 5.7(a), and they are shown to be similar for all iterations, even when significant fluctuation occurs, such as around iteration 160. This consistent similarity suggests that the analytical sample allocation in Lemma 13 is practically effective.

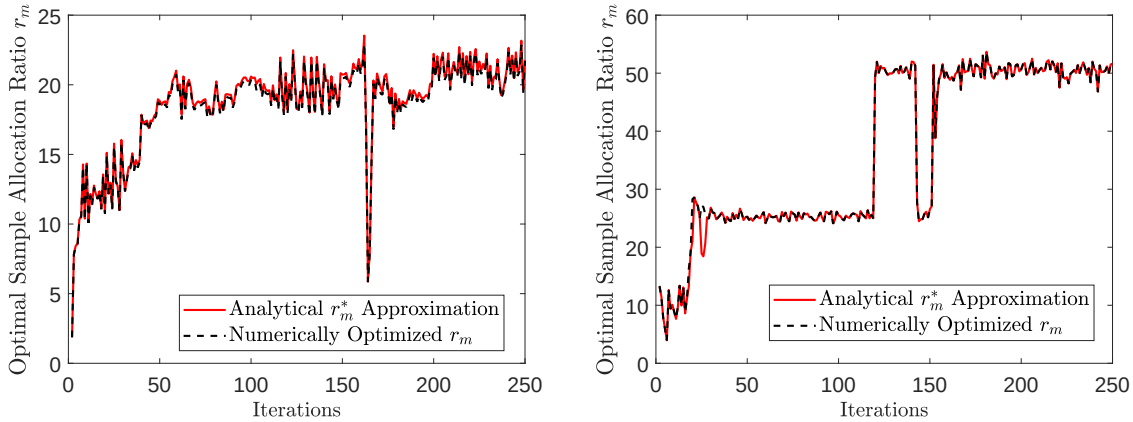

(a) Case of MBB beam. **(b)** Case of carrier plate.

Figure 5.7 Comparison between numerically optimized sample allocation ratio and approximated analytical optimal r_m^* from Lemma 13 over the first 250 MFTO-CSn iterations for the MBB beam and carrier plate.

The bootstrap analysis of the $\widehat{c_{R,MF}}$ estimator at three MFTO-CSn optimization iterations is presented in Table 5.6. The general trend is similar to the previous

observations from the MFTO-CSt case. The key point is that the robust compliance estimator formulated from the CSn strategy leads to lower MSE compared to the regular MC, as well as the MF-μ^* and MF-σ^* schemes. Hence, selecting the optimal α and r_m by minimizing $\text{MSE}[\widehat{c_R}]_{\text{cs}}^{\text{ub,MF}}$ is a feasible strategy for obtaining a robust compliance estimator with minimal MSE.

Table 5.6 Bootstrap analysis results of the robust compliance estimator using $\boldsymbol{\rho}$ at different optimization iterations of MFTO-CSn.

MFTO-CSn	$\text{MSE}\left[\widehat{c_{R,MF}}\right]^B$	$\mathbb{E}_B\left[\text{MSE}[\widehat{c_R}]_{\text{cs}}^{\text{ub,MF}}\right]$	$\text{MSE}\left[\widehat{c_{R,MC}}\right]^B$	$n_{c_R}^{eq,B}$	$\text{MSE}\left[\widehat{c_{R,\mu^*}}\right]^B$	$\text{MSE}\left[\widehat{c_{R,\sigma^*}}\right]^B$
Iter 5	3.42	22.1	4.78	732	4.69	3.42
Iter 40	1.13	6.62	2.26	1067	1.67	1.14
Iter 200	0.882	4.95	1.76	948	1.17	0.893

The last MFTO variant, denoted as the EVan scheme, selects all the MFMC variables (α_μ, α_σ, and r_m) by numerically minimizing the $\text{MSE}[\widehat{c_R}]_{\mu\sigma}^{\text{MF}}$, which is an approximation of the exact MSE of the robust compliance estimator. The bootstrapping computations for MFTO-EVan are reported in Table 5.7. In Table 5.1, $\text{MSE}[\widehat{c_R}]_{\mu\sigma}$ closely resembles the MSE computed from bootstrapping, affirming the result of Theorem 1. However, in the case of the MFMC estimator, a comparison of $\text{MSE}\left[\widehat{c_{R,MF}}\right]^B$ and $\mathbb{E}_B\left[\text{MSE}[\widehat{c_R}]_{\mu\sigma}^{\text{MF}}\right]$ shows that $\text{MSE}[\widehat{c_R}]_{\mu\sigma}$ leads to inaccuracies ranging from 10% to 40%, especially for later iterations. Recall that $n_{plt} = 50$ samples are used to compute the various unbiased estimators required in $\text{MSE}\left[\widehat{c_{R,MF}}\right]^B$. In this case, this sample size is insufficient to achieve high accuracy. If n_{plt} is increased to 500, which is P_b, and $\mathbb{E}_B\left[\text{MSE}[\widehat{c_R}]_{\mu\sigma}^{\text{MF}}\right]$ is recomputed using the bootstrap procedure, then this leads to 4.04 at 5th iteration, 1.26 at 40th iteration, and 0.923 at 200th iteration. These values are closer to $\text{MSE}\left[\widehat{c_{R,MF}}\right]^B$. To demonstrate this further, the $\text{MSE}[\widehat{c_R}]_{\mu\sigma}$ of the MFMC estimator is recomputed using $n_{plt} = n_p = 20,000$ samples, and the results are $\text{MSE}[\widehat{c_R}]_{\mu\sigma}^{\text{MF},n_p}$. The values of $\text{MSE}[\widehat{c_R}]_{\mu\sigma}^{\text{MF},n_p}$ are very close to the bootstrap estimations in $\text{MSE}\left[\widehat{c_{R,MF}}\right]^B$. Hence, this indicates the feasibility of $\text{MSE}[\widehat{c_R}]_{\mu\sigma}$ from Theorem 1, as well as the $\mathbb{E}\left[\widehat{\widehat{\mu_{c,MF}}\widehat{\sigma^2_{c,MF}}}\right]$ expression in Lemma 12. Additionally, this result shows that caution about the general application of the MFMC schemes is required. For a high degree of statistical accuracy, a sizeable number of pilot samples may be required.

Despite the inaccuracies in the estimation of $\text{MSE}[\widehat{c_R}]_{\mu\sigma}$, comparing $\text{MSE}\left[\widehat{c_{R,MF}}\right]^B$ to $\text{MSE}\left[\widehat{c_{R,MC}}\right]^B$ demonstrates that the MFMC-EVan scheme provides significant MSE reductions compared to the regular MC for the same computational cost. Com-

Table 5.7 Bootstrap analysis results of the robust compliance estimator using $\boldsymbol{\rho}$ at different optimization iterations of MFTO-EVan.

MFTO-EVan	MSE $\left[\widehat{c_{R,MF}}\right]^B$	$\mathbb{E}_B\left[\text{MSE}[\widehat{c_R}]^{\text{MF}}_{\mu\sigma}\right]$	MSE $\left[\widehat{c_{R,MC}}\right]^B$	MSE $\left[\widehat{c_{R,\mu^*}}\right]^B$	MSE $\left[\widehat{c_{R,\sigma^*}}\right]^B$	$\text{MSE}[\widehat{c_R}]^{\text{MF},n_p}_{\mu\sigma}$
Iter 5	3.88	3.44	5.81	4.26	3.75	3.85
Iter 40	1.23	0.851	2.60	1.54	1.21	1.24
Iter 200	0.890	0.516	1.75	1.06	0.892	0.874

pared to MSE $\left[\widehat{c_{R,\mu^*}}\right]^B$ and MSE $\left[\widehat{c_{R,\sigma^*}}\right]^B$, the EVan strategy is more effective than the strategy that focuses only on the mean and is as effective as the strategy that focuses only on the variance. Hence, even when $\text{MSE}[\widehat{c_R}]_{\mu\sigma}$ is not approximated accurately, the numerically optimized MFMC parameters result in a low MSE. One explanation for this phenomenon is that the sources of the difference between the true MSE and its approximation $\text{MSE}[\widehat{c_R}]_{\mu\sigma}$ are mainly statistical, and thus only weakly related to the MFMC variables. The estimation error of the statistics is greatly reduced when sufficient accuracy is ensured, as in the case of $\text{MSE}[\widehat{c_R}]^{\text{MF},n_p}_{\mu\sigma}$. The optimal variables for minimizing $\text{MSE}[\widehat{c_R}]^{\text{MF}}_{\mu\sigma}$ also approximately minimize MSE $\left[\widehat{c_{R,MF}}\right]^B$.

The difference between the EVan approach and other MFMC strategies is that in minimizing the MSE, EVan selects α_μ and α_σ through numerical optimization, whereas other approaches employ analytical expressions for α^*_μ and α^*_σ. The differences in their values are illustrated in Figure 5.8 through the iterations of the MFTO-EVan algorithm. The values of α_σ are similar, but the values of α_μ are noticeably different. The expression of α^*_μ only depends on statistical parameters, but the $\text{MSE}[\widehat{c_R}]^{\text{MF}}_{\mu\sigma}$ expression is influenced by the sample numbers n_s and m_s. Hence, compared to α^*_μ, more fluctuations are expected in the numerically optimized α_μ, which is influenced by changes in r_m. The expression of α^*_σ depends on the model distribution, it is sensitive to adjustments in r_m and hence, it is similar to numerically optimized α_σ.

5.3.3 Carrier Plate

The spatial domain of the carrier plate problem is shown in Figure 5.1(b). It is a square with side lengths of 100 units. The distributed load is 0.01 per unit length in the negative y direction on the top-most edge, leading to a total load of one. The boundary condition is zero vertical and horizontal displacements on the bottom edge. The volume constraint in the RTO is 50% of the design domain, which is equivalent to 5000 units squared.

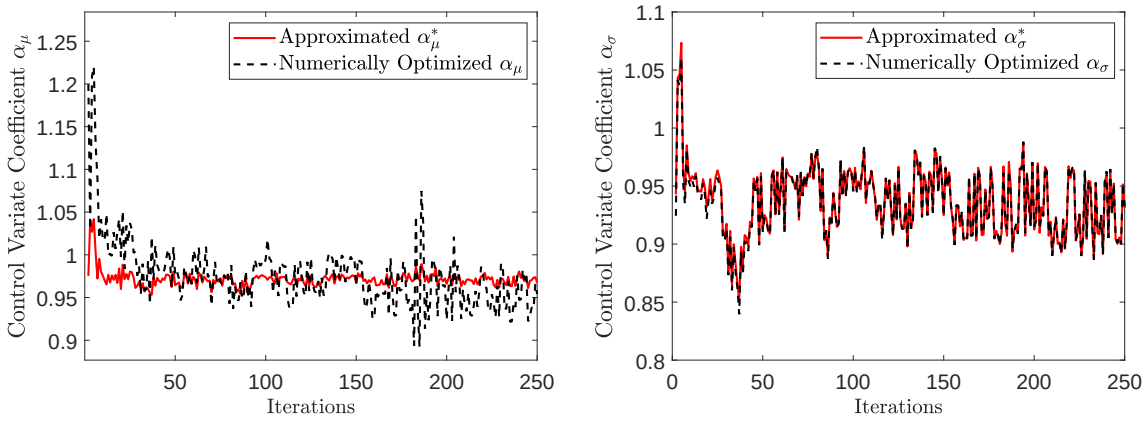

(a) α_μ comparison. **(b)** α_σ comparison.

Figure 5.8 Comparison between the values of α_μ^* and α_σ^* with numerically optimized α_μ and α_σ that minimizes $\text{MSE}[\widehat{c_R}]_{\mu\sigma}^{\text{MF}}$ over the first 250 MFTO-EVan iterations for the MBB problem.

The DTO design is shown in Figure 5.10(a). The design is symmetric about the horizontal center of the domain. The main load-bearing component is an arch structure in the center of the domain, and due to the distributed load applied, the design has many small members near the top surface where the force is applied.

For computing the ground truth parameters, an MC scheme employs 20,000 random samples of the Young's modulus random field. The mean and variance of the Young's modulus at the centroid of each element are evaluated using these random samples and illustrated in Figure 5.9. Due to the short correlation lengths of the random field, the length scale of variability in these plots is on the order of a few elements.

Carrier Plate RTO Designs

The RTO designs are shown in Figure 5.10. Compared to the DTO design, the robust designs have asymmetrical features. This is caused by the RTO designs having many small branches. The statistics of the sampled Young's modulus fields in Figure 5.9 show that modulus exhibit significant variations in a small length scale. Hence, these small regions of variability influenced the positioning of the members in the RTO designs. The phenomenon of short correlation lengths leading to generation of small members for structural reinforcement is observed in other studies [52, 53]. The robust compliances of the RTO designs are all smaller than for DTO. This shows the effectiveness of MFTO and MCTO in accounting for material uncertainties.

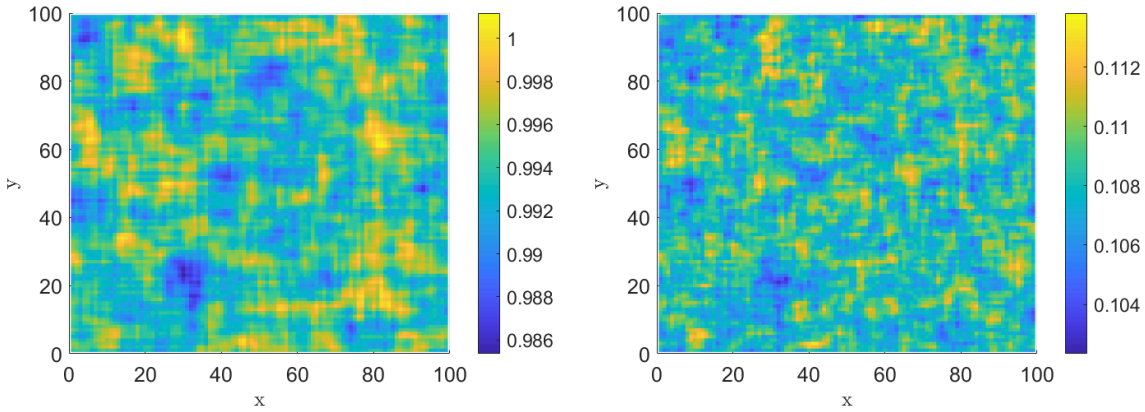

(a) Mean of the sampled modulus. **(b)** Variance of the sampled modulus.

Figure 5.9 Mean and variance of the Young's modulus at the centroid of elements over the domain of carrier plate, computed using the 20,000 random samples.

Comparatively, the MFTO-EVan obtained the smallest c_R, while MFTO-Pn had the largest amongst the RTO algorithms. This test case again encourages confidence in the MFTO algorithms and demonstrates their effectiveness in reaching high quality minima.

Identical to the MBB beam problem, the bootstrap analyses for the carrier plate problem use the 5th, 40th, and 200th material distributions, which are representative intermediate iterations.

Analyses of MC Estimators

The bootstrap computation of the MC robust compliance estimator is shown in Table 5.8. The observations for the carrier plate problem are very similar to the MBB beam. The relative L^2 error (Δ_{c_R}) of the objective has an order of magnitude in between that of the individual statistical moments (Δ_μ and Δ_{σ^2}). Comparing the quantities derived in Theorem 1 with the bootstrap estimated MSE $\left[\widehat{c_{R,MC}}\right]^B$, the values of $\mathbb{E}_B\left[\mathrm{MSE}[\widehat{c_R}]_{\mathrm{p}}^{\mathrm{ub,MC}}\right]$ and $\mathbb{E}_B\left[\mathrm{MSE}[\widehat{c_R}]_{\mathrm{cs}}^{\mathrm{ub,MC}}\right]$ are both higher, suggesting that both $\mathrm{MSE}[\widehat{c_R}]_{\mathrm{cs}}^{\mathrm{ub}}$ and $\mathrm{MSE}[\widehat{c_R}]_{\mathrm{p}}^{\mathrm{ub}}$ are acceptable upper bounds. The values of $\mathbb{E}_B\left[\mathrm{MSE}[\widehat{c_R}]_{\mu\sigma}^{\mathrm{MC}}\right]$ are very similar to MSE $\left[\widehat{c_{R,MC}}\right]^B$, showing that $\mathrm{MSE}[\widehat{c_R}]_{\mu\sigma}$ is a good approximation of the exact MSE of the MC robust compliance estimator.

Analyses of MFMC Mean and Variance Estimators

For analyses on the MFMC mean and variance estimators, the results based on MFTO-CSt iterations are presented. The kernel density approximated PDFs of HFM

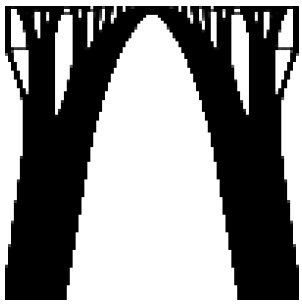

(a) DTO:
$(2.464, 0.1013, 2.869)$

(b) MCTO:
$(2.361, 0.0866, 2.707, -5.63\%)$

(c) MFTO-Pn:
$(2.446, 0.0927, 2.816, -1.82\%)$

(d) MFTO-CSt:
$(2.341, 0.0883, 2.694, -6.09\%)$

(e) MFTO-CSn:
$(2.389, 0.0915, 2.755, -3.98\%)$

(f) MFTO-EVan:
$(2.322, 0.0885, 2.676, -6.71\%)$

Figure 5.10 Structural designs for the carrier plate problem produced by DTO and different RTO algorithms with $\kappa = 4$. The subcaption details their ground truth statistics in brackets: (μ_c, σ_c, c_R). For the RTO algorithms, the difference in c_R between the RTO design and DTO design is also reported as a percentage. Note that a negative difference means a reduction in c_R.

Table 5.8 Bootstrap analysis results of the MC estimators using $\boldsymbol{\rho}$ at different optimization iterations of MCTO.

MCTO	MSE $\left[\widehat{c_{R,MC}}\right]^B$	$\mathbb{E}_B\left[\mathrm{MSE}[\widehat{c_R}]_{\mathrm{p}}^{\mathrm{ub,MC}}\right]$	$\mathbb{E}_B\left[\mathrm{MSE}[\widehat{c_R}]_{\mathrm{cs}}^{\mathrm{ub,MC}}\right]$	$\mathbb{E}_B\left[\mathrm{MSE}[\widehat{c_R}]_{\mu\sigma}^{\mathrm{MC}}\right]$	Δ_μ	Δ_{σ^2}	Δ_{c_R}
Iter 5	1.27e-3	2.18e-3	1.05e-2	1.34e-3	2.04e-6	3.80e-3	1.41e-5
Iter 40	1.91e-4	3.07e-4	1.32e-3	1.89e-4	2.82e-6	3.81e-3	1.91e-5
Iter 200	1.36e-4	2.19e-4	9.49e-4	1.34e-4	2.52e-6	3.76e-3	1.86e-5

and LFM compliances at intermediate iterations are depicted in Figure 5.6(b). These PDFs again exhibit Gaussian shapes similar to the MBB problem and hence the approximate confidence interval from Corollary 4.1 is applicable.

The bootstrap data associated with the $\widehat{\mu_{c,MF}}$ and $\widehat{\sigma^2_{c,MF}}$ estimators are reported in Tables 5.9 and 5.10. The similarity between the MSE $\left[\widehat{\mu_{c,MF}}\right]^B$ and $\mathbb{E}_B\left[\mathrm{MSE}[\widehat{\mu_{c,MF}}]\right]$

shows that the MSE of the MFMC mean estimator is accurately estimated by the $\text{MSE}[\widehat{\mu_{c,MF}}]$ expression with n_{plt} pilot samples. The same is said for the $\widehat{\sigma^2_{c,MF}}$ estimator. The data related to P_{CI} demonstrate the applicability of Corollary 4.1 in estimating the confidence intervals for the mean and variance using the MFMC estimators.

Table 5.9 Bootstrap analysis results of the MFMC mean estimator using $\boldsymbol{\rho}$ at different optimization iterations of MFTO-CSt.

MFTO-CSt	$\text{MSE}\left[\widehat{\mu_{c,MF}}\right]^B$	$\mathbb{E}_B\left[\text{MSE}[\widehat{\mu_{c,MF}}]\right]$	$P^B_{90\%}$	$P^B_{99\%}$	Δ_μ
Iter 5	1.14e-4	1.09e-4	89.2%	99.4%	1.47e-6
Iter 40	1.76e-5	1.77e-5	90.8%	99.0%	1.85e-6
Iter 200	5.81e-6	5.87e-6	91.2%	99.2%	1.05e-6

Table 5.10 Bootstrap analysis results of the MFMC variance estimator using $\boldsymbol{\rho}$ at different optimization iterations of MFTO-CSt.

MFTO-CSt	$\text{MSE}\left[\widehat{\sigma^2_{c,MF}}\right]^B$	$\mathbb{E}_B\left[\text{MSE}[\widehat{\sigma^2_{c,MF}}]\right]$	$P^B_{90\%}$	$P^B_{99\%}$	Δ_{σ^2}
Iter 5	2.66e-5	2.62e-5	91.6%	99.2%	3.95e-3
Iter 40	8.16e-7	7.72e-7	89.4%	98.2%	3.91e-3
Iter 200	1.63e-7	1.73e-7	91.0%	99.2%	2.52e-3

Analyses of MFMC Robust Compliance Estimator

The analyses of the four MFMC variants are presented in Tables 5.11, 5.12, 5.13, and 5.14. These variants differ due to their strategies for selecting the optimal control variate coefficients and the sample allocation. These variables are selected based on minimizing either $\text{MSE}[\widehat{c_R}]^{\text{ub}}_{\text{p}}$, $\text{MSE}[\widehat{c_R}]^{\text{ub}}_{\text{cs}}$, or $\text{MSE}[\widehat{c_R}]_{\mu\sigma}$. The analyses here are focused on demonstrating the effectiveness of these strategies for calculating $\widehat{c_{R,MF}}$ with a small MSE.

Table 5.11 Bootstrap analysis results of the robust compliance estimator using $\boldsymbol{\rho}$ at different optimization iterations of MFTO-Pn.

MFTO-Pn	$\text{MSE}\left[\widehat{c_{R,MF}}\right]^B$	$\mathbb{E}_B\left[\text{MSE}[\widehat{c_R}]^{\text{ub,MF}}_{\text{p}}\right]$	$\text{MSE}\left[\widehat{c_{R,MC}}\right]^B$	$n^{eq,B}_{c_R}$	$\text{MSE}\left[\widehat{c_{R,\mu^*}}\right]^B$	$\text{MSE}\left[\widehat{c_{R,\sigma^*}}\right]^B$
Iter 5	2.40e-3	3.87e-3	2.23e-3	494	2.61e-3	3.53e-3
Iter 40	3.09e-4	4.53e-4	3.48e-4	524	2.36e-4	3.17e-4
Iter 200	1.19e-4	1.79e-4	1.91e-4	706	7.50e-5	1.19e-4

Table 5.12 Bootstrap analysis results of the robust compliance estimator using $\boldsymbol{\rho}$ at different optimization iterations of MFTO-CSt.

MFTO-CSt	MSE $\left[\widehat{c_{R,MF}}\right]^B$	$\mathbb{E}_B\left[\text{MSE}[\widehat{c_R}]_{\text{cs}}^{\text{ub,MF}}\right]$	MSE $\left[\widehat{c_{R,MC}}\right]^B$	$n_{c_R}^{eq,B}$	MSE $\left[\widehat{c_{R,\mu^*}}\right]^B$	MSE $\left[\widehat{c_{R,\sigma^*}}\right]^B$
Iter 5	1.49e-3	1.23e-2	1.53e-3	517	2.24e-3	2.82e-3
Iter 40	2.55e-4	1.81e-3	2.84e-3	547	3.12e-4	3.12e-4
Iter 200	9.05e-5	7.22e-4	1.64e-4	848	1.35e-4	1.60e-4

Table 5.13 Bootstrap analysis results of the robust compliance estimator using $\boldsymbol{\rho}$ at different optimization iterations of MFTO-CSn.

MFTO-CSn	MSE $\left[\widehat{c_{R,MF}}\right]^B$	$\mathbb{E}_B\left[\text{MSE}[\widehat{c_R}]_{\text{cs}}^{\text{ub,MF}}\right]$	MSE $\left[\widehat{c_{R,MC}}\right]^B$	$n_{c_R}^{eq,B}$	MSE $\left[\widehat{c_{R,\mu^*}}\right]^B$	MSE $\left[\widehat{c_{R,\sigma^*}}\right]^B$
Iter 5	1.71e-3	1.31e-2	2.18e-3	554	1.98e-3	3.90e-3
Iter 40	2.21e-4	1.50e-3	3.36e-4	781	2.47e-4	3.25e-4
Iter 200	6.15e-5	4.43e-4	1.60e-4	1323	6.90e-5	1.21e-4

Table 5.14 Bootstrap analysis results of the robust compliance estimator using $\boldsymbol{\rho}$ at different optimization iterations of MFTO-EVan.

MFTO-EVan	MSE $\left[\widehat{c_{R,MF}}\right]^B$	$\mathbb{E}_B\left[\text{MSE}[\widehat{c_R}]_{\mu\sigma}^{\text{MF}}\right]$	MSE $\left[\widehat{c_{R,MC}}\right]^B$	MSE $\left[\widehat{c_{R,\mu^*}}\right]^B$	MSE $\left[\widehat{c_{R,\sigma^*}}\right]^B$	$\text{MSE}[\widehat{c_R}]_{\mu\sigma}^{\text{MF},n_p}$
Iter 5	1.67e-3	1.62e-3	1.85e-3	2.57e-3	3.68e-3	1.66e-3
Iter 40	1.87e-4	1.57e-4	2.26e-4	2.71e-4	2.71e-4	1.85e-4
Iter 200	5.84e-5	4.78e-5	1.40e-4	1.03e-4	1.19e-4	5.87e-5

The comparisons between the MFMC estimators with the regular MC estimator of equal computational cost are carried out by contrasting the MSE $\left[\widehat{c_{R,MF}}\right]^B$ columns with the MSE $\left[\widehat{c_{R,MC}}\right]^B$ columns, and also by the $n_{c_R}^{eq,B}$ metric. The MFMC variants for all cases lead to a noticeable improvement of MSE for later iterations, and $n_{c_R}^{eq,B}$ shows that it would require about double the computational cost to achieve the same L^2 error using the regular MC robust compliance estimator. The CSn and EVan variants lead to the largest MSE reduction, while the Pn scheme has the smallest. Both the MBB beam and the carrier plate problems demonstrate the improvement of the inner loop UQ procedure using MFMC schemes in place of standard MC.

The existing MFMC strategies in literature mainly target the optimal estimation of either the mean or variance. These strategies denoted as MF-μ^* and MF-σ^*, are employed to construct a robust compliance estimator at MFTO iterations, and the bootstrap computations of their MSE are reported in the MSE $\left[\widehat{c_{R,\mu^*}}\right]^B$ and MSE $\left[\widehat{c_{R,\sigma^*}}\right]^B$ columns. For the carrier plate problem, MSE $\left[\widehat{c_{R,\sigma^*}}\right]^B$ generally has a much larger value than MSE $\left[\widehat{c_{R,\mu^*}}\right]^B$. This is the reverse of the MBB beam problem and shows

that it is difficult to know *a priori* which statistical moment should be prioritized, and focusing on one statistical moment does not always minimize the MSE of the robust compliance.

A qualitative explanation of this contrasting behavior is attributed to the topologies of the designs, shown in Figure 5.2 for MBB beam and Figure 5.10 for carrier plate. The designs of the MBB beam are all very similar, suggesting the existence of a primary underlying load path. On the other hand, the designs of carrier plate vary and have small members, suggesting that multiple load paths with equal prominence exist. Hence, for the MBB beam, accurate prediction of the mean displacement field is easier to achieve compared to the variance. Consequently, MFMC scheme targeting optimal variance estimation performs better. For the carrier plate, accurate prediction of the mean displacement is difficult due to various load paths and hence the MFMC scheme focusing on optimal mean estimation has better performance.

The MFMC variants in this work, based on minimizing quantities related to the MSE of robust compliance, offer alternative methods to construct an optimal MFMC estimator. Observing the MSE $\left[\widehat{c_{R,MF}}\right]^B$ columns, the CSt, CSn, and EVan variants all lead to a reduction of MSE compared to the $\widehat{c_{R,\mu^*}}$ and $\widehat{c_{R,\sigma^*}}$ estimators. This is a consistent observation for both the MBB beam and the carrier plate problems, showing that the MFTO variants are effective for problems with differing behaviors. Also, this emphasizes the importance of focusing on the proper objective when selecting the MFMC variables. The MF-μ^* and MF-σ^* strategies diminish the effectiveness of the MFMC robust compliance estimator in reducing the MSE. However, the Pn strategy leads to MSE values similar to $\widehat{c_{R,\sigma^*}}$, but higher than $\widehat{c_{R,\mu^*}}$. In the carrier plate problem, the Pn strategy is not very effective.

Furthermore, the values of $\mathbb{E}_B\left[\mathrm{MSE}[\widehat{c_R}]_{\mathrm{p}}^{\mathrm{ub,MF}}\right]$ and $\mathbb{E}_B\left[\mathrm{MSE}[\widehat{c_R}]_{\mathrm{cs}}^{\mathrm{ub,MF}}\right]$ are greater than MSE $\left[\widehat{c_{R,MF}}\right]^B$. This confirms that both $\mathrm{MSE}[\widehat{c_R}]_{\mathrm{p}}^{\mathrm{ub,MF}}$ and $\mathrm{MSE}[\widehat{c_R}]_{\mathrm{cs}}^{\mathrm{ub,MF}}$ are acceptable upper bounds of the MSE of $\widehat{c_{R,MF}}$, with $\mathrm{MSE}[\widehat{c_R}]_{\mathrm{cs}}^{\mathrm{ub,MF}}$ being more conservative. The $\mathbb{E}_B\left[\mathrm{MSE}[\widehat{c_R}]_{\mu\sigma}^{\mathrm{MF}}\right]$ differs with MSE $\left[\widehat{c_{R,MF}}\right]^B$ ranging from 5% to 20%. This difference is induced by n_{plt} not being large enough to ensure high statistical accuracy. Despite this inaccuracy, the EVan strategy is still effective in reducing the MSE of the estimator for c_R. Increasing the n_{plt} leads to improvement in accuracy. Setting $n_{plt} = P_b = 500$ and recomputing $\mathbb{E}_B\left[\mathrm{MSE}[\widehat{c_R}]_{\mu\sigma}^{\mathrm{MF}}\right]$ with the bootstrapping procedure, the approximated MSEs of the c_R estimator are: 1.66×10^{-3} at 5th iteration, 1.85×10^{-4} at 40th iteration, and 5.87×10^{-5} at 200th iteration. These values of $\mathbb{E}_B\left[\mathrm{MSE}[\widehat{c_R}]_{\mu\sigma}^{\mathrm{MF}}\right]$ computed with $n_{plt} = 500$ are similar to MSE $\left[\widehat{c_{R,MF}}\right]^B$. Furthermore, computing $\mathrm{MSE}[\widehat{c_R}]_{\mu\sigma}^{\mathrm{MF}}$ with $n_p = 20,000$ samples, as reported in $\mathrm{MSE}[\widehat{c_R}]_{\mu\sigma}^{\mathrm{MF},n_p}$,

the estimated MSE value is now very similar to bootstrap estimate of MSE $\left[\widehat{c_{R,MF}}\right]^B$, as statistical noise has been removed due to the law of large numbers. Ultimately, these observations add confidence to the results of Theorem 1 and Lemma 12.

The sample allocation in Lemma 13 is assessed by comparing the optimal sample allocation ratio from CSn and CSt. The CSn scheme numerically optimizes the r_m, while CSt employs the limiting distribution approximation. Through MFTO-CSn optimization, the approximate r_m^* are computed according to Lemma 13, and compared with the numerical optimum in Figure 5.7(b). Just like the MBB beam case, they are consistently similar, which shows the effectiveness of Lemma 13 in estimating the optimal r_m.

5.4 Conclusion

In this chapter, a MFMC-based RTO algorithm is developed which generates high quality structural designs under high dimensional material uncertainties and is more efficient than the MC-based RTO, which is typically used for these problems.

The MFTO algorithm consists of two novel ingredients. The first is the application of the MFMC scheme developed in Chapter 4 to generate accurate estimations of the statistic of interest, which is c_R. The second is the incorporation of the on-the-fly RB model as the LFM and the full FE model as the HFM in MFMC. The RB model is attractive for MFTO since it is much cheaper to evaluate than the FE model, and its output has a high correlation with that of the FE model. Also, the on-the-fly approach to RB does not interact with the spatial discretization, which is important for uncertainties with short correlation lengths.

The variables in the MFMC scheme are selected to minimize the MSE of the estimator for c_R, which is a linear combination of the mean and standard deviation of the compliance. This approach leads to four variants, which are CSt and CSn from minimizing $\text{MSE}[\widehat{c_R}]^{\text{ub}}_{\text{cs}}$, an upper bound of the MSE; Pn from minimizing $\text{MSE}[\widehat{c_R}]^{\text{ub}}_{\text{p}}$, another upper bound of the MSE; and EVan from minimizing the $\text{MSE}[\widehat{c_R}]_{\mu\sigma}$, which is an approximation of the MSE. Numerical cases demonstrate that given a fixed computational budget, these MFMC variants provide a better estimation of c_R compared to the standard MC, as well as MFMC schemes that target the optimal estimation of either the mean or the variance.

Comparing the numerical results of the four MFMC variants, the CSt and CSn variants are the most effective in reducing the MSE of the estimator of c_R given a computational budget. The EVan variant is also effective, but, the expression

of $\mathrm{MSE}[\widehat{c_R}]_{\mu\sigma}$ requires estimations of the product of raw moments for which high statistical accuracy is difficult to achieve using only a small set of n_{plt}. The Pn variant is the least effective in optimal estimation of c_R. However, the $\mathrm{MSE}[\widehat{c_R}]_{\mathrm{p}}^{\mathrm{ub}}$ upper bound is tighter compared to $\mathrm{MSE}[\widehat{c_R}]_{\mathrm{cs}}^{\mathrm{ub}}$, and since it is only dependent on the MSEs of mean and variance estimators, it is easier to approximate accurately with a small set of n_{plt}. For applications where the computational budget constraint is relaxed and instead a maximum of MSE is considered, if sufficient statistical accuracy is achievable the EVan strategy should be employed. If sufficient statistical accuracy cannot be achieved for $\mathrm{MSE}[\widehat{c_R}]_{\mu\sigma}$, then the $\mathrm{MSE}[\widehat{c_R}]_{\mathrm{p}}^{\mathrm{ub}}$ upper bound should be used as the threshold.

Chapter 6

Conclusion

This thesis develops robust topology optimization (RTO) algorithms that are efficient and produce uncertainty-aware structures under material variability induced by additive manufacturing. RTO has a nested loop framework, where the statistic of interest is computed in the inner loop using an uncertainty quantification (UQ) scheme, while the design variables are updated in the outer loop using filters and a gradient-based optimizer. The governing equation in RTO is the static linear elasticity system and the statistic of interest is the robust compliance (c_R), which is a weighted sum of the mean and standard deviation of the compliance. Having an accurate estimation of c_R leads to high quality designs. The material uncertainties, modeled using the Karhunen–Loève expansion, are high dimensional and only the Monte Carlo (MC) method is tractable while other UQ schemes suffer from the curse of dimensionality. This thesis presents two novel UQ schemes for the efficient and reliable computation of c_R in the presence of high stochastic dimensions, and they are made compatible with gradient-based optimization to form RTO algorithms.

The first UQ scheme is the Neumann expansion (NE) scheme, presented in Chapter 3, alongside the associated RTO algorithm, denoted as NETO. The NE scheme represents the compliance as a perturbed series, where each expansion term is approximated as a product between a power of the random variable α and a constant. This is a dimension reduction approach since all of the variability of the system is accounted for by the powers of α. For RTO, the expected values and gradients of the expansion terms are evaluated using sampling methods each iteration, which are then employed to compute the c_R and its gradient. Since sampling methods are costly to re-evaluate each iteration, a storage and update algorithm is developed to enable rapid computation of the quantities following the update of design variables.

The NETO algorithm is efficient in the sense of reduced computational cost compared to the MC-based RTO (MCTO) algorithm. The numerical cases demonstrate

that NETO can produce designs with a similar level of optimality as the MCTO designs generated using 1000 random samples while being a factor of 300 to 400 faster. Since the NETO approximates the randomness of the system using only the α associated variables, it leads to an offset error compared to the true c_R. For the optimization cases considered, the relative errors are less than 2% and depend on the characteristics of the uncertainty. This is the shortcoming of the NETO method and would require further development. Ultimately, for high dimensional material uncertainties, NETO can provide a substantial improvement in computational efficiency compared to MCTO while generating robust designs with similar quality, albeit admitting a higher estimation error of the robust compliance.

The second UQ scheme is the multi-fidelity Monte Carlo (MFMC) scheme, presented in Chapter 4. The standard MC approach estimates c_R by sampling from a high fidelity model (HFM), and the quality of the MC estimator is assessed using the mean-squared error (MSE). The MFMC scheme employs a low fidelity model (LFM) and estimates c_R by combining the samples from both the HFM and LFM. If evaluating the LFM is cheaper and the ouput of the LFM has a good statistical correlation with the output of the HFM, then the MFMC estimator of the c_R has a lower MSE, leading to a more accurate estimation of c_R. The existing MFMC approaches are only applicable to the optimal estimation of either the mean or the variance, which may not be optimal for the estimation of c_R. This thesis develops strategies for minimizing the MSE of the estimator for c_R. Also, unbiased estimators are developed to enable the MSE of c_R to be computed in optimization setting.

The MFMC-based RTO (MFTO) algorithm is detailed in Chapter 5. The MFTO algorithm is efficient in the sense of reduced estimation error compared to MCTO for the same computational cost. The HFM employed is the finite element model and the LFM corresponds to the on-the-fly reduced basis model. The RB model is attractive for RTO since it does not interfere with spatial discretization, which is important for uncertainties with short length scales. The numerical cases demonstrate that comparing the MFTO and MCTO algorithms with the same computational budget, the MSEs of the MFMC estimators are about 20% to 60% lower than the MC estimators. For MCTO to achieve the same accuracy, about two to three times more computational cost is required. In addition, the MFMC strategies focusing on the optimal estimation of c_R are shown to be more effective than the strategies from the literature which target either the mean or the variance. The designs from the MFTO are as optimal as the designs from the MCTO, which demonstrates the efficacy of the MFTO in producing uncertainty-aware structures.

Appendix A

Supplementary Information for Chapter 4

A.1 Estimators for the Monte Carlo Scheme

A.1.1 MC Estimators for Mean and Variance

Let $\boldsymbol{\xi} = \{\xi_d\}, d = 1, \cdots, n_d$ be the set of input random variables, with n_d being the dimension of the input variable. Consider n_s independent samples of $\boldsymbol{\xi}$, leading to $\boldsymbol{\xi}_q = \{\xi_d\}_q, q = 1, \cdots, n_s$. Evaluating the HFM or LFM using this set of samples leads to n_s independent samples of the output of interest, which is the compliance in this thesis, denoted as $\boldsymbol{c} = \{c_q\}, q = 1, \cdots, n_s$. Define the mean parameter of the compliance as μ_c, the unbiased MC estimator for μ_c is:

$$\widehat{\mu_{c,MC}} = \frac{1}{n_s} \sum_{i=1}^{n_s} c_i. \tag{A.1}$$

The unbiased MC estimator for the variance is:

$$\widehat{\sigma^2_{c,MC}} = \frac{1}{n_s - 1} \sum_{i=1}^{n_s} (c_i - \widehat{\mu_{c,MC}})^2. \tag{A.2}$$

For the MC mean estimator, the MSE is:

$$\mathrm{MSE}[\widehat{\mu_{c,MC}}] = \mathbb{E}\big[(\widehat{\mu_{c,MC}} - \mu_c)^2\big] = \frac{\sigma_c^2}{n_s}, \tag{A.3}$$

where σ_c^2 is the population variance parameter of the compliance. The MSE for the

MC variance estimator is:

$$\mathrm{MSE}[\widehat{\sigma^2_{c,MC}}] = \mathbb{E}\big[(\widehat{\sigma_{c,MC}} - \sigma_c^2)^2\big] = \frac{1}{n_s}(\delta_c - \frac{n_s-3}{n_s-1}\sigma_c^4), \tag{A.4}$$

where $\delta_c = \mathbb{E}[(c-\mu_c)^4]$ is the 4th central moment parameter of compliance.

A.1.2 MC Estimator for Standard Deviation

The biased MC standard deviation estimator is:

$$\widehat{\sigma_{c,MC}} = \sqrt{\widehat{\sigma^2_{c,MC}}}. \tag{A.5}$$

For a general standard deviation estimator, $\widehat{\sigma_c}$, the square root imposes challenges in obtaining a closed form of its MSE. A Taylor series approximation of the square root function centered at σ_c^2 allows the derivation of MSE for a generic $\widehat{\sigma_c}$ estimator [113]. The result is described in the following lemma.

Lemma 14. *Given the population variance parameter σ_c^2 and an unbiased sample variance estimator $\widehat{\sigma_c^2}$, the biased standard deviation estimator $\widehat{\sigma_c} = \sqrt{\widehat{\sigma_c^2}}$ has the following properties:*

Bias: $\mathbb{E}\left[\sqrt{\widehat{\sigma_c^2}} - \sigma_c\right] = \frac{-1}{8\sigma_c^3} MSE[\widehat{\sigma_c^2}] + O(\mathbb{E}\Big[(\widehat{\sigma_c^2} - \sigma_c^2)^3\Big])$,

Mean Squared Error: $\mathbb{E}\left[\left(\sqrt{\widehat{\sigma_c^2}} - \sigma_c\right)^2\right] = \frac{1}{4\sigma_c^2} MSE[\widehat{\sigma_c^2}] + O(\mathbb{E}\Big[(\widehat{\sigma_c^2} - \sigma_c^2)^3\Big])$.

Proof of Lemma 14: The Taylor series expansion of the function $f(x) = \sqrt{x}$ about x_0 is to 2nd order

$$\sqrt{x} = \sqrt{x_0} + \frac{1}{2\sqrt{x_0}}(x - x_0) - \frac{1}{8x_0^{3/2}}(x-x_0)^2 + O((x-x_0)^3).$$

Subtracting $\sqrt{x_0}$ from both side of the equation, substitute in $x_0 = \sigma_c^2$ and $x = \widehat{\sigma_c^2}$, then taking the expected value of both sides, the result is:

$$\mathbb{E}\left[\sqrt{\widehat{\sigma_c^2}} - \sigma_c\right] = \frac{1}{2\sigma_c}\mathbb{E}\Big[\widehat{\sigma_c^2} - \sigma_c^2\Big] - \frac{1}{8\sigma_c^3}\mathbb{E}\Big[(\widehat{\sigma_c^2} - \sigma_c^2)^2\Big] + O(\mathbb{E}\Big[(\widehat{\sigma_c^2} - \sigma_c^2)^3\Big]).$$

Since $\widehat{\sigma_c^2}$ is an unbiased estimator, the first term vanishes. The second expected value

term is the definition of $\text{MSE}[\widehat{\sigma_c^2}]$, and hence the equation is simplified to

$$\mathbb{E}\left[\sqrt{\widehat{\sigma_c^2}} - \sigma_c\right] = -\frac{1}{8\sigma_c^3}\text{MSE}[\widehat{\sigma_c^2}] + O(\mathbb{E}\left[(\widehat{\sigma_c^2} - \sigma_c^2)^3\right]),$$

which is the equation for the estimator bias presented in the lemma.

For the MSE of the estimator, first expand:

$$\mathbb{E}\big[(\widehat{\sigma_c} - \sigma_c)^2\big] = \mathbb{E}\left[\widehat{\sigma_c^2} - \sigma_c^2\right] + 2\mathbb{E}\big[\sigma_c^2 - \widehat{\sigma_c}\sigma_c^2\big].$$

The first term vanishes since $\widehat{\sigma_c^2}$ is unbiased, and the second term is equivalent to $2\sigma_c$ multiplied with the negative of the bias of the estimator, and hence

$$\mathbb{E}\big[(\widehat{\sigma_c} - \sigma_c)^2\big] = 2\sigma_c\left(\frac{-1}{8\sigma_c^3}\mathbb{E}\left[(\widehat{\sigma_c^2} - \sigma_c^2)^2\right] + O(\mathbb{E}\left[(\widehat{\sigma_c^2} - \sigma_c^2)^3\right])\right) = \frac{1}{4\sigma_c^2}\text{MSE}[\widehat{\sigma_c^2}] + O(\mathbb{E}\left[(\widehat{\sigma_c^2} - \sigma_c^2)^3\right]).$$

The expression for the MSE is obtained. □

This lemma can be directly applied to the MC standard deviation estimator by substituting in $\widehat{\sigma_{c,MC}}$. Since $\widehat{\sigma_{c,MC}}$ is biased, its MSE is not equal to its variance.

A.1.3 Practical MSE Computations

Computing $\text{MSE}[\widehat{\mu_{c,MC}}]$, $\text{MSE}[\widehat{\sigma^2_{c,MC}}]$, and $\text{MSE}[\widehat{\sigma_{c,MC}}]$ requires parameters including: σ_c, μ_c, δ_c, etc. Practically, these parameters are unknown and unbiased MC estimators are employed estimate their values.

The σ_c^2 is approximated by the standard MC estimator $\widehat{\sigma^2_{c,MC}}$. The unbiased MC estimator of δ_c is provided by Lemma 15.

Lemma 15. *Unbiased MC estimator of the fourth central moment δ_c given n_s samples is:*

$$\widehat{\delta_c} = \frac{-3n_s(2n_s-3)}{(n_s-1)(n_s-2)(n_s-3)}\widehat{m_2}^2 + \frac{n_s(n_s^2-2n_s+3)}{(n_s-1)(n_s-2)(n_s-3)}\widehat{m_4}. \tag{A.6}$$

The $\widehat{m_2}$ and $\widehat{m_4}$ are the biased second and fourth central moment estimator from MC:

$$\widehat{m_2} = \frac{1}{n_s}\sum_{i=1}^{n_s}(c_i - \widehat{\mu_{c,MC}})^2, \text{ and } \widehat{m_4} = \frac{1}{n_s}\sum_{i=1}^{n_s}(c_i - \widehat{\mu_{c,MC}})^4. \tag{A.7}$$

Proof of Lemma 15: See Gerlovina and Hubbard [114]. □

The unbiased estimator of σ_c^4 is provided by Lemma 5. For estimating the σ_c^3 parameter, it is difficult to develop a general unbiased estimator due to the difficulties

introduced by the square root operator, just like the case of σ_c. Hence, $\widehat{\sigma^2_{c,MC}}^{3/2}$ is used as an approximation.

A.2 Proofs, Lemma, and Corollary for Section 4.2

A.2.1 Proof of Lemma 2

Proof of Lemma 2: Since $\widehat{\sigma^2_{c,MF}}$ is unbiased, its MSE is equivalent to its variance ($\mathbb{V}[\cdot]$) and hence:

$$\text{MSE}[\widehat{\sigma^2_{c,MF}}] = \mathbb{V}\big[\widehat{\mu_{h,MC}}^{n_s}\big] + \alpha_\sigma^2 \mathbb{V}\big[(\widehat{\mu_{l,MC}}^{m_s} - \widehat{\mu_{l,MC}}^{n_s})\big] + 2\alpha_\sigma \text{Cov}\big[\widehat{\mu_{h,MC}}^{n_s}, (\widehat{\mu_{l,MC}}^{m_s} - \widehat{\mu_{l,MC}}^{n_s})\big]. \quad \text{(A.8)}$$

Using Lemma 3.2 from Qian et al. [85], the terms in the above equation are expanded:

$$\begin{aligned}\mathbb{V}\big[(\widehat{\mu_{l,MC}}^{m_s} - \widehat{\mu_{l,MC}}^{n_s})\big] &= \mathbb{V}\big[\widehat{\mu_{l,MC}}^{m_s}\big] + \mathbb{V}\big[\widehat{\mu_{l,MC}}^{n_s}\big] - 2\text{Cov}\big[\widehat{\mu_{l,MC}}^{m_s}, \widehat{\mu_{l,MC}}^{n_s}\big], \\ &= \frac{1}{n_s}(\delta_l - \frac{n_s-3}{n_s-1}\sigma_l^4) - \frac{1}{m_s}(\delta_l - \frac{m_s-3}{m_s-1}\sigma_l^4).\end{aligned}$$

Also,

$$\text{Cov}\big[\widehat{\mu_{h,MC}}^{n_s}, (\widehat{\mu_{l,MC}}^{m_s} - \widehat{\mu_{l,MC}}^{n_s})\big] = \left[-\tfrac{1}{m_s}\left(\text{Cov}[\vartheta_h,\vartheta_l] + \tfrac{2}{m_s-1}\text{Cov}[c_h,c_l]^2\right) + \tfrac{1}{n_s}\left(\text{Cov}[\vartheta_h,\vartheta_l] + \tfrac{2}{n_s-1}\text{Cov}[c_h,c_l]^2\right)\right].$$

The MSE expressions in Equation (4.6) and Equation (A.8) are identical. Since the variance is strictly positive, Equation (4.6) is a convex quadratic in α_σ. Applying Proposition 2 from Gorodetsky et al. [87], the stationary point of $\frac{\partial \text{MSE}[\widehat{\sigma^2_{c,MF}}]}{\partial \alpha_\sigma} = 0$ is:

$$\alpha_\sigma^* = \frac{\frac{1}{n_s}\left(\text{Cov}[\vartheta_h,\vartheta_l]+\frac{2}{n_s-1}\text{Cov}[c_h,c_l]^2\right)-\frac{1}{m_s}\left(\text{Cov}[\vartheta_h,\vartheta_l]+\frac{2}{m_s-1}\text{Cov}[c_h,c_l]^2\right)}{\frac{1}{n_s}(\delta_l-\frac{n_s-3}{n_s-1}\sigma_l^4)-\frac{1}{m_s}(\delta_l-\frac{m_s-3}{m_s-1}\sigma_l^4)},$$

which leads to the expression for α_σ^*.

□

A.2.2 Proof of Lemma 3

Proof of Lemma 3: Recalling the definition of $\widehat{\mu_{\Gamma,MF}}$:

$$\widehat{\mu_{\Gamma,MF}} = \widehat{\mu_{\Gamma,MC}}^{n_s} + \alpha(\widehat{\mu_{\gamma,MC}}^{m_s} - \widehat{\mu_{\gamma,MC}}^{n_s}), \quad m_s > n_s.$$

If the first assumption holds true, then each of the MC estimators are just a sum of Γ or γ. The MFMC estimator is thus composed of sum of jointly normal random variables, hence the estimator itself is a normally distributed variable. By extension, $\widehat{\mu_{\Gamma,MF}} - \mu_\Gamma$ is also a normal random variable, and its variance is the sum of the variances of all the Γ and γ involved in the MC estimators, in addition to the covariances between them.

If the second assumption holds, then:

$$\widehat{\mu_{\Gamma,MF}} - \mu_\Gamma = (\widehat{\mu_{\Gamma,MC}}^{n_s} - \mu_\Gamma) + \alpha(\widehat{\mu_{\gamma,MC}}^{m_s} - \widehat{\mu_{\gamma,MC}}^{n_s}).$$

Using CLT, the first term is normally distributed with

$$\widehat{\mu_{\Gamma,MC}}^{n_s} - \mu_\Gamma \sim \mathcal{N}(0, \frac{\mathbb{V}[\Gamma]}{n_s}).$$

For the second term, using "Result 14" from O'Neill [115], it is also a normal random variable:

$$\widehat{\mu_{\gamma,MC}}^{m_s} - \widehat{\mu_{\gamma,MC}}^{n_s} \sim \mathcal{N}(0, \frac{m_s - n_s}{n_s m_s}\mathbb{V}[\gamma]).$$

Since α and μ_Γ are constants, $\widehat{\mu_{\Gamma,MF}} - \mu_\Gamma$ is from a sum of jointly normal random variables, and hence it is also a normal random variable with variance equal to the sum of the individual variances of the two terms as well as their covariance.

Consider the following rearrangement of $\widehat{\mu_{\Gamma,MF}} - \mu_\Gamma$:

$$\begin{aligned}\widehat{\mu_{\Gamma,MF}} - \mu_\Gamma &= \widehat{\mu_{\Gamma,MC}}^{n_s} + \alpha(\widehat{\mu_{\gamma,MC}}^{m_s} - \widehat{\mu_{\gamma,MC}}^{n_s}) - \mu_\Gamma + \alpha\mu_\gamma - \alpha\mu_\gamma, \\ &= \alpha\left(\widehat{\mu_{\gamma,MC}}^{m_s} - \mu_\gamma\right) + \left((\widehat{\mu_{\Gamma,MC}}^{n_s} - \alpha\widehat{\mu_{\gamma,MC}}^{n_s}) - (\mu_\Gamma - \alpha\mu_\gamma)\right).\end{aligned}$$

By the application of CLT to MC estimators, both terms are normal random variables:

$$\widehat{\mu_{\gamma,MC}}^{m_s} - \mu_\gamma \sim \mathcal{N}(0, \alpha^2\frac{\mathbb{V}[\gamma]}{m_s}),$$

and

$$(\widehat{\mu_{\Gamma,MC}}^{n_s} - \alpha\widehat{\mu_{\gamma,MC}}^{n_s}) - (\mu_\Gamma - \alpha\mu_\gamma) \sim \mathcal{N}(0, \frac{\mathbb{V}[\Gamma - \alpha\gamma]}{n_s}).$$

If the third assumption holds, since μ_γ and $\mu_\Gamma - \alpha\mu_\gamma$ are both constants, $\widehat{\mu_{\gamma,MC}}^{m_s} - \mu_\gamma$ and $(\widehat{\mu_{\Gamma,MC}}^{n_s} - \alpha\widehat{\mu_{\gamma,MC}}^{n_s}) - (\mu_\Gamma - \alpha\mu_\gamma)$ are jointly normal, and hence $\widehat{\mu_{\Gamma,MF}} - \mu_\Gamma$ is also normally distributed. The variance of this difference is the variances of the two terms plus their covariances.

All three assumptions lead to a normally distributed $\widehat{\mu_{\Gamma,MF}} - \mu_\Gamma$. The $\widehat{\mu_{\Gamma,MF}}$

estimator is unbiased, hence the mean of the distribution is zero. For the variance, all cases resulted in some form of the sum of variances and covariances of individual variables, where these variables are different depending on the arrangement of the equation. However, in all cases, from the properties of variance and covariance, this sum is equivalent to $\mathbb{V}\big[\widehat{\mu_{\Gamma,MF}}\big]$, and hence also to MSE $\big[\widehat{\mu_{\Gamma,MF}}\big]$. Ultimately, these assumptions result in $(\widehat{\mu_{\Gamma,MF}} - \mu_\Gamma) \sim \mathcal{N}(0, \text{MSE}\left[\widehat{\mu_{\Gamma,MF}}\right])$, and using the standard CI formulation for a normal distribution, the CI approximation in Lemma 3 is achieved. □

A.2.3 Proof of Lemma 4

Proof of Lemma 4: The full expression for $\widehat{\mu_{\vartheta_h,MF}}$ is shown to clarify its contrast from $\widehat{\sigma^2_{c,MF}}$:

$$\widehat{\mu_{\vartheta_h,MF}} = \widehat{\mu_{\vartheta_h,MC}}^{n_s} + \alpha_\sigma(\widehat{\mu_{\vartheta_l,MC}}^{m_s} - \widehat{\mu_{\vartheta_l,MC}}^{n_s}) = \tfrac{1}{n_s}\textstyle\sum_{i=1}^{n_s}(c_{h,i} - \mu_h)^2 + \alpha_\sigma\left(\tfrac{1}{m_s}\sum_{i=1}^{m_s}(c_{l,i} - \mu_l)^2 - \tfrac{1}{n_s}\sum_{i=1}^{n_s}(c_{l,i} - \mu_l)^2\right).$$

Note that $\widehat{\mu_{\vartheta_h,MF}}$ is also an unbiased estimator for σ^2_h, but unlike $\widehat{\sigma^2_{c,MF}}$, the Bessel's correction $(n_s - 1)$ is not required since the parameters μ_l and μ_h are used directly. Since these mean parameters are typically unknown, $\widehat{\mu_{\vartheta_h,MF}}$ cannot be computed.

In $\widehat{\sigma^2_{c,MF}}$, the μ_l and μ_h are approximated by $\widehat{\mu_{h,MC}}^{n_s}$, $\widehat{\mu_{l,MC}}^{m_s}$, and $\widehat{\mu_{l,MC}}^{n_s}$. The $\widehat{\sigma^2_{c,MF}}$ is rewritten to include $\widehat{\mu_{\vartheta_h,MF}}$ in its expression:

$$\begin{aligned}
\widehat{\sigma^2_{h,MC}}^{n_s} &= \frac{1}{n_s - 1}\sum_{i=1}^{n_s}(c_{h,i} - \widehat{\mu_{h,MC}}^{n_s})^2 = \frac{1}{n_s - 1}\sum_{i=1}^{n_s}((c_{h,i} - \mu_h) + (\mu_h - \widehat{\mu_{h,MC}}^{n_s}))^2, \\
&= \left[\frac{1}{n_s}\sum_{i=1}^{n_s}(c_{h,i} - \mu_h)^2\right] + (\mu_h - \widehat{\mu_{h,MC}}^{n_s})^2 + \frac{1}{n_s}\widehat{\sigma^2_{h,MC}}^{n_s}.
\end{aligned}$$

Similar derivation can be done for $\widehat{\sigma^2_{l,MC}}^{m_s}$ and $\widehat{\sigma^2_{l,MC}}^{n_s}$, hence $\widehat{\sigma^2_{c,MF}}$ can be rewritten as:

$$\begin{aligned}
\widehat{\sigma^2_{c,MF}} &= \widehat{\sigma^2_{h,MC}}^{n_s} + \alpha_\sigma\left(\widehat{\sigma^2_{l,MC}}^{m_s} - \widehat{\sigma^2_{l,MC}}^{n_s}\right), \\
&= \left\{\frac{1}{n_s}\sum_{i=1}^{n_s}(c_{h,i} - \mu_h)^2 + \alpha_\sigma\frac{1}{m_s}\sum_{i=1}^{m_s}(c_{l,i} - \mu_l)^2 - \alpha_\sigma\frac{1}{n_s}\sum_{i=1}^{n_s}(c_{l,i} - \mu_l)^2\right\} \\
&\quad + \left\{(\mu_h - \widehat{\mu_{h,MC}}^{n_s})^2 + \alpha_\sigma(\mu_l - \widehat{\mu_{l,MC}}^{m_s})^2 - \alpha_\sigma(\mu_l - \widehat{\mu_{l,MC}}^{n_s})^2\right\} \\
&\quad + \left\{\frac{1}{n_s}\widehat{\sigma^2_{h,MC}}^{n_s} + \alpha_\sigma\frac{1}{m_s}\widehat{\sigma^2_{l,MC}}^{m_s} - \alpha_\sigma\frac{1}{n_s}\widehat{\sigma^2_{l,MC}}^{n_s}\right\}.
\end{aligned} \tag{A.9}$$

The α_σ is assumed to be a bounded constant. In the right hand side of the last equality in Equation (A.9), the first curly bracket term is the definition of $\widehat{\mu_{\vartheta_h,MF}}$. For the second curly bracket term, by the weak law of large numbers, the MC mean estimators converges in probability to the true parameters, meaning $\lim_{n_s\to\infty} \widehat{\mu_{h,MC}}^{n_s} \xrightarrow{\text{P}} \mu_h$, $\lim_{m_s\to\infty} \widehat{\mu_{l,MC}}^{m_s} \xrightarrow{\text{P}} \mu_l$, and $\lim_{n_s\to\infty} \widehat{\mu_{l,MC}}^{n_s} \xrightarrow{\text{P}} \mu_l$, where $\xrightarrow{\text{P}}$ denote convergence in probability. By the Slutsky's theorem or by the Continuous mapping theorem, the squared differences converges in probability to zero. Hence, the second term overall converges in probability to zero:

$$\lim_{n_s\to\infty}\lim_{m_s\to\infty}\left\{(\mu_h - \widehat{\mu_{h,MC}}^{n_s})^2 + \alpha_\sigma(\mu_l - \widehat{\mu_{l,MC}}^{m_s})^2 - \alpha_\sigma(\mu_l - \widehat{\mu_{l,MC}}^{n_s})^2\right\} \xrightarrow{\text{P}} 0.$$

For the third curly bracket term, since the c_h and c_l are second order random variables, they have finite variance and the unbiased variance estimators are also bounded. Hence, the $\widehat{\sigma^2_{h,MC}}^{n_s}$, $\widehat{\sigma^2_{l,MC}}^{m_s}$, and $\widehat{\sigma^2_{l,MC}}^{n_s}$ converges to their distributions, which are bounded in the support. Taking $\lim_{n_s\to\infty}$ or $\lim_{m_s\to\infty}$, the $\frac{1}{n_s}$ and $\frac{1}{m_s}$ are convergent deterministic sequences, and they converge almost surely to zero, which implies convergence in probability. Combining these behaviors, by Slutsky's theorem,

$$\lim_{n_s\to\infty}\lim_{m_s\to\infty}\left\{\frac{1}{n_s}\widehat{\sigma^2_{h,MC}}^{n_s} + \alpha_\sigma\frac{1}{m_s}\widehat{\sigma^2_{l,MC}}^{m_s} - \alpha_\sigma\frac{1}{n_s}\widehat{\sigma^2_{l,MC}}^{n_s}\right\} \xrightarrow{\text{d}} 0.$$

In summary, taking $\lim_{n_s\to\infty}\lim_{m_s\to\infty}$ in the last equality in Equation (A.9), the first curly bracket term converges in distribution to $\widehat{\mu_{\vartheta_h,MF}}$, the second curly bracket term converges in probability to zero, and the third term converges in distribution to zero. Hence, applying Slutsky's theorem again, $\lim_{n_s\to\infty}\lim_{m_s\to\infty}\widehat{\sigma^2_{c,MF}} \xrightarrow{\text{d}} \widehat{\mu_{\vartheta_h,MF}}$. This shows that the limiting distribution of $\widehat{\sigma^2_{c,MF}}$ follows that of $\widehat{\mu_{\vartheta_h,MF}}$. □

A.2.4 Proof of Lemma 5

Proof of Lemma 5: Since $\widehat{\sigma^2_{c,MC}}$ is unbiased, its MSE is equivalent to its variance:

$$\mathbb{E}\left[\left(\widehat{\sigma^2_{c,MC}} - \mathbb{E}\left[\widehat{\sigma^2_{c,MC}}\right]\right)^2\right] = \text{MSE}[\widehat{\sigma^2_{c,MC}}] = \mathbb{E}\left[(\widehat{\sigma^2_{c,MC}})^2\right] - (\sigma^2_c)^2.$$

Applying the MSE expression in Equation (A.4) to the above equation:

$$\sigma^4_c = \mathbb{E}\left[(\widehat{\sigma^2_{c,MC}})^2\right] - \frac{1}{n_s}(\delta_c - \frac{n_s-3}{n_s-1}\sigma^4_c).$$

Rearranging to isolate σ_c^4 to obtain:

$$\sigma_c^4 = \frac{n_s(n_s-1)}{n_s^2-2n_s+3}\mathbb{E}\Big[\widehat{(\sigma_{c,MC}^2)^2}\Big] - \frac{n_s-1}{n_s^2-2n_s+3}\delta_c.$$

Replacing δ_c with its unbiased estimator $\widehat{\delta_c}$ as presented in Equation (A.6), removing the $\mathbb{E}[]$ operator for $\widehat{(\sigma_{c,MC}^2)^2}$, and replacing σ_c^4 with $\widehat{\sigma_c^4}$, the final expression for $\widehat{\sigma_c^4}$ is obtained.

$$\widehat{\sigma_c^4} = \frac{n_s(n_s-1)}{n_s^2-2n_s+3}\widehat{(\sigma_{c,MC}^2)^2} - \frac{n_s-1}{n_s^2-2n_s+3}\widehat{\delta_c}.$$

Since $\mathbb{E}\Big[\widehat{\delta_c}\Big] = \delta_c$, the estimator $\widehat{\sigma_c^4}$ is unbiased as applying $\mathbb{E}[\cdot]$ to the right hand side of the above equation leads to σ_c^4. □

A.2.5 Corollary 15.1

Corollary 15.1. *Given n_{plt} pilot samples of c_h evaluated from the HFM and c_l evaluated from the LFM, the unbiased estimators of σ_h^2, σ_l^2, δ_h, and δ_l are:*

$$\widehat{\sigma_h^2} = \frac{1}{n_{plt}-1}\sum_{i=1}^{n_{plt}}\left(c_{h,i} - \left(\frac{1}{n_{plt}}\sum_{j=1}^{n_{plt}} c_{h,j}\right)\right)^2; \tag{A.10}$$

$$\widehat{\sigma_l^2} = \frac{1}{n_{plt}-1}\sum_{i=1}^{n_{plt}}\left(c_{l,i} - \left(\frac{1}{n_{plt}}\sum_{j=1}^{n_{plt}} c_{l,j}\right)\right)^2; \tag{A.11}$$

$$\widehat{\delta_h} = \frac{-3n_{plt}(2n_{plt}-3)}{(n_{plt}-1)(n_{plt}-2)(n_{plt}-3)}\widehat{m_{2,h}}^2 + \frac{n_{plt}(n_{plt}^2-2n_{plt}+3)}{(n_{plt}-1)(n_{plt}-2)(n_{plt}-3)}\widehat{m_{4,h}}; \tag{A.12}$$

$$\widehat{\delta_l} = \frac{-3n_{plt}(2n_{plt}-3)}{(n_{plt}-1)(n_{plt}-2)(n_{plt}-3)}\widehat{m_{2,l}}^2 + \frac{n_{plt}(n_{plt}^2-2n_{plt}+3)}{(n_{plt}-1)(n_{plt}-2)(n_{plt}-3)}\widehat{m_{4,l}}. \tag{A.13}$$

Proof of Corollary 15.1: The expressions for $\widehat{\sigma_h^2}$ and $\widehat{\sigma_l^2}$ follow the regular MC variance estimator with $n_s = n_{plt}$ samples from Equation (A.2), where c is replaced with c_h or c_l. The expressions for $\widehat{\delta_h}$ and $\widehat{\delta_l}$ follow the unbiased MC estimator in Equation (A.6) with $n_s = n_{plt}$ samples. The c are replaced with c_h or c_l. Similar procedure is also used to obtain $\widehat{m_{2,h}}$ and $\widehat{m_{2,l}}$ from Equation (A.7), in addition to $\widehat{m_{4,h}}$ and $\widehat{m_{4,l}}$ from Equation (A.7). □

A.2.6 Proof of Lemma 6

Proof of Lemma 6: Taking the expected value of $\widehat{\mu_A}\widehat{\mu_B}$ leads to:

$$\mathbb{E}[\widehat{\mu_A}\widehat{\mu_B}] = \frac{1}{n_s^2}\mathbb{E}\left[\left(\sum_{i=1}^{n_s} A_i\right)\left(\sum_{j=1}^{n_s} B_j\right)\right].$$

The product of sum inside $\mathbb{E}[\cdot]$ has n_s^2 total terms, n_s of them have $i = j$, while $n_s(n_s - 1)$ has $i \neq j$. Hence, the above equation simplifies to:

$$\mathbb{E}[\widehat{\mu_A}\widehat{\mu_B}] = \frac{1}{n_s^2}\left(n_s\mathbb{E}[AB] + n_s(n_s-1)\mathbb{E}[A]\mathbb{E}[B]\right).$$

Re-arranging and isolating for $\mathbb{E}[A]\mathbb{E}[B]$:

$$\mathbb{E}[A]\mathbb{E}[B] = \frac{1}{n_s - 1}\left(n_s\mathbb{E}[\widehat{\mu_A}\widehat{\mu_B}] - \mathbb{E}[AB]\right).$$

Replacing $\mathbb{E}[A]\mathbb{E}[B]$ with $\widehat{\mu_A\mu_B}$, replacing $\mathbb{E}[AB]$ with $\widehat{\mu_{AB}}$ and removing $\mathbb{E}[\cdot]$ from $\mathbb{E}[\widehat{\mu_A}\widehat{\mu_B}]$ leads to the unbiased estimator shown in Lemma 6. Taking $\mathbb{E}[\cdot]$ on the right hand side of the equation leads to $\mathbb{E}[A]\mathbb{E}[B] = \mu_A\mu_B$, hence the estimator is unbiased. □

A.2.7 Proof for Lemma 7

Proof of Lemma 7: Taking the expected value of $\widehat{\mu_A}\widehat{\mu_B}\widehat{\mu_C}$ leads to:

$$\mathbb{E}[\widehat{\mu_A}\widehat{\mu_B}\widehat{\mu_C}] = \frac{1}{n_s^3}\mathbb{E}\left[\left(\sum_{i=1}^{n_s} A_i\right)\left(\sum_{i=1}^{n_s} B_i\right)\left(\sum_{i=1}^{n_s} C_i\right)\right].$$

The product of the sums inside $\mathbb{E}[\cdot]$ has n_s^3 total terms. n_s terms have $i = j = k$, three cases of $n_s(n_s - 1)$ terms have either $(i = j \neq k)$ or $(i = k \neq j)$ or $(j = k \neq i)$, and $n_s(n_s - 1)(n_s - 2)$ terms of $i \neq j \neq k$. Gathering the like terms and simplifying:

$$\mathbb{E}[\widehat{\mu_A}\widehat{\mu_B}\widehat{\mu_C}] = \frac{1}{n_s^3}\Big(n_s\mathbb{E}[ABC] + n_s(n_s-1)(\mathbb{E}[AB]\mathbb{E}[C] + \mathbb{E}[AC]\mathbb{E}[B] + \mathbb{E}[BC]\mathbb{E}[A]) + n_s(n_s-2)(n_s-1)\mathbb{E}[A]\mathbb{E}[B]\mathbb{E}[C]\Big).$$

Isolating for $\mathbb{E}[A]\mathbb{E}[B]\mathbb{E}[C]$ leads to

$$\mathbb{E}[A]\mathbb{E}[B]\mathbb{E}[C] = \frac{1}{(n_s-1)(n_s-2)}\Big(n_s^2\mathbb{E}[\widehat{\mu_A}\widehat{\mu_B}\widehat{\mu_C}] - \mathbb{E}[ABC] - (n_s-1)\left(\mathbb{E}[AB]\mathbb{E}[C] + \mathbb{E}[AC]\mathbb{E}[B] + \mathbb{E}[BC]\mathbb{E}[A]\right)\Big).$$

Removing the $\mathbb{E}[\cdot]$ from $\mathbb{E}[\widehat{\mu_A}\widehat{\mu_B}\widehat{\mu_C}]$, replacing $\mathbb{E}[A]\mathbb{E}[B]\mathbb{E}[C]$ by $\widehat{\mu_A\mu_B\mu_C}$, $\mathbb{E}[ABC]$ by $\widehat{\mu_{ABC}}$, as well as $\mathbb{E}[AB]\mathbb{E}[C]$, $\mathbb{E}[AC]\mathbb{E}[B]$, and $\mathbb{E}[BC]\mathbb{E}[A]$ by $\widehat{\mu_{AB}\mu_C}$, $\widehat{\mu_{AC}\mu_B}$, and $\widehat{\mu_{BC}\mu_A}$ leads to the estimator in Lemma 7. This estimator $\widehat{\mu_A}\widehat{\mu_B}\widehat{\mu_C}$ is unbiased since taking the expected value of the right hand side of the expression leads to $\mu_A\mu_B\mu_C = \mathbb{E}[A]\mathbb{E}[B]\mathbb{E}[C]$. □

A.2.8 Lemma 16

Lemma 16. *Given two random variables of interest A and B, and n_{plt} MC samples. The unbiased MC estimators of their mean $\mu_A = \mathbb{E}[A]$ and $\mu_B = \mathbb{E}[B]$ are $\widehat{\mu_A} = \frac{1}{n_{plt}}\sum_{i=1}^{n_{plt}} A_i$ and $\widehat{\mu_B} = \frac{1}{n_{plt}}\sum_{i=1}^{n_{plt}} B_i$. The unbiased MC estimators of their product $\mu_{AB} = \mathbb{E}[AB]$ is $\widehat{\mu_{AB}} = \frac{1}{n_{plt}}\sum_{i=1}^{n_{plt}} A_iB_i$. An unbiased MC estimator for approximating their covariance $Cov[A, B]$ is:*

$$\widehat{Cov[A, B]} = \frac{n_{plt}}{n_{plt} - 1}\left(\widehat{\mu_{AB}} - \widehat{\mu_A}\widehat{\mu_B}\right). \tag{A.14}$$

Proof of Lemma 16: Re-expressing the covariance as $\mathrm{Cov}[A, B] = \mu_{AB} - \mu_A\mu_B$, an unbiased estimator for $\mathbb{E}[AB] = \mu_{AB}$ is the MC mean estimator $\widehat{\mu_{AB}}$. Following the result from Lemma 6, an unbiased estimator for $\mu_A\mu_B$ is:

$$\widehat{\mu_A\mu_B} = \frac{1}{n_{plt} - 1}\left(n_{plt}\widehat{\mu_A}\widehat{\mu_B} - \widehat{\mu_{AB}}\right),$$

where $\widehat{\mu_A}$, $\widehat{\mu_B}$, and $\widehat{\mu_{AB}}$ are the MC unbiased estimators of μ_A, μ_B, and μ_{AB}. Hence, $\widehat{\mathrm{Cov}[A, B]}$ is obtained by combining these two unbiased estimators according to the definition of $\mathrm{Cov}[A, B]$:

$$\widehat{\mathrm{Cov}[A, B]} = \widehat{\mu_{AB}} - \widehat{\mu_A\mu_B} = \frac{n_{plt}}{n_{plt} - 1}\left(\widehat{\mu_{AB}} - \widehat{\mu_A}\widehat{\mu_B}\right).$$

This estimator is unbiased since taking $\mathbb{E}[\cdot]$ on the right hand side of the equation leads to $\mathbb{E}[AB] - \mathbb{E}[A]\mathbb{E}[B] = \mu_{AB} - \mu_A\mu_B$, which recovers $\mathrm{Cov}[A, B]$. □

A.2.9 Proof for Lemma 8

Proof of Lemma 8: Although $\widehat{\mu_h}^2\widehat{\mu_l}^2$ is an biased estimator of $\mu_h^2\mu_l^2$, additional terms can be added to correct for an unbiased estimator. To do so, consider the expected

value of the biased estimator:

$$\mathbb{E}\big[\widehat{\mu_h}^2\widehat{\mu_l}^2\big] = \frac{1}{n_{plt}^4}\mathbb{E}\left[\left(\sum_{i=1}^{n_{plt}} c_{h,i}\right)\left(\sum_{j=1}^{n_{plt}} c_{h,j}\right)\left(\sum_{k=1}^{n_{plt}} c_{l,k}\right)\left(\sum_{w=1}^{n_{plt}} c_{l,w}\right)\right].$$

The expected value consists of the product of four sums, which leads to n_{plt}^4 total terms. To simplify the expression, the idea is to assess the indices using the combinatorics Pascal's triangle. The number of cases where all four indices are equal is $\binom{4}{4} = 1$, corresponding to $i = j = k = w$, which has n_{plt} terms. The number of cases with three identical indices is $\binom{4}{3} = 4$, corresponding to $i = j = k \neq w$, $i = j = w \neq k$, $i = k = w \neq j$, and $j = k = w \neq i$, each of which results in $n_{plt}(n_{plt} - 1)$ terms. The number of unique cases with two pairs of identical indices is $\binom{3}{2} = 3$, corresponding to $(i = j) \neq (k = w)$, $(i = k) \neq (j = w)$, and $(i = w) \neq (j = k)$, each of which results in $n_{plt}(n_{plt} - 1)$ terms. The number of cases with only two identical indices is $\binom{4}{2} = 6$, corresponding to $i = j \neq k \neq w$, $i = k \neq j \neq w$, $i = w \neq j \neq k$, $j = k \neq i \neq w$, $j = w \neq i \neq k$, and $k = w \neq i \neq j$, each of which results in $n_{plt}(n_{plt} - 1)(n_{plt} - 2)$ terms. Lastly, the number of cases with no equal index is $\binom{4}{0} = 1$, corresponding to $i \neq j \neq k \neq w$, which has $n_{plt}(n_{plt} - 1)(n_{plt} - 2)(n_{plt} - 3)$ terms. Using these index patterns, the expected value expression above is expanded into:

$$\begin{aligned}
\mathbb{E}\big[\widehat{\mu_h}^2\widehat{\mu_l}^2\big] = \frac{1}{n_{plt}^4}\Big(& n_{plt}\mathbb{E}\big[c_h^2c_l^2\big] + 2n_{plt}(n_{plt}-1)\mathbb{E}\big[c_h^2c_l\big]\mathbb{E}[c_l] + 2n_{plt}(n_{plt}-1)\mathbb{E}\big[c_hc_l^2\big]\mathbb{E}[c_h] \\
&+ 2n_{plt}(n_{plt}-1)\mathbb{E}[c_hc_l]^2 + n_{plt}(n_{plt}-1)\mathbb{E}\big[c_h^2\big]\mathbb{E}\big[c_l^2\big] \\
&+ n_{plt}(n_{plt}-1)(n_{plt}-2)\mathbb{E}\big[c_h^2\big]\mathbb{E}[c_l]^2 + n_{plt}(n_{plt}-1)(n_{plt}-2)\mathbb{E}\big[c_l^2\big]\mathbb{E}[c_h]^2 \\
&+ 4n_{plt}(n_{plt}-1)(n_{plt}-2)\mathbb{E}[c_hc_l]\mathbb{E}[c_h]\mathbb{E}[c_l] \\
&+ n_{plt}(n_{plt}-1)(n_{plt}-2)(n_{plt}-3)\mathbb{E}[c_h]^2\mathbb{E}[c_l]^2\Big).
\end{aligned}$$

Rearranging and isolating for $\mathbb{E}[c_h]^2\mathbb{E}[c_l]^2 = \mu_h^2\mu_l^2$ leads to:

$$\begin{aligned}
\mu_h^2\mu_l^2 = \frac{1}{(n_{plt}-2)(n_{plt}-3)}\Bigg(& \frac{n_{plt}^3}{n_{plt}-1}\mathbb{E}\big[\widehat{\mu_h}^2\widehat{\mu_l}^2\big] - \frac{1}{n_{plt}-1}\mu_{h^2l^2} - 2\mu_{h^2l}\mu_l \\
&- 2\mu_{hl^2}\mu_h - 2\mu_{hl}^2 - \mu_{h^2}\mu_{l^2} - (n_{plt}-2)\mu_{h^2}\mu_l^2 \\
&- (n_{plt}-2)\mu_{l^2}\mu_h^2 - 4(n_{plt}-2)\mu_{hl}\mu_h\mu_l\Bigg),
\end{aligned}$$

Removing the $\mathbb{E}[\cdot]$ from $\widehat{\mu_h}^2\widehat{\mu_l}^2$, and replacing the rest of the parameters with their respective unbiased estimators (see Remark 1) leads to the expression for $\widehat{\mu_h^2\mu_l^2}$ in

Lemma 8. The estimator $\widehat{\mu_{h^2}\mu_{l^2}}$ is unbiased since taking the expected value of the right hand side of the above equation, after the said augmentations, leads to $\mu_h^2\mu_l^2 = \mathbb{E}[c_h]^2\mathbb{E}[c_l]^2$. □

A.2.10 Proof for Lemma 10

Proof of Lemma 10: Expanding based on the definition of $\mathrm{Cov}[\vartheta_h, \vartheta_l]$ and using the properties of covariance:

$$\begin{aligned}
\mathrm{Cov}[\vartheta_h, \vartheta_l] &= \mathrm{Cov}\big[(c_h - \mu_h)^2, (c_l - \mu_l)^2\big], \\
&= \mathrm{Cov}\big[c_h^2 - 2c_h\mu_h + \mu_h^2, c_l^2 - 2c_l\mu_l + \mu_l^2\big], \\
&= \mathrm{Cov}\big[c_h^2 - 2c_h\mu_h, c_l^2 - 2c_l\mu_l\big], \\
&= \mathrm{Cov}\big[c_h^2, c_l^2\big] - 2\mu_l\mathrm{Cov}\big[c_h^2, c_l\big] - 2\mu_h\mathrm{Cov}\big[c_h, c_l^2\big] + 4\mu_h\mu_l\mathrm{Cov}[c_h, c_l].
\end{aligned}$$

Hence, an unbiased estimator for $\mathrm{Cov}[\vartheta_h, \vartheta_l]$ is obtained by replacing the four parameters in the right hand side with their unbiased estimators.

Applying Lemma 16, an unbiased estimator for $\mathrm{Cov}[c_h^2, c_l^2]$ is obtained by $A = c_h^2$ and $B = c_l^2$, leading to $\widehat{\mathrm{Cov}[c_h^2, c_l^2]}$ shown in Equation (4.18).

Expanding $\mu_l\mathrm{Cov}[c_h^2, c_l]$ as:

$$\mu_l\mathrm{Cov}\big[c_h^2, c_l\big] = \mathbb{E}[c_l](\mathbb{E}\big[c_h^2c_l\big] - \mathbb{E}\big[c_h^2\big]\mathbb{E}[c_l]) = \mathbb{E}[c_l]\mathbb{E}\big[c_h^2c_l\big] - \mathbb{E}\big[c_h^2\big]\mathbb{E}[c_l]^2,$$

using the unbiased estimators discussed in Remark 1, replace $\mathbb{E}[c_l]\mathbb{E}[c_h^2c_l] = \mu_{h^2l}\mu_l$ with $\widehat{\mu_{h^2l}\mu_l}$ and $\mathbb{E}[c_h^2]\mathbb{E}[c_l]^2 = \mu_{h^2}\mu_l^2$ with $\widehat{\mu_{h^2}\mu_l^2}$, an unbiased estimator for $\mu_l\mathrm{Cov}[c_h^2, c_l]$ is obtained as shown in Equation (4.19).

Similarly, expanding $\mu_h\mathrm{Cov}[c_h, c_l^2]$ as:

$$\mu_h\mathrm{Cov}\big[c_h, c_l^2\big] = \mathbb{E}[c_h]\mathbb{E}\big[c_hc_l^2\big] - \mathbb{E}\big[c_l^2\big]\mathbb{E}[c_h]^2,$$

using the unbiased estimators discussed in Remark 1, replace $\mathbb{E}[c_h]\mathbb{E}[c_hc_l^2] = \mu_{hl^2}\mu_h$ with $\widehat{\mu_{hl^2}\mu_h}$ and $\mathbb{E}[c_l^2]\mathbb{E}[c_h]^2 = \mu_{l^2}\mu_h^2$ with $\widehat{\mu_{l^2}\mu_h^2}$, an unbiased estimator for $\mu_h\mathrm{Cov}[c_h, c_l^2]$ is obtained as shown in Equation (4.20).

Lastly, expanding $\mu_h\mu_l\mathrm{Cov}[c_h, c_l]$ as:

$$\mu_h\mu_l\mathrm{Cov}[c_h, c_l] = \mathbb{E}[c_h]\mathbb{E}[c_l]\mathbb{E}[c_hc_l] - \mathbb{E}[c_h]^2\mathbb{E}[c_l]^2,$$

using the unbiased estimators discussed in Remark 1, replace $\mathbb{E}[c_h]\mathbb{E}[c_l]\mathbb{E}[c_hc_l] = \mu_{hl}\mu_h\mu_l$ with $\widehat{\mu_{hl}\mu_h\mu_l}$ and $\mathbb{E}[c_h]^2\mathbb{E}[c_l]^2 = \mu_h^2\mu_l^2$ with $\widehat{\mu_h^2\mu_l^2}$, an unbiased estimator for $\mu_h\mu_l\mathrm{Cov}[c_h, c_l]$

as shown in Equation (4.21) is obtained. □

A.3 Proofs for Section 4.3

A.3.1 Proof of Theorem 1

Proof of Theorem 1: Apply the definition of MSE to the estimator $\widehat{c_R}$:

$$\mathbb{E}\big[(\widehat{c_R} - c_R)^2\big] = \mathbb{E}\big[(\widehat{\mu_c} - \mu_c)^2\big] + \kappa^2\mathbb{E}\bigg[(\sqrt{\widehat{\sigma_c^2}} - \sigma_c)^2\bigg] + 2\kappa\mathbb{E}\bigg[(\widehat{\mu_c} - \mu_c)(\sqrt{\widehat{\sigma_c^2}} - \sigma_c)\bigg]. \tag{A.15}$$

The first term is by definition MSE$[\widehat{\mu_c}]$. The second term, is further expanded as:

$$\kappa^2\mathbb{E}\bigg[(\sqrt{\widehat{\sigma_c^2}} - \sigma_c)^2\bigg] = \kappa^2\mathbb{E}\bigg[\widehat{\sigma_c^2} - \sigma_c^2\bigg] + 2\kappa^2\mathbb{E}\bigg[(\sigma_c^2 - \sqrt{\widehat{\sigma_c^2}}\sigma_c)\bigg].$$

The first value is 0 as $\widehat{\sigma_c^2}$ is unbiased, and $\sqrt{\widehat{\sigma_c^2}}$ is approximated using the same Taylor expansion presented in the proof of Lemma 14, and hence:

$$\begin{aligned}\kappa^2\mathbb{E}\bigg[(\sqrt{\widehat{\sigma_c^2}} - \sigma_c)^2\bigg] &= 2\kappa^2\sigma_c\mathbb{E}\bigg[\sigma_c - \sqrt{\widehat{\sigma_c^2}}\bigg], \\ &= \frac{\kappa^2}{4\sigma_c^2}\text{MSE}\left[\widehat{\sigma_c^2}\right] + O(\mathbb{E}\bigg[(\widehat{\sigma_c^2} - \sigma_c^2)^3\bigg]).\end{aligned} \tag{A.16}$$

The further expansion of the third term in Equation (A.15) leads to the different MSE bounds or approximation.

Firstly, consider

$$\begin{aligned}\mathbb{E}\bigg[(\widehat{\mu_c} - \mu_c)(\sqrt{\widehat{\sigma_c^2}} - \sigma_c)\bigg] &= \mathbb{E}\bigg[\widehat{\mu_c}\sqrt{\widehat{\sigma_c^2}}\bigg] - \mathbb{E}\bigg[\sqrt{\widehat{\sigma_c^2}}\mu_c\bigg] - \mathbb{E}[\widehat{\mu_c}\sigma_c] + \mathbb{E}[\mu_c\sigma_c], \\ &= \mathbb{E}\bigg[\widehat{\mu_c}\sqrt{\widehat{\sigma_c^2}}\bigg] - \mu_c\left(\sigma_c - \frac{1}{8\sigma_c^3}\text{MSE}\left[\widehat{\sigma_c^2}\right]\right) - \mu_c\sigma_c \\ &\quad + \mu_c\sigma_c + O(\mathbb{E}\bigg[(\widehat{\sigma_c^2} - \sigma_c^2)^3\bigg]), \\ &= \mathbb{E}\bigg[\widehat{\mu_c}\sqrt{\widehat{\sigma_c^2}}\bigg] - \mu_c\sigma_c + \frac{\mu_c}{8\sigma_c^3}\text{MSE}\left[\widehat{\sigma_c^2}\right] + O(\mathbb{E}\bigg[(\widehat{\sigma_c^2} - \sigma_c^2)^3\bigg]).\end{aligned} \tag{A.17}$$

Note that since both $\widehat{\mu_c}$ and $\widehat{\sigma_c^2}$ are unbiased estimators, they converge in expected value to their corresponding true population statistics. The Cauchy-Schwarz bound

can be applied to upper bound $\mathbb{E}\left[\widehat{\mu_c}\sqrt{\widehat{\sigma_c^2}}\right]$, leading to:

$$\mathbb{E}\left[\widehat{\mu_c}\sqrt{\widehat{\sigma_c^2}}\right] \leq \sqrt{\mathbb{E}\left[\widehat{\mu_c}^2\right]\mathbb{E}\left[\widehat{\sigma_c^2}\right]} = \sqrt{\mathbb{E}\left[\widehat{\mu_c}^2\right]\sigma_c^2}.$$

Using the unbiased property of $\widehat{\mu_c}$, the $\mathbb{E}\left[\widehat{\mu_c}^2\right]$ can then be rewritten in terms of $\text{MSE}[\widehat{\mu_c}]$, leading to:

$$\sqrt{\mathbb{E}\left[\widehat{\mu_c}^2\right]} = \sqrt{\text{MSE}[\widehat{\mu_c}] + \mathbb{E}[\widehat{\mu_c}]^2} = \mu_c\sqrt{\frac{\text{MSE}[\widehat{\mu_c}]}{\mu_c^2} + 1}.$$

In practical problems, $\text{MSE}[\widehat{\mu_c}]$ is orders of magnitudes less than μ_c, hence $\frac{\text{MSE}[\widehat{\mu_c}]}{\mu_c^2}$ tends to be much less than 1. Thus, the Taylor expansion of the function $f(x) = \sqrt{1+x}$ about $x = 0$ can be used to approximate the above expression. The Taylor expansion is:

$$\sqrt{1+x} = 1 + \frac{1}{2}x + O(x^2)$$

Substituting $x = \frac{\text{MSE}[\widehat{\mu_c}]}{\mu_c^2}$ leads to:

$$\sqrt{\mathbb{E}\left[\widehat{\mu_c}^2\right]} = \mu_c + \frac{\text{MSE}[\widehat{\mu_c}]}{2\mu_c} + O\left(\left(\frac{\text{MSE}[\widehat{\mu_c}]}{\mu_c^2}\right)^2\right).$$

Hence, the upper bound for Equation (A.17) is:

$$\begin{aligned}\mathbb{E}\left[(\widehat{\mu_c} - \mu_c)(\sqrt{\widehat{\sigma_c^2}} - \sigma_c)\right] \leq \frac{\sigma_c}{2\mu_c}\text{MSE}[\widehat{\mu_c}] + \frac{\mu_c}{8\sigma_c^3}\text{MSE}\left[\widehat{\sigma_c^2}\right] \\ + O\left(\left(\frac{\text{MSE}[\widehat{\mu_c}]}{\mu_c^2}\right)^2\right) + O(\mathbb{E}\left[(\widehat{\sigma_c^2} - \sigma_c^2)^3\right]).\end{aligned} \tag{A.18}$$

Finally, substituting $\text{MSE}[\widehat{\mu_c}]$, expressions in Equations (A.18) and (A.16) into Equation (A.15), the $\text{MSE}[\widehat{c_R}]^{\text{ub}}_{\text{cs}}$ upper bound is obtained:

$$\begin{aligned}\text{MSE}[\widehat{c_R}] &\leq \text{MSE}[\widehat{\mu_c}] + \frac{\kappa^2}{4\sigma_c^2}\text{MSE}\left[\widehat{\sigma_c^2}\right] + 2\kappa\frac{\sigma_c}{2\mu_c}\text{MSE}[\widehat{\mu_c}] + 2\kappa\frac{\mu_c}{8\sigma_c^3}\text{MSE}\left[\widehat{\sigma_c^2}\right] + O\left(\left(\frac{\text{MSE}[\widehat{\mu_c}]}{\mu_c^2}\right)^2\right) + O(\mathbb{E}\left[(\widehat{\sigma_c^2} - \sigma_c^2)^3\right]), \\ &= (1 + \kappa\frac{\sigma_c}{\mu_c})\text{MSE}[\widehat{\mu_c}] + \left(\frac{\kappa^2}{4\sigma_c^2} + \frac{\kappa\mu_c}{4\sigma_c^3}\right)\text{MSE}\left[\widehat{\sigma_c^2}\right] + O\left(\left(\frac{\text{MSE}[\widehat{\mu_c}]}{\mu_c^2}\right)^2 + \mathbb{E}\left[(\widehat{\sigma_c^2} - \sigma_c^2)^3\right]\right) \approx \text{MSE}[\widehat{c_R}]^{\text{ub}}_{\text{cs}}.\end{aligned}$$

For the second $\widehat{c_R}$ MSE bound, consider Cauchy-Schwarz inequality applied to the $\mathbb{E}\left[(\widehat{\mu_c} - \mu_c)(\sqrt{\widehat{\sigma_c^2}} - \sigma_c)\right]$ and the result in Lemma 14:

$$\begin{aligned}
\mathbb{E}\Big[(\widehat{\mu_c}-\mu_c)(\sqrt{\widehat{\sigma_c^2}}-\sigma_c)\Big] &\leq \sqrt{\mathbb{E}[(\widehat{\mu_c}-\mu_c)^2]\mathbb{E}\Big[(\sqrt{\widehat{\sigma_c^2}}-\sigma_c)^2\Big]}, \\
&= \sqrt{\text{MSE}[\widehat{\mu_c}]}\sqrt{\text{MSE}\,[\widehat{\sigma_c}]}, \\
&= \sqrt{\text{MSE}[\widehat{\mu_c}]}\sqrt{\frac{1}{4\sigma_c^2}\text{MSE}\left[\widehat{\sigma_c^2}\right]+O(\mathbb{E}\Big[(\widehat{\sigma_c^2}-\sigma_c^2)^3\Big])}, \\
&\approx \frac{1}{2\sigma_c}\sqrt{\text{MSE}[\widehat{\mu_c}]}\sqrt{\text{MSE}\left[\widehat{\sigma_c^2}\right]}.
\end{aligned} \tag{A.19}$$

Substituting the bound in Equation (A.19) into Equation (A.15) leads to the $\text{MSE}[\widehat{c_R}]_{\text{p}}^{\text{ub}}$ expression:

$$\begin{aligned}
\text{MSE}[\widehat{c_R}] &\leq \text{MSE}[\widehat{\mu_c}]+\frac{\kappa^2}{4\sigma_c^2}\text{MSE}\left[\widehat{\sigma_c^2}\right]+\frac{\kappa}{\sigma_c}\sqrt{\text{MSE}[\widehat{\mu_c}]}\sqrt{\text{MSE}\left[\widehat{\sigma_c^2}\right]}+O(\mathbb{E}\Big[(\widehat{\sigma_c^2}-\sigma_c^2)^3\Big]), \\
&\approx \text{MSE}[\widehat{c_R}]_{\text{p}}^{\text{ub}}.
\end{aligned}$$

For the $\text{MSE}[\widehat{c_R}]_{\mu\sigma}$ approximation, $\mathbb{E}\Big[(\widehat{\mu_c}-\mu_c)(\sqrt{\widehat{\sigma_c^2}}-\sigma_c)\Big]$ is exactly expanded alongside the Taylor series approximation of $\sqrt{\widehat{\sigma_c^2}}$:

$$\begin{aligned}
\mathbb{E}\Big[(\widehat{\mu_c}-\mu_c)(\sqrt{\widehat{\sigma_c^2}}-\sigma_c)\Big] &= \mathbb{E}[(\mu_c-\widehat{\mu_c})\sigma_c]+\mathbb{E}\Big[(\widehat{\mu_c}-\mu_c)\sqrt{\widehat{\sigma_c^2}}\Big], \\
&\approx \mathbb{E}[(\mu_c-\widehat{\mu_c})]\sigma_c+\mathbb{E}[(\widehat{\mu_c}-\mu_c)]\sigma_c+\mathbb{E}\Big[\widehat{\mu_c}\widehat{\sigma_c^2}\Big]\frac{1}{2\sigma_c}-\frac{\mu_c}{2\sigma_c}\mathbb{E}\Big[\widehat{\sigma_c^2}\Big] \\
&\quad -\frac{\sigma_c^2}{2\sigma_c}\mathbb{E}[\widehat{\mu_c}]+\frac{\mu_c\sigma_c^2}{2\sigma_c}-\frac{1}{8\sigma_c^3}\mathbb{E}\Big[(\widehat{\mu_c}-\mu_c)(\widehat{\sigma_c^2}-\sigma_c^2)^2\Big], \\
&= \mathbb{E}\Big[\widehat{\mu_c}\widehat{\sigma_c^2}\Big]\frac{1}{2\sigma_c}-\frac{\mu_c\sigma_c}{2}-\frac{1}{8\sigma_c^3}\mathbb{E}\Big[(\widehat{\mu_c}-\mu_c)(\widehat{\sigma_c^2}-\sigma_c^2)^2\Big].
\end{aligned} \tag{A.20}$$

Considering $\mathbb{E}\Big[(\widehat{\mu_c}-\mu_c)(\widehat{\sigma_c^2}-\sigma_c^2)^2\Big]$ as negligible and substituting Equation (A.20) into Equation (A.15), the $\text{MSE}[\widehat{c_R}]_{\mu\sigma}$ approximation is obtained:

$$\begin{aligned}
\text{MSE}[\widehat{c_R}] &\approx \text{MSE}[\widehat{\mu_c}]+\frac{\kappa^2}{4\sigma_c^2}\text{MSE}\left[\widehat{\sigma_c^2}\right]+2\kappa\left(\mathbb{E}\Big[\widehat{\mu_c}\widehat{\sigma_c^2}\Big]\frac{1}{2\sigma_c}-\frac{\mu_c\sigma_c}{2}\right) \\
&\quad +O\left(\mathbb{E}\Big[(\widehat{\mu_c}-\mu_c)(\widehat{\sigma_c^2}-\sigma_c^2)^2\Big]\right), \\
&\approx \text{MSE}[\widehat{c_R}]_{\mu\sigma}.
\end{aligned}$$

□

A.3.2 Proof of Lemma 11

Proof of Lemma 11: Let $q = \max(n_A, n_B)$, expand $\mathbb{E}\Big[\widehat{\mu_{A,MC}}^{n_A}\widehat{\sigma^2_{B,MC}}^{n_B}\Big]$ by its definition:

$$\begin{aligned}\mathbb{E}\Big[\widehat{\mu_{A,MC}}^{n_A}\widehat{\sigma^2_{B,MC}}^{n_B}\Big] &= \mathbb{E}\left[\left(\frac{1}{n_A}\sum_{i=1}^{n_A}A_i\right)\left(\frac{1}{n_B-1}\sum_{j=1}^{n_B}\left(B_j-\left(\frac{1}{n_B}\sum_{k=1}^{n_B}B_k\right)\right)^2\right)\right],\\ &= \frac{1}{n_A(n_B-1)}\left(\mathbb{E}\left[\left(\sum_{i=1}^{n_A}A_i\right)\left(\sum_{j=1}^{n_B}B_j^2\right)\right]-\frac{2}{n_B}\mathbb{E}\left[\left(\sum_{i=1}^{n_A}A_i\right)\left(\sum_{j=1}^{n_B}\sum_{k=1}^{n_B}B_jB_k\right)\right]\right.\\ &\quad\left.+\frac{1}{n_B}\mathbb{E}\left[\left(\sum_{i=1}^{n_A}A_i\right)\left(\sum_{j=1}^{n_B}B_j\right)\left(\sum_{k=1}^{n_B}B_k\right)\right]\right)\end{aligned}$$

Let $w = \min(n_A, n_B)$, the first $\mathbb{E}[\cdot]$ expression in the second equality results in n_An_B terms, with w terms having $i = j$, and the rest having $i \neq j$. Hence, this leads to:

$$\mathbb{E}\left[\left(\sum_{i=1}^{n_A}A_i\right)\left(\sum_{j=1}^{n_B}B_j^2\right)\right] = w\mathbb{E}\big[AB^2\big]+(n_An_B-w)\mathbb{E}[A]\mathbb{E}\big[B^2\big].$$

The second $\mathbb{E}[\cdot]$ expression in the second equality leads to $n_An_B^2$ terms, with w terms of $i = j = k$, $w(n_B - 1)$ terms of $(i = j \neq k)$ or $(i = k \neq j)$, $n_An_B - w$ terms of $(j = k \neq i)$, and $(1 - n_B)(2w - n_An_B)$ terms of $i \neq j \neq k$. Hence, this expression simplifies to:

$$\begin{aligned}\mathbb{E}\left[\left(\sum_{i=1}^{n_A}A_i\right)\left(\sum_{j=1}^{n_B}\sum_{k=1}^{n_B}B_jB_k\right)\right] &= 2w(n_B-1)\mathbb{E}[AB]\mathbb{E}[B]+(n_An_B-w)\mathbb{E}[A]\mathbb{E}\big[B^2\big]\\ &\quad+w\mathbb{E}\big[AB^2\big]+(1-n_B)(2w-n_An_B)\mathbb{E}[A]\mathbb{E}[B]^2.\end{aligned}$$

The third $\mathbb{E}[\cdot]$ expression in the second equality leads to the same outcome as the second $\mathbb{E}[\cdot]$ expression above, with the only difference of having a multiplier of $\frac{1}{n_B}$ instead of $\frac{2}{n_B}$. Lastly, putting everything together and simplifying to obtain:

$$\begin{aligned}\mathbb{E}\Big[\widehat{\mu_{A,MC}}^{n_A}\widehat{\sigma^2_{B,MC}}^{n_B}\Big] &= \frac{1}{n_A(n_B-1)}\Big[w\mathbb{E}\big[AB^2\big]+(n_An_B-w)\mathbb{E}[A]\mathbb{E}\big[B^2\big]-\frac{1}{n_B}\Big(w\mathbb{E}\big[AB^2\big]+(1-n_B)(2w-n_An_B)\mathbb{E}[A]\mathbb{E}[B]^2\\ &\quad+2w(n_B-1)\mathbb{E}[AB]\mathbb{E}[B]+(n_An_B-w)\mathbb{E}[A]\mathbb{E}\big[B^2\big]\Big)\Big],\\ &= \frac{w}{n_An_B}\mathbb{E}\big[AB^2\big]+\frac{n_An_B-w}{n_An_B}\mathbb{E}[A]\mathbb{E}\big[B^2\big]-\frac{2w}{n_An_B}\mathbb{E}[AB]\mathbb{E}[B]-\frac{n_An_B-2w}{n_An_B}\mathbb{E}[A]\mathbb{E}[B]^2.\end{aligned}$$

Recall that $w = \min(n_A, n_B)$ and $q = \max(n_A, n_B)$, the above expression leads to the result in Lemma 11 for any A and B, and any n_A and n_B. □

A.3.3 Proof of Lemma 13

Proof of Lemma 13: As shown in Peherstorfer et al. [86], the results in Lemma 1 is obtained from solving the necessary Karush–Kuhn–Tucker (KKT) conditions of the optimization problem where the MSE of $\widehat{\mu_{c,MF}}$ is minimized under the P_b constraint, and hence the stationary points of α and r_m are achieved. This procedure can be extended for the case of linear combination of MSE posed in Lemma 13.

Firstly, note that the MSE in Lemma 1 with the optimal α substituted in leads to:

$$\text{MSE}\left[\hat{\mu}_\Gamma^{MF}\right] = \frac{1}{P_b}(1+\frac{r_m}{w_c})\left[\mathbb{V}[\Gamma](1-\text{Corr}[\Gamma,\gamma]^2) + \frac{1}{r_m}\mathbb{V}[\Gamma]\text{Corr}[\Gamma,\gamma]^2\right].$$

Since the new objective is to minimize the positive weighted sum of two MSEs, the α that minimizes individual MSE will remain optimal in this case. Hence, the equations for α_μ and α_σ are obtained by substitute the appropriate parameters into the α expression in Lemma 1. Subsequently, using the MSE equation in Lemma 1, the expression for the linear combination of MSE is obtained, and substituting α_μ and α_σ leads to:

$$\begin{aligned}
\chi_1\text{MSE}\left[\widehat{\mu_{c,MF}}\right] + \chi_2\text{MSE}\left[\widehat{\mu_{\vartheta_h,MF}}\right] &= \frac{\chi_1}{P_b}(1+\frac{r_m}{w_c})\left[\sigma_h^2 + \frac{r_m-1}{r_m}(\alpha_\mu^2\sigma_h^2 - 2\alpha_\mu\text{Cov}[c_h,c_l])\right] \\
&\quad + \frac{\chi_2}{P_b}(1+\frac{r_m}{w_c})\left[\tau_h + \frac{r_m-1}{r_m}(\alpha_\sigma^2\tau_h - 2\alpha_\mu\text{Cov}[\vartheta_h,\vartheta_l])\right], \\
&= \frac{1}{P_b}(1+\frac{r_m}{w_c})\Big[\chi_1\sigma_h^2(1-\text{Corr}[c_h,c_l]^2) + \chi_2\tau_h(1-\text{Corr}[\vartheta_h,\vartheta_l]^2) \\
&\quad + \frac{1}{r_m}(\chi_1\sigma_h^2\text{Corr}[c_h,c_l]^2 + \chi_2\tau_h\text{Corr}[\vartheta_h,\vartheta_l]^2)\Big].
\end{aligned}$$

Comparing this equation with the one above defined in terms of Γ and γ, it is evident that they have the same form, and the multiplicative coefficients of the terms with r_m matches:

$$\mathbb{V}[\Gamma](1-\text{Corr}[\Gamma,\gamma]^2) \sim \chi_1\sigma_h^2(1-\text{Corr}[c_h,c_l]^2) + \chi_2\tau_h(1-\text{Corr}[\vartheta_h,\vartheta_l]^2)$$

and

$$\mathbb{V}[\Gamma]\text{Corr}[\Gamma,\gamma]^2 \sim \chi_1\sigma_h^2\text{Corr}[c_h,c_l]^2 + \chi_2\tau_h\text{Corr}[\vartheta_h,\vartheta_l]^2.$$

Hence, the KKT minimum for r_m in Lemma 1 is still applicable here. For the expression under the square root, substitute the numerator $\mathbb{V}[\Gamma]\text{Corr}[\Gamma,\gamma]^2$ and the denominator $\mathbb{V}[\Gamma](1-\text{Corr}[\Gamma,\gamma]^2)$ with the equivalent expressions above leads to the final outcome for optimal r_m^* shown in Lemma 13. □

Bibliography

[1] J. H. Zhu, W. H. Zhang, and L. Xia. "Topology optimization in aircraft and aerospace structures design". In: *Archives of Computational Methods in Engineering* 23 (2016), pp. 595–622. DOI: 10.1007/s11831-015-9151-2.

[2] D. Pepler. "Modelling additively manufactured material for applications in topology optimization". Doctoral Dissertation. University of Toronto, 2023.

[3] L. Li and C. A. Steeves. "Random matrix theory for robust topology optimization with material uncertainty". In: *Structural and Multidisciplinary Optimization* 66.11 (2023). DOI: 10.1007/s00158-023-03665-y.

[4] M. P. Bendsøe and N. Kikuchi. "Generating optimal topologies in structural design using a homogenization method". In: *Computer Methods in Applied Mechanics and Engineering* 71.2 (1988), pp. 197–224. DOI: 10.1016/0045-7825(88)90086-2.

[5] M. Bendsøe and O. Sigmund. *Topology optimization: theory, method and applications*. 2nd ed. Springer Berlin, Heidelberg, Jan. 2003. DOI: 10.1007/978-3-662-05086-6.

[6] G. Allaire, F. Jouve, and A. Toader. "A level-set method for shape optimization". In: *Comptes Rendus Mathematique* 334.12 (2002), pp. 1125–1130. DOI: 10.1016/S1631-073X(02)02412-3.

[7] P. Hajela, E. Lee, and C.-Y. Lin. "Genetic algorithms in structural topology optimization". In: *Topology Design of Structures*. Ed. by M. P. Bendsøe and C. A. Mota Soares. Springer Netherlands, 1993, pp. 117–133. DOI: 10.1007/978-94-011-1804-0_10.

[8] X. Guo, W. Zhang, and W. Zhong. "Doing topology optimization explicitly and geometrically—a new moving morphable components based framework". In: *Journal of Applied Mechanics* 81.8 (2014), p. 081009. DOI: 10.1115/1.4027609.

[9] M. Bendsøe. "Optimal shape design as a material distribution problem". In: *Structural Optimization* 1 (1989), pp. 193–202. DOI: 10.1007/BF01650949.

[10] V. Keshavarzzadeh, F. Fernandez, and D. A. Tortorelli. "Topology optimization under uncertainty via non-intrusive polynomial chaos expansion". In: *Computer Methods in Applied Mechanics and Engineering* 318 (2017), pp. 120–147. DOI: 10.1016/j.cma.2017.01.019.

[11] S. Xu, Y. Cai, and G. Cheng. "Volume preserving nonlinear density filter based on heaviside funtions". In: *Structural and Multidisciplinary Optimization* 41 (2010), pp. 495–505. DOI: 10.1007/s00158-009-0452-7.

[12] F. Wang, B. Lazarov, and O. Sigmund. "On projection methods, convergence and robust formulations in topology optimization". In: *Structural and Multidisciplinary Optimization* 43 (2011), pp. 767–784. DOI: 10.1007/s00158-010-0602-y.

[13] G. Allaire. "A review of adjoint methods for sensitivity analysis, uncertainty quantification and optimization in numerical codes". In: *Ingénieurs de l'Automobile* 836 (2015), pp. 33–36.

[14] K. Svanberg. "The method of moving asymptotes — A new method for structural optimization". In: *International Journal for Numerical Methods in Engineering* 24.2 (1987), pp. 359–373. DOI: 10.1002/nme.1620240207.

[15] G. I. Schuëller and H. A. Jensen. "Computational methods in optimization considering uncertainties – An overview". In: *Computer Methods in Applied Mechanics and Engineering* 198.1 (2008), pp. 2–13. DOI: 10.1016/j.cma.2008.05.004.

[16] Y. Tsompanakis, N. D. Lagaros, and M. Papadrakakis. *Structural design optimization considering uncertainties: structures & infrastructures book*. Ed. by D. M. Frangopol. 1st ed. Vol. 1. CRC Press, 2008. DOI: 10.1201/b10995.

[17] K. Maute. "Topology optimization under uncertainty". In: *Topology Optimization in Structural and Continuum Mechanics*. Ed. by G. I. N. Rozvany and T. Lewiński. Vienna: Springer Vienna, 2014, pp. 457–471. DOI: 10.1007/978-3-7091-1643-2_20.

[18] H. G. Beyer and B. Sendhoff. "Robust optimization – A comprehensive survey". In: *Computer Methods in Applied Mechanics and Engineering* 196.33 (2007), pp. 3190–3218. DOI: 10.1016/j.cma.2007.03.003.

[19] G. Kharmanda, N. Olhoff, A. Mohamed, and M. Lemaire. "Reliability-based topology optimization". In: *Structural and Multidisciplinary Optimization* 26 (2004), pp. 295–307. DOI: 10.1007/s00158-003-0322-7.

[20] A. Vishwanathan and G. A. Vio. "Efficient quantification of material uncertainties in reliability-based topology optimization using random matrices". In: *Computer Methods in Applied Mechanics and Engineering* 351 (2019), pp. 548–570. DOI: 10.1016/j.cma.2019.03.047.

[21] M. Tootkaboni, A. Asadpoure, and J. K. Guest. "Topology optimization of continuum structures under uncertainty – A Polynomial Chaos approach". In: *Computer Methods in Applied Mechanics and Engineering* 201-204 (2012), pp. 263–275. DOI: 10.1016/j.cma.2011.09.009.

[22] B. Lazarov, M. Schevenels, and O. Sigmund. "Topology optimization considering material and geometric uncertainties using stochastic collocation methods". In: *Structural and Multidisciplinary Optimization* 46 (2012), pp. 597–612. DOI: 10.1007/s00158-012-0791-7.

[23] B. Sudret and A. Der Kiureghian. "Stochastic finite element methods and reliability a state-of-the-art report". In: Department of Civil and Environmental Engineering, University of California: Berkeley, Nov. 2000.

[24] B. Sudret. "Uncertainty propagation and sensitivity analysis in mechanical models - contributions to structural reliability and stochastic spectral methods". In: Clermont-Ferrand, France: Université Blaise-Pascal, Jan. 2007.

[25] M. Schevenels, B. S. Lazarov, and O. Sigmund. "Robust topology optimization accounting for spatially varying manufacturing errors". In: *Computer Methods in Applied Mechanics and Engineering* 200.49 (2011), pp. 3613–3627. DOI: 10.1016/j.cma.2011.08.006.

[26] O. U. Gungor and R. M. Gorguluarslan. "Experimental characterization of spatial variability for random field modeling on struts of additively manufactured lattice structures". In: *Additive Manufacturing* 36 (2020). DOI: 10.1016/j.addma.2020.101471.

[27] Z. Kazemi and C. A. Steeves. "Uncertainty quantification in material properties of additively manufactured materials for application in topology optimization". In: *ASME International Mechanical Engineering Congress and Exposition*. Vol. 3. IMECE, 2022. DOI: 10.1115/IMECE2022-95195.

[28] B. Sudret and A. Der Kiureghian. "Comparison of finite element reliability methods". In: *Probabilistic Engineering Mechanics* 17.4 (2002), pp. 337–348. DOI: 10.1016/S0266-8920(02)00031-0.

[29] N. Feng, G. Zhang, and K. Khandelwal. "On the performance evaluation of stochastic finite elements in linear and nonlinear problems". In: *Computers & Structures* 243 (2021), p. 106408. DOI: 10.1016/j.compstruc.2020.106408.

[30] V. Papadopoulos and D. Giovanis. *Stochastic finite element methods: An introduction*. 1st ed. Mathematical Engineering. Springer Cham, Jan. 2018. DOI: 10.1007/978-3-319-64528-5.

[31] S. De, J. Hampton, K. Maute, and A. Doostan. "Topology optimization under uncertainty using a stochastic gradient-based approach". In: *Structural and Multidisciplinary Optimization* 62.5 (2020), pp. 2255–2278. DOI: 10.1007/s00158-020-02599-z.

[32] R. J. Gladstone, M. A. Nabian, V. Keshavarzzadeh, and H. Meidani. *Robust topology optimization using variational autoencoders*. 2021. URL: https://arxiv.org/abs/2107.10661.

[33] W. Li and X. S. Zhang. "Momentum-based accelerated mirror descent stochastic approximation for robust topology optimization under stochastic loads". In: *International Journal for Numerical Methods in Engineering* 122.17 (2021), pp. 4431–4457. DOI: doi.org/10.1002/nme.6672.

[34] S. De, K. Maute, and A. Doostan. "Topology optimization under microscale uncertainty using stochastic gradients". In: *Structural and Multidisciplinary Optimization* 66.1 (2022). DOI: 10.1007/s00158-022-03417-4.

[35] S. De, K. Maute, and A. Doostan. "Bi-fidelity stochastic gradient descent for structural optimization under uncertainty". In: *Computational Mechanics* 66.4 (2020), pp. 745–771. DOI: 10.1007/s00466-020-01870-w.

[36] H. Robbins and S. Monro. "A stochastic approximation method". In: *The Annals of Mathematical Statistics* 22.3 (1951), pp. 400–407. DOI: 10.1214/aoms/1177729586.

[37] L. W. T. Ng and K. Willcox. "Multifidelity approaches for optimization under uncertainty". In: *International Journal for Numerical Methods in Engineering* 100.10 (2014), pp. 746–772. DOI: 10.1002/nme.4761.

[38] M. Jansen, G. Lombaert, M. Diehl, B. S. Lazarov, O. Sigmund, and M. Schevenels. "Robust topology optimization accounting for misplacement of material". In: *Structural and Multidisciplinary Optimization* 47 (2013), pp. 317–333. DOI: 10.1007/s00158-012-0835-z.

[39] V. Keshavarzzadeh and K. A. James. "Robust multiphase topology optimization accounting for manufacturing uncertainty via stochastic collocation". In: *Structural and Multidisciplinary Optimization* 60.6 (2019), pp. 2461–2476. DOI: 10.1007/s00158-019-02333-4.

[40] F. Heiss and V. Winschel. "Likelihood approximation by numerical integration on sparse grids". In: *Journal of Econometrics* 144.1 (2008), pp. 62–80. DOI: 10.1016/j.jeconom.2007.12.004.

[41] O. Amir, O. Sigmund, B. S. Lazarov, and M. Schevenels. "Efficient reanalysis techniques for robust topology optimization". In: *Computer Methods in Applied Mechanics and Engineering* 245-246 (2012), pp. 217–231. DOI: 10.1016/j.cma.2012.07.008.

[42] V. Keshavarzzadeh, R. M. Kirby, and A. Narayan. "Robust topology optimization with low rank approximation using artificial neural networks". In: *Computational Mechanics* 68.6 (2021), pp. 1297–1323. DOI: 10.1007/s00466-021-02069-3.

[43] K. M. Hamdia, H. Ghasemi, X. Zhuang, and T. Rabczuk. "Multilevel Monte Carlo method for topology optimization of flexoelectric composites with uncertain material properties". In: *Engineering Analysis with Boundary Elements* 134 (2022), pp. 412–418. DOI: 10.1016/j.enganabound.2021.10.008.

[44] J. Hyun, A. Chaudhuri, K. E. Willcox, and H. A. Kim. "Multifidelity robust topology optimization for material uncertainties with digital manufacturing". In: *AIAA SCITECH 2023 Forum*. Jan. 2023. DOI: 10.2514/6.2023-2038.

[45] M. Jansen, G. Lombaert, and M. Schevenels. "Robust topology optimization of structures with imperfect geometry based on geometric nonlinear analysis". In: *Computer Methods in Applied Mechanics and Engineering* 285 (2015), pp. 452–467. DOI: 10.1016/j.cma.2014.11.028.

[46] B. S. Lazarov, M. Schevenels, and O. Sigmund. "Topology optimization with geometric uncertainties by perturbation techniques". In: *International Journal for Numerical Methods in Engineering* 90.11 (2012), pp. 1321–1336. DOI: 10.1002/nme.3361.

[47] A. Asadpoure, J. Guest, and T. Igusa. "Structural topology optimization considering correlated uncertainties in elastic modulus". In: *51st AIAA/ASME/ASCE/AHS/ASC Structures, Structural Dynamics, and Materials Conference*. 2012. DOI: 10.2514/6.2010-2943.

[48] N. Changizi and M. Jalalpour. "Robust topology optimization of frame structures under geometric or material properties uncertainties". In: *Structural and Multidisciplinary Optimization* 56.4 (2017), pp. 791–807. DOI: 10.1007/s00158-017-1686-4.

[49] Z. Fu nad C. Wang and J. Zhao. "Truss topology optimization under uncertain nodal locations with proportional topology optimization method". In: *Mechanics Based Design of Structures and Machines* 45.2 (2017), pp. 190–206. DOI: 10.1080/15397734.2016.1163640.

[50] J. C. Krüger, M. Kranz, T. Schmidt, R. Seifried, and B. Kriegesmann. "An efficient and non-intrusive approach for robust design optimization with the first-order second-moment method". In: *Computer Methods in Applied Mechanics and Engineering* 414 (2023), p. 116136. DOI: 10.1016/j.cma.2023.116136.

[51] K. Steltner, C. B. W. Pedersen, and B. Kriegesmann. "Semi-intrusive approach for stiffness and strength topology optimization under uncertainty". In: *Optimization and Engineering* 24 (3 2023), pp. 2181–2211. DOI: 10.1007/s11081-022-09770-z.

[52] G. A. da Silva and E. L. Cardoso. "Topology optimization of continuum structures subjected to uncertainties in material properties". In: *International Journal for Numerical Methods in Engineering* 106.3 (2016), pp. 192–212. DOI: 10.1002/nme.5126.

[53] G. A. da Silva and E. L. Cardoso. "Stress-based topology optimization of continuum structures under uncertainties". In: *Computer Methods in Applied Mechanics and Engineering* 313 (2017), pp. 647–672. DOI: 10.1016/j.cma.2016.09.049.

[54] R. Filomeno Coelho J. N. Richardson and S. Adriaenssens. "A unified stochastic framework for robust topology optimization of continuum and truss-like structures". In: *Engineering Optimization* 48.2 (2016), pp. 334–350. DOI: 10.1080/0305215X.2015.1011152.

[55] S. Chen and W. Chen. "A new level-set based approach to shape and topology optimization under geometric uncertainty". In: *Structural and Multidisciplinary Optimization* 44.1 (2011), pp. 18–44. DOI: 10.1007/s00158-011-0660-9.

[56] S. Chen, W. Chen, and S. Lee. "Level set based robust shape and topology optimization under random field uncertainties". In: *Structural and Multidisciplinary Optimization* 41.4 (2010), pp. 507–524. DOI: 10.1007/s00158-009-0449-2.

[57] J. Zheng, Z. Luo, H. Li, and C. Jiang. "Robust topology optimization for cellular composites with hybrid uncertainties". In: *International Journal for Numerical Methods in Engineering* 115.6 (2018), pp. 695–713. DOI: 10.1002/nme.5821.

[58] J. Zheng, Z. Luo, C. Jiang, and J. Gao. "Robust topology optimization for concurrent design of dynamic structures under hybrid uncertainties". In: *Mechanical Systems and Signal Processing* 120 (2019), pp. 540–559. DOI: 10.1016/j.ymssp.2018.10.026.

[59] C. Audouze, A. Klein, A. Butscher, N. Morris, P. Nair, and M. Yano. "Robust Level-Set-Based Topology Optimization Under Uncertainties Using Anchored ANOVA Petrov–Galerkin Method". In: *SIAM/ASA Journal on Uncertainty Quantification* 11.3 (2023), pp. 877–905. DOI: 10.1137/22M1524722.

[60] I. Ben-Yelun, A. O. Yuksel, and F. Cirak. "Robust topology optimisation of lattice structures with spatially correlated uncertainties". In: *Structural and Multidisciplinary Optimization* 67.2 (2024). DOI: 10.1007/s00158-023-03716-4.

[61] F. Yamazaki, M. Shinozuka, and G. Dasgupta. "Neumann expansion for stochastic finite element analysis". In: *Journal of Engineering Mechanics* 114.8 (1988), pp. 1335–1354. DOI: 10.1061/(ASCE)0733-9399(1988)114:8(1335).

[62] M. Shinozuka and G. Deodatis. "Response variability Of stochastic finite element systems". In: *Journal of Engineering Mechanics* 114.3 (1988), pp. 499–519. DOI: 10.1061/(ASCE)0733-9399(1988)114:3(499).

[63] R. G. Ghanem and P. D. Spanos. *Stochastic finite elements: a spectral approach*. Berlin, Heidelberg: Springer-Verlag, 1991.

[64] G. W. Stewart. *Matrix algorithms*. Society for Industrial and Applied Mathematics, 1998. DOI: 10.1137/1.9781611971408.

[65] R. B. Flavell. "Approximate matrix inversion". In: *Operational Research Quarterly (1970-1977)* 28.3 (1977), pp. 517–520.

[66] C. F. Li, S. Adhikari, S. Cen, Y. T. Feng, and D. R. J. Owen. "A joint diagonalisation approach for linear stochastic systems". In: *Computers & Structures* 88.19 (2010), pp. 1137–1148. DOI: 10.1016/j.compstruc.2010.06.013.

[67] X. Wang, S. Cen, and C. Li. "Generalized neumann expansion and its Aapplication in stochastic finite element methods". In: *Mathematical Problems in Engineering* 2013.1 (2013), p. 325025. DOI: 10.1155/2013/325025.

[68] P. B. Nair. "Equivalence between the combined approximations technique and krylov subspace methods". In: *AIAA Journal* 40.5 (2002), pp. 1021–1023. DOI: 10.2514/2.1747.

[69] P. D. Hill. "Kernel estimation of a distribution function". In: *Communications in Statistics - Theory and Methods* 14.3 (1985), pp. 605–620. DOI: 10.1080/03610928508828937.

[70] B. W. Silverman. *Density estimation for statistics and data analysis*. 1st ed. Monographs on Statistics and Applied Probability. New York: Routledge, 1998. DOI: 10.1201/9781315140919.

[71] F. Menhorn, G. Geraci, D. T. Seidl, Y. M. Marzouk, M. S. Eldred, and H. J. Bungartz. "Multilevel Monte Carlo estimators for derivative-free optimization under uncertainty". In: *International Journal for Uncertainty Quantification* 14.3 (2024), pp. 21–65. DOI: 10.1615/Int.J.UncertaintyQuantification.2023048049.

[72] F. Vidal-Codina, N. C. Nguyen, M. B. Giles, and J. Peraire. "A model and variance reduction method for computing statistical outputs of stochastic elliptic partial differential equations". In: *Journal of Computational Physics* 297 (2015), pp. 700–720. DOI: 10.1016/j.jcp.2015.05.041.

[73] Q. Ayoul-Guilmard, S. Ganesh, S. Krumscheid, and F. Nobile. "Quantifying uncertain system outputs via the multi-level Monte Carlo method - Distribution and robustness measures". In: *International Journal for Uncertainty Quantification* 13.5 (2023), pp. 61–98.

[74] I. M. Sobol. "On quasi-Monte Carlo integrations". In: *Mathematics and Computers in Simulation* 47.2 (1998), pp. 103–112. DOI: 10.1016/S0378-4754(98)00096-2.

[75] W. J. Morokoff and R. E. Caflisch. "Quasi-Monte Carlo integration". In: *Journal of Computational Physics* 122.2 (1995), pp. 218–230. DOI: 10.1006/jcph.1995.1209.

[76] S. T. Tokdar and R. E. Kass. "Importance sampling: a review". In: *WIREs Computational Statistics* 2.1 (2010), pp. 54–60. DOI: 10.1002/wics.56.

[77] A. Tabandeh, G. Jia, and P. Gardoni. "A review and assessment of importance sampling methods for reliability analysis". In: *Structural Safety* 97 (2022), p. 102216. DOI: 10.1016/j.strusafe.2022.102216.

[78] W.-L. Loh. "On Latin hypercube sampling". In: *The Annals of Statistics* 24.5 (1996), pp. 2058–2080. DOI: 10.1214/aos/1069362310.

[79] M. Stein. "Large sample properties of simulations using Latin hypercube sampling". In: *Technometrics* 29.2 (1987), pp. 143–151. DOI: 10.1080/00401706.1987.10488205.

[80] S. Krumscheid, F. Nobile, and M. Pisaroni. "Quantifying uncertain system outputs via the multilevel Monte Carlo method — Part I: Central moment estimation". In: *Journal of Computational Physics* 414 (2020), p. 109466. DOI: 10.1016/j.jcp.2020.109466.

[81] M. B. Giles. "Multilevel Monte Carlo path simulation". In: *Operations Research* 56.3 (2008), pp. 607–617. DOI: 10.1287/opre.1070.0496.

[82] S. Heinrich. "Multilevel Monte Carlo methods". In: *Large-Scale Scientific Computing*. Ed. by S. Margenov, J. Waśniewski, and P. Yalamov. Vol. 2179. Berlin, Heidelberg: Springer Berlin Heidelberg, Dec. 2001, pp. 58–67. DOI: 10.1007/3-540-45346-6_5.

[83] A. L. Haji-Ali, F. Nobile, and R. Tempone. "Multi-index Monte Carlo: when sparsity meets sampling". In: *Numerische Mathematik* 132.4 (2016), pp. 767–806. DOI: 10.1007/s00211-015-0734-5.

[84] B. Peherstorfer, K. Willcox, and M. Gunzburger. "Survey of multifidelity methods in uncertainty propagation, inference, and optimization". In: *SIAM Review* 60.3 (2018), pp. 550–591. DOI: 10.1137/16M1082469.

[85] E. Qian, B. Peherstorfer, D. O'Malley, V. V. Vesselinov, and K. Willcox. "Multifidelity Monte Carlo estimation of variance and sensitivity indices". In: *SIAM/ASA Journal on Uncertainty Quantification* 6.2 (2018), pp. 683–706. DOI: 10.1137/17M1151006.

[86] B. Peherstorfer, K. Willcox, and M. Gunzburger. "Optimal model management for multifidelity Monte Carlo estimation". In: *SIAM Journal on Scientific Computing* 38.5 (2016), A3163–A3194. DOI: 10.1137/15M1046472.

[87] A. A. Gorodetsky, G. Geraci, M. S. Eldred, and J. D. Jakeman. "A generalized approximate control variate framework for multifidelity uncertainty quantification". In: *Journal of Computational Physics* 408 (2020), p. 109257. DOI: 10.1016/j.jcp.2020.109257.

[88] S. Pauli and P. Arbenz. "Determining optimal multilevel Monte Carlo parameters with application to fault tolerance". In: *Computers & Mathematics with Applications* 70.11 (2015), pp. 2638–2651. DOI: 10.1016/j.camwa.2015.07.011.

[89] G. Balokas, B. Kriegesmann, S. Czichon, and R. Rolfes. "A variable-fidelity hybrid surrogate approach for quantifying uncertainties in the nonlinear response of braided composites". In: *Computer Methods in Applied Mechanics and Engineering* 381 (2021), p. 113851. DOI: 10.1016/j.cma.2021.113851.

[90] A. Tran, P. Robbe, and H. Lim. "Multi-fidelity microstructure-induced uncertainty quantification by advanced Monte Carlo methods". In: *Materialia* 27 (2023), p. 101705. DOI: 10.1016/j.mtla.2023.101705.

[91] T. J. Dodwell, S. Kynaston, R. Butler, R. T. Haftka, N. H. Kim, and R. Scheichl. "Multilevel Monte Carlo simulations of composite structures with uncertain manufacturing defects". In: *Probabilistic Engineering Mechanics* 63 (2021), p. 103116. DOI: 10.1016/j.probengmech.2020.103116.

[92] P. Khodabakhshi, O. Burkovska, K. Willcox, and M. Gunzburger. "Multifidelity methods for uncertainty quantification of a nonlocal model for phase changes in materials". In: *Computers & Structures* 297 (2024), p. 107328. DOI: 10.1016/j.compstruc.2024.107328.

[93] G. Aitken, L. Beevers, and M. A. Christie. "Multi-level Monte Carlo models for flood inundation uncertainty quantification". In: *Water Resources Research* 58.11 (2022). DOI: 10.1029/2022WR032599.

[94] G. Donoghue and M. Yano. "A multi-fidelity ensemble Kalman filter with hyperreduced reduced-order models". In: *Computer Methods in Applied Mechanics and Engineering* 398 (2022), p. 115282. DOI: 10.1016/j.cma.2022.115282.

[95] B. Peherstorfer, P. S. Beran, and K. E. Willcox. "Multifidelity Monte Carlo estimation for large-scale uncertainty propagation". In: *2018 AIAA Non-Deterministic Approaches Conference*. 2018. DOI: 10.2514/6.2018-1660.

[96] A. Guibert, A. F. Diaz, A. Chaudhuri, and H. A. Kim. "Multifidelity uncertainty quantification in battery performance for eVTOL flights under material and loading uncertainties". In: *VFS Forum Preceedings - Vertical Flight Society 80th Annual Forum & Technology Display*. 2024. DOI: 10.4050/F-0080-2024-1167.

[97] A. Beck, J. Dürrwächter, T. Kuhn, F. Meyer, C. D. Munz, and C. Rohde. "hp-Multilevel Monte Carlo methods for uncertainty quantification of compressible Navier-Stokes equations". In: *SIAM Journal on Scientific Computing* 42.4 (2020), B1067–B1091. DOI: 10.1137/18M1210575.

[98] F. Menhorn, G. Geraci, M. S. Eldred, and Y. Marzouk. "Multifidelity optimization under uncertainty for a scramjet-inspired problem". In: *Proceedings of ECCM 6 and ECFD 7*. June 2018, pp. 2771–2782.

[99] F. Vidal-Codina, N. C. Nguyen, M. B. Giles, and J. Peraire. "An empirical interpolation and model-variance reduction method for computing statistical outputs of parametrized stochastic partial differential equations". In: *SIAM/ASA Journal on Uncertainty Quantification* 4.1 (2016), pp. 244–265. DOI: 10.1137/15M1016783.

[100] V. A. Profillidis and G. N. Botzoris. "Chapter 5 - Statistical methods for transport demand modeling". In: *Modeling of Transport Demand*. Elsevier, 2019, pp. 163–224. DOI: 10.1016/B978-0-12-811513-8.00005-4.

[101] N. Alemazkoor, A. Louhghalam, and M. Tootkaboni. "A multi-fidelity polynomial chaos-greedy Kaczmarz approach for resource-efficient uncertainty quantification on limited budget". In: *Computer Methods in Applied Mechanics and Engineering* 389 (2022), p. 114290. DOI: 10.1016/j.cma.2021.114290.

[102] C. Gogu. "Improving the efficiency of large scale topology optimization through on-the-fly reduced order model construction". In: *International Journal for Numerical Methods in Engineering* 101.4 (2015), pp. 281–304. DOI: 10.1002/nme.4797.

[103] M. Xiao, D. Lu, P. Breitkopf, B. Raghavan, S. Dutta, and W. Zhang. "On-the-fly model reduction for large-scale structural topology optimization using principal components analysis". In: *Structural and Multidisciplinary Optimization* 62.1 (2020), pp. 209–230. DOI: 10.1007/s00158-019-02485-3.

[104] C. Nguyen, X. Zhuang, L. Chamoin, X. Zhao, H. Nguyen-Xuan, and T. Rabczuk. "Three-dimensional topology optimization of auxetic metamaterial using isogeometric analysis and model order reduction". In: *Computer Methods in Applied Mechanics and Engineering* 371 (2020), p. 113306. DOI: 10.1016/j.cma.2020.113306.

[105] A. T. Patera and I. B. Oliveira. "Reduced-basis techniques for rapid reliable optimization of systems described by affinely parametrized coercive elliptic partial differential equations". In: *Optimization and Engineering* 8.1 (2007), pp. 43–65. DOI: 10.1007/s11081-007-9002-6.

[106] Y. Yue and K. Meerbergen. "Accelerating optimization of parametric linear systems by model order reduction". In: *SIAM Journal on Optimization* 23.2 (2013), pp. 1344–1370. DOI: 10.1137/120869171.

[107] P. Benner, E. Sachs, and S. Volkwein. "Model order reduction for PDE constrained optimization". In: *Trends in PDE Constrained Optimization*. Ed. by G. Leugering, P. Benner, S. Engell, A. Griewank, H. Harbrecht, M. Hinze, R. Rannacher, and S. Ulbrich. Springer International Publishing, 2014, pp. 303–326. DOI: 10.1007/978-3-319-05083-6_19.

[108] S. Boyaval, C. Le Bris, T. Lelièvre, Y. Maday, N. C. Nguyen, and A. T. Patera. "Reduced basis techniques for stochastic problems". In: *Archives of Computational Methods in Engineering* 17.4 (2010), pp. 435–454. DOI: 10.1007/s11831-010-9056-z.

[109] S. Boyaval, C. Le Bris, Y. Maday, N. C. Nguyen, and A. T. Patera. "A reduced basis approach for variational problems with stochastic parameters: Application to heat conduction with variable Robin coefficient". In: *Computer Methods in Applied Mechanics and Engineering* 198.41 (2009), pp. 3187–3206. DOI: 10.1016/j.cma.2009.05.019.

[110] P. Chen, A. Quarteroni, and G. Rozza. "Reduced basis methods for uncertainty quantification". In: *SIAM/ASA Journal on Uncertainty Quantification* 5.1 (2017), pp. 813–869. DOI: 10.1137/151004550.

[111] B. Efron and R. J. Tibshirani. *An introduction to the bootstrap*. 1st ed. Chapman and Hall/CRC, May 1994, p. 456. DOI: 10.1201/9780429246593.

[112] B. Efron and T. Hastie. *Computer age statistical inference, student edition: Algorithms, evidence, and data science*. Institute of Mathematical Statistics Monographs. Cambridge University Press, 2021.

[113] X. Liu. "Appendix A: The Delta method". In: *Survival Analysis*. John Wiley & Sons, Ltd, July 2012, pp. 405–406. ISBN: 9781118307656. DOI: 10.1002/9781118307656.app1.

[114] I. Gerlovina and A. E. Hubbard. "Computer algebra and algorithms for unbiased moment estimation of arbitrary order". In: *Cogent Mathematics & Statistics* 6.1 (2019), p. 1701917. DOI: 10.1080/25742558.2019.1701917.

[115] B. O'Neill. "Some useful moment results in sampling problems". In: *The American Statistician* 68.4 (2014), pp. 282–296. DOI: 10.1080/00031305.2014.966589.